Proteomics and metabolism of the mesophilic cellulolytic bacterium, *Clostridium termitidis* strain CT1112

by

Umesh Ramachandran

A Thesis Submitted to the Faculty of Graduate Studies of
The University of Manitoba
in partial fulfillment of the requirements for the degree of

DOCTOR OF PHILOSOPHY

Department of Biosystems Engineering
University of Manitoba
Winnipeg

Proteomics and metabolism of the mesophilic cellulolytic bacterium, *Clostridium termitidis* strain CT1112

by

Umesh Ramachandran

Ph.D., University of Manitoba, 2013

Supervisory Committee

Dr. David B. Levin (Department of Biosystems Engineering, University of Manitoba)
Supervisor

Dr. Nazim Cicek (Department of Biosystems Engineering, University of Manitoba)
Departmental Member

Dr. Richard Sparling (Department of Microbiology, University of Manitoba)
Departmental Member

Dr. Patrick C. Hallenbeck (Department of Microbiology and Immunology, University of Montreal)
External Examiner

Supervisory Committee

Dr. David B. Levin (Department of Biosystems Engineering, University of Manitoba)
Supervisor

Dr. Nazim Cicek (Department of Biosystems Engineering, University of Manitoba)
Co-supervisor or Departmental Member

Dr. Richard Sparling (Department of Microbiology, University of Manitoba)
Departmental Member

Dr. Patrick C. Hallenbeck (Department of Microbiology and Immunology, University of Montreal)
External Examiner

Abstract

Consolidated bioprocessing, a method that involves cellulase production, substrate hydrolysis, and fermentation all in one step, requires lower energy input and aims at achieving reduced biofuel production costs than traditional processes. It is an economically appealing strategy for the efficient production of biofuels such as ethanol or H_2. At present, the yields of fermentative hydrogen and ethanol production are less than the theoretical maximum and vary between anaerobic Clostridia due to the presence of highly branched metabolic pathways. With the recent advancements in 'Omic technologies, the selected cellulolytic species, in this case, *C. termitidis*, was extensively studied to identify the key enzymes that are involved in hydrogen and ethanol synthesis pathways in both the genome and proteome under different culture conditions. Metabolic characterization involving growth and end-product synthesis patterns were performed on 2 g L^{-1} cellobiose and α-cellulose under batch conditions to determine its metabolic potential for hydrogen and/or ethanol production. Initial characterization has shown the ability of *C. termitidis* to produce hydrogen, ethanol, and various other end-products on the two susbtrates. Continous N_2 sparging in the pH-controlled bioreactors with cellobiose and α-cellulose showed a consistent increase in the H_2 synthesis and lowered ethanol production compared to batch studies, with the H_2 yields of 1.03 and 1.34 mol product per mol hexose equivalent added, respectively. Shotgun 2-D proteome analyses were performed to compare cellulose versus cellobiose grown cultures across exponential and stationary phases of growth. Most of the glycolytic proteins were detected in the proteome with some exceptions and no significant change was observed across both

growth conditions. Hydrogen synthesis was regulatd via PFOR and ferredoxin-dependent hydrogenase, where as ethanol synthesis was regulated primarily via bifunctional AdhE activity. Proteomic analyses of *C. termitidis* cultured on hexose sugars in the absence of xylose suggested possible sequential utilization of xylose and cellobiose for the first time. Putative proteins consistent with xylose fermentation were observed at high levels. The hypothesis that *C. termitidis* can sequentially utilize xylose and cellobiose was further validated using batch fermentations tests on pure (xylose, cellobiose, xylan) and mixed substrates (xylose + cellobiose).

Table of Contents

List of Abbreviations

ABC	ATP-binding cassette
ack	Acetate kinase gene
adh	Alcohol dehydrogenase gene
AdhE	Acetaldehyde/alcohol dehydrogenase gene
aldh	Aldehyde dehydrogenase gene
AMP	Adenosine monophosphate
ARDI	Agricultural and Rural Development Initiative
ATCC	American type culture collection
atk	Acetate thiokinase gene
ATP	Adenosine triphosphate
BK	Butyrate kinase
BCA	Bi-cinnachoic acid
CBP	Consolidated bioprocessing
CO	Carbon monoxide
CO_2	Carbon dioxide
COGs	Clusters of orthologous groups
D	Dimensional
DTT	Dithiothreitol
E:A	Ethanol-to-acetate ratio
Ech	Enery conserving hydrogenase
EDTA	Ethylenediaminetetraacetic acid
Fd	Ferredoxin

FDP	Fructose-1,6-bisphosphate
GADPH	Glyceraldehyde-3-phosphate dehydrogenase
GAPFOR	Glyceraldehyde-3-phosphate:ferredoxin oxidoreductase
GHG	Greenhouse gasses
GTP	Guanosine triphosphate
H_2	Hydrogen gas
H_2ase	Hydrogenase
HPLC	High pressure liquid chromatography
IMG	Integrated microbial genomics
KO	KEGG ontology
LDH	Lactate dehydrogenase
MalE	Malic enzyme
MDH	Malate dehydrogenase
N_2	Nitrogen gas
NAD(P)H	Nicotinamide adenine dinucleotide (phosphate)
ND	Not determined
NFO	NADH:ferredoxin oxidoreductase
NSERC	Natural Sciences and Engineering Research Council of Canada
OAADC	Oxaloacetate decarboxylase
OD	Optical density
PEP	Phosphoenol pyruvate
PEPCK	Phosphoenolpyruvate carboxykinase
PFK	Phosphofructokinase

PFL	Pruvate formate lyase
PFOR	Pyruvate:ferredoxin oxidoreductase
PPDK	Pyruvate phosphate dikinase
PP_i	Pyrophosphate
PPK	Pyruvate phosphate kinase
PTA	Phosphotransacetylase
SSF	Simultaneous Saccharification and Fermentation

List of Tables

List of Figures

List of Supplementary Tables and Figures

Acknowledgments

The support and help of many individuals is gratefully acknowledged. Firstly, I would like to thank Dr. David Levin for providing me an opportunity to pursue this research, for his mentorship, optimism and unwavering support throughout the duration of my studies. I would like to thank all members of our lab, past and present, for their friendship and support. Nathan Wrana, Warren Blunt, Marcel Taillefer, Tobin Verbeke, Joe Ackerman, Tom Rydzak, Carlo Carere, and Scott Wushke were all supportive of my studies. A special thanks to Victor Spicer and Dmitry Shamshurin for their constant help with respect to proteomic analyses. I would also, at this time, like to extend my appreciation to my supervisory committee members, Dr. Nazim Cicek and Dr. Richard Sparling for their support, ongoing mentoring advice, good critique, and technical assistance.

My sincerest thanks go to my colleagues and collaborators both at the University of Manitoba and abroad. I would also like to thank all the members of Dr. John Wilkins and Dr. Oleg Krokhin's lab at the Manitoba Centre for Proteomics and Systems Biology for graciously hosting me during my time there and assisting with the Proteomic studies.

I am grateful of the administrative assistance provided by Evelyn Fehr and Debby Watson in the Biosystems Engineering office. This work was supported by funds provided by the Natural Sciences and Engineering Research Council of Canada (NSERC), through a Strategic Programs grant, by Genome Canada, through the Applied Genomics Research in Bioproducts or Crops (ABC) program for the grant titled, "Microbial Genomics for Biofuels and CoProducts from Biorefining Processes", and by the Province of Manitoba, Agricultural and Rural Development Initiative (ARDI), grant. I

would like to thank all my friends and family for their moral support and sincere encouragement.

Dedication

I would like to dedicate this work to my parents, Ramachandran Raghavan and Saraswathi Macheth, and my wife Aswathi Menon for their unbelievable patience and support, consistent encouragement and ability to elucidate the important things in my life. Thank you.

Chapter 1: Literature Review

This Chapter is based, in-part, on the following publication: "Levin DB, Carere C, Ramachandran U, Rydzak T, Saunders J. 2011. Fermentative Biofuels: Prospects of Practical Application. Chapter 12, pp. 601-634. In, Carbon Neutral Fuels and Energy Carriers, TE Veziroglu & N. Muradov (Eds.). Taylor & Francis Group, Publishers, Boca Raton, Florida, USA". My contribution to this publication was with the "Bioethanol" sections that include 1.8, 1.9, 1.10, and 1.11.

1.1 Introduction- Importance of alternate fuels

Increased demand for the fossil fuels from the developing nations along with decreased refining capacity resulted in alarming price hikes for crude oil that had significant impacts on the global economy, underscoring the urgent need for the production of alternative biofuels. By 2025, the global energy demand will increase by 50% with much of the demand coming from many developing nations (Lovins 2004; Ragauskas et al. 2006).

The threat of global climate change associated with greenhouse gas emissions from fossil fuel combustion has created a sense of urgency to develop renewable fuels with lower carbon emissions. There is great interest in the use of cellulosic biomass as a renewable source of energy (Demain et al. 2005). Renewable sources of energy and chemicals maybe derived from biomass (plants, animals, microbes and their waste products) through biorefining processes. Currently, biomass contributes approximately 14% of the world's energy needs, and as much as 35% of the energy demands in developing countries with limited fossil fuel supplies. In addition to renewable fuels, many industrial products such as dyes, synthetic fibers and solvents were made from trees and agricultural crops in the early 20^{th} century. By the end of 1960s, most of these bio-based chemical products were derived from petroleum (Van Wyk 2001).

If biomass is to become a viable alternative source of renewable energy (and bioproducts), new more efficient biorefining technologies will have to be developed. Consolidated bioprocessing (CBP) is a process in which all the three essential steps involved in the production of "the next generation biofuels": a) cellulase production; b) susbstrate hydrolysis; and c) fermentation, all occur in single process (Lynd et al. 2002 and 2005). For the efficient production of lignocellulose-based biofuels, a detailed understanding of the metabolism of the cellulolytic bacteria is essential. Hence, bioprospecting for novel biofuels producing bacteria is important for hydrogen (H_2), ethanol and other soluble end-products that could be used for biorefineries. Microorganisms that produce cellulose and lignocellulose degrading enzymes can be used to hydrolyze this biomass and convert the bulk of the substrate into various fermentation end-products, including H_2 (Levin et al. 2006; Lynd et al. 2002).

Cellulose fibers are embedded in a complex, intertwined matrix of other structural biopolymers, primarily hemicelluloses and lignin, which account for 20 to 35% and 5 to 25% of plant dry weight respectively (Lynd et al. 2002). Apart from its diverse architecture and complex nature, the presence of a complex intertwined matrix preventing enzyme docking on the cellulose, has become the rate-limiting step in the conversion of cellulose to fuels.

Biochemical analyses have been conducted on the cellulase systems of aerobic and anaerobic bacteria and fungi (Levin et al. 2006). Some cellulolytic bacteria express a suite of cellulolytic enzymes that are assembled into a complex structure on the cell surface called a cellulosome (Demain et al. 2005; Desvaux et al. 2000; Lynd et al. 2002). The bacteria attach to cellulose particles via the cellulosome. Cellulases within the

cellulosome act in a coordinated manner to efficiently hydrolyze cellulose to cellobiose and other soluble cellulodextrans (Zhang and Lynd 2005a; Zhang and Lynd 2005b). Currently, the cellulases and cellulosome complexes of various Clostridia have been studied extensively (Demain et al. 2005; Desvaux et al. 2000; Lynd et al. 2002; Zhang and Lynd 2005b). This chapter focuses on the importance of the clear elucidation of central carbon metabolism in anaerobic cellulolytic bacteria, especially Clostridia, for improved lignocellulose-based biofuels (H_2 and ethanol) production.

1.2 Limitations of First generation Biofuels

Bioethanol was traditionally produced using batch fermentations of sugars obtained from starch grain (US and Canada) or sugarcane (Brazil), and ethanol is recovered from the fermentation broths by distillation. Corn-based ethanol is the predominant feedstock used in the US and Eastern Canada, and wheat in the prairie provinces of Canada. Biofuels (primarily ethanol) obtained using these processes are called as “first generation biofuels”. Prolonged viablility of grain-based ethanol production is debatable due to various environmental concerns (Groom et al. 2008; Searchinger et al. 2008; Simpson et al. 2008). For example, according to Searchinger et al. (2008) corn-based ethanol production increased the rate of greenhouse gas (GHG) emissions. Moreover, grain-based ethanol production raises the concern of the use of agricultural crops/and or land for fuel instead of food (Brown 2006).

1.3 Second and next generation biofuels

Cellulose hydrolysis is complex and difficult due to its crystalline structure and presence of complex polymers such as lignin. Second-generation biofuels are biofuels that are produced from lignocellulosic biomass. Bioethanol produced from

lignocellulosics involve simultaneous saccharification and fermentation (SSF) or simultaneous saccharification and co-fermentation (SSCF) (Lynd et al. 2005; Lynd et al. 2002). These fermentation methods require additional pre-treatment of the cellulosic feedstock such as acid treatment and/or steam-explosion, followed by enzymatic hydrolysis using exogenously derived cocktails of cellulolytic enzymes to breakdown cellulose fibers into glucose monomers necessary for fermentation (Agbor et al. 2011). These techniques used for pre-treatment are cost-intensive and further result in the production of some end-products such as furfurals that can inhibit some downstream processes.

1.4 Importance of biorefineries

Biorefineries are essential for sustainable development and green processing in many industrial countries. These facilities utilize all the forestry and/or agricultural residues derived biomass conversion processes to produce biofuels, such as ethanol, and other value-added co-products, such as bio-plastics. In Canada, biorefinery development is at preliminary stages and more focus is on the production of exclusive bioproducts based on sugars obtained by the hydrolysis of lignocellulosic biomass derived from forests (Mabee et al. 2005). One of the major objectives of biorefinery development is to generate low-volume, high-value co-products when compared with high-volume, low-value products such as ethanol derived from lignocellulosics that show poor economics. This constraint could be overcome by utilizing processes that increase product generation from lignocellulosic process stream and coalesce biofuels production along with the generation of value-added products, like lignin for adhesive and resin production, further establishing better economic feasibility (Kadam et al. 2008; Pan et al. 2005).

1.5 Potential feedstocks for biofuels production

In general, approximately 50% of the total cost of biofuel production constitutes the cost of feedstock used for fermentation. Low-cost feedstocks are abundant and hence very important for the commercial feasibility of biofuels production. Increase in the energy costs has triggered the necessity of large-scale use of biomass for fuel production as an alternative to oil and gas. Currently, the prices for cellulosic biomass are lower when compared with crude oil and natural gas; the wellhead prices have been significantly higher during the last 10 years. Lignocellulosics constitute the most abundant biopolymer in the entire world. Cellulosic biomass from agriculture, municipal sources, and forestry could be used as impending feedstocks for biofuels and value-added bioproducts production ousting fossil fuels and diminishing green house gas emissions (Levin et al. 2007; Mabee et al. 2006). Canada possesses abundant low value agricultural crop residues such as hemp hurds, flax shives, and wheat straw. Biofuels crop such as switch grass also offer great potential for the production of third-generation biofuels. Lower costs for biomass as fuel feedstocks versus crude oil has created a significant interest for the development of strategies for production of biofuels using low value lignocellulosic feedstocks.

1.6 Consolidated Bioprocessing (CBP)

Substrate hydrolysis, cellulase production, and fermentation may be achieved in a single step alternative process called consolidated bioprocessing (CBP), using different microorganisms that produce cellulolytic and hemicellulolytic enzymes (Demain et al. 2005; Lynd 1996; Lynd et al. 2005; Lynd et al. 2002). This process may significantly reduce costs by eradicating the requirement for cellulosic enzyme production in a

separate biorefinery. Conventional methods used for cellulose conversion (second generation biofuels) involve four essential processes namely: i) production of saccharolytic cellulase and hemicellulase enzymes, ii) hydrolysis of carbohydrates present in pretreated biomass to sugars, iii) fermentation of hexoses including glucose, mannose, galactose, and iv) fermentation of pentoses like xylose and arabinose. Consolidated bioprocessing combines all four of these processes into a single-step. In this manner, biofuels production costs may be reduced due to higher conversion efficiencies of substrate when compared with separate hydrolysis and fermentation techniques (SHF), easier processing of the feedstocks, and reduced energy inputs resulting in better energy balance. Hence, CBP is an economically viable system for the production of "next generation biofuels" (Demain et al. 2005; Lynd et al. 2005; Lynd et al. 2002).

1.7 Biohydrogen

Although there is intensive research on a range of alternative fuels, cellulosic ethanol is the most possible alternative transportation fuel with immediate application. Biohydrogen ($BioH_2$), however, can be used as a transportation fuel, either via direct combustion in modified internal combustion engines, or in fuel cells in fuel cell powered vehicles. Hydrogen has tremendous potential to reduce greenhouse gas emissions generated by hydrocarbon combustion and thereby reducing fossil fuel consumption.

Presently, Canada is the largest producer and consumer of H_2, both in the Organization for Economic Co-operation and Development (OECD) and globally (NRCan 2004). The different methods that are used currently to produce $bioH_2$, include indirect biophotolysis, direct biophotolysis, dark-fermentation, and photo-fermentation. Current research on the comparison of the rates of H_2 production using various biological

systems indicate that dark-fermentation methods offer a good potential for effective bioH_2, production and further amalgamation with promising H_2, and fuel cell systems (Levin et al. 2004). Anaerobic bacteria that utilize cellulosic feedstocks as sole source of carbon can produce good amounts of H_2 in conventional bioreactors (Carere et al. 2008; Islam et al. 2006; Levin et al. 2006; Ramachandran et al. 2008).

BioH_2 technologies are at a very earlier stage of development. Fermentation of substrates containing cellulose, starch, or sugars by anaerobic bacteria generates both H_2 and CO_2 at low density and pressure. Commercial existence of the different BioH_2 systems depends on adequate amounts of H_2 for practical application. Currently, more focus is on developing systems that aim at higher yield and synthesis of H_2 using appropriate bacterial strains along with the optimization of bioreactor designs, and further genetically manipulating metabolic pathways favoring H_2 synthesis (Carere et al. 2008).

1.8 Ethanol as a biofuel

Ethyl alcohol, also known as ethanol or grain alcohol, is a flammable, clear and colorless liquid that melts at -114.1° C and has a boiling point of 78.5° C. Ethanol is widely used as a gasoline additive providing cleaner-burning fuel with higher octane. The largest ethanol producing industries, representing over 95% of the world production are located in Brazil and the U.S. (Market Research Analyst, 2008). Ethanol production by fermentation of sugars has been conducted for many years and can be produced from any feedstock containing hexose sugars (beet or sugarcane) or substrates that could be converted into sugar such as starch or cellulose. In Canada, ethanol is produced mainly from grade 2 wheat grains (used primarily as animal feed), although, currently more focus is on lignocellulosic based ethanol production.

Ethanol is already used as a transportation fuel (or fuel additive) in large scale in Brazil, USA, and other European countries, and it is expected that it will be one of the most potential renewable biofuels in the transportation sector in the next 20 years (Farell 2006; Brown et al. 1998). There are numerous advantages for ethanol's use as an energy carrier in today's transportation economy. Most significant is the potential for ethanol to serve as an essential renewable and domestic source of fuel acting to decrease the dependence on foreign oil. The addition of ethanol to gasoline also increases the fuel octane rating and and results in cleaner and more complete combustion, offering mitigation to the growing global concerns regarding GHG (green house gas) emissions and climate change. Emissions from combustion of ten percent (10%) ethanol-blended gasoline have 30% less carbon monoxide (CO), 10% less carbon dioxide (CO_2), and 7% less NOx/SOx (Ethanol clean air facts, American coalition for ethanol, 2004).

1.9 Ethanol production from starch

Most fermentation industrial alcohol and potable alcohol are currently produced from grains. Fermentation of starch from grain is a little more complex than fermentation of sugars, as starch has to be first broken down to sugars, which are then used to culture yeast for ethanol production (Van Maris et al. 2006). Starch is converted to glucose enzymatically, either by the presence of diastase present in the sprouting grains or by fungal amylase. The resulting hexose is converted to ethanol via fermentation by yeast (*Saccharomyces cerevisiae*). Dried distiller's grain (DDGS), a second co-product that is used as a high protein cattle feed, is derived from the residual starch, fiber, protein, and ash of the fermentation reactor (Van Maris et al. 2006). Strategies to enhance ethanol

production from grain include genetic modification of microorganisms so that they are capable of metabolizing pentose sugar as well as glucose (hexose sugar) (Walker 2011).

1.10 Cellulosic ethanol using anaerobic bacteria

Advancement in biotechnology, genetics, engineering and process chemistry are paving way for the concept of converting renewable biomass to valuable fuels and products. The paradigm shift from fossil fuels like petroleum to bio-based feedstocks will open up new opportunities for chemical processing industry. Feedstocks containing carbohydrates can be used as chemical raw materials and this will replace the requirement for various expensive, oxidative processes used in the petroleum industry. Biomass carbohydrates will provide a suitable route to products like alcohols, carboxylic acids and esters. The conversion of biomass to ethanol begins with characterizing the structural and chemical complexity of the three primary polymers that make up plant cell walls: cellulose, hemicellulose and lignin (US department of energy office of science report).

At present, bioethanol plant processes depend mainly on the fermentation of sugars from sugarcane in Brazil, or corn in the US (Lovins 2004; Parikka 2004). Also, there is more interest in the strategies involving bioethanol production from corn stover, trees, and low-cost municipal and agricultural wastes (Britt et al. 2000; Walker 2011). Most of these biomaterials consist of higher amounts of cellulose and hemicellulose, and the efficient “deconstruction” of these products remains a challenge. In order to reduce the cost of de-polymerization, the lignocellulosics are pre-treated so that the biomass matrix is more accessible to certain enzymes. In the future, cost-effective bioprocessing will be obtained by the combination of cellulase/hemicellulase treatments with other

essential processing steps. Hence, fermentation process could be combined with cellulase production using engineered anaerobic bacteria capable of producing both ethanol and cellulase, further providing appropriate delivery of the optimal mixture of the hydrolytic enzymes (Lynd et al. 2002). An additional feature of this method de-polymerization enzymes could be used for the cost-effective conversion of plant polysaccharides to mono- or oligosaccharides, providing further fermentation or separation processes.

Cellulose is the most abundant biopolymer available on the planet. The plant cell wall consists of chains of cellulose molecules linked with other polymers to form linear structures of considerably high tensile strength called as microfibrils (Pauly et al. 2008; Fernandes et al. 2011; Fry 2001). Each microfibril consists of approximately 40 cellulose chains and is about 10-20 nm in diameter. A microfibril's cellulose core is surrounded by hemicellulose, a branched polymer consisting of the combination of pentose sugars like arabinose, xylose and few hexoses like galactose, mannose, and glucose. Hemicellulose also forms covalent associations with lignin, a rigid polymer (Pauly et al. 2008). The structure and organization of lignin is poorly understood. Hence, pretreatment of biomass with acids or enzymes is essential to eliminate the surrounding matrix of hemicellulose and lignin from the cellulose core before hydrolysis.

The sugar residues within the cellulose molecule are linked together by a high degree of hydrogen bonding that determines its crystallinity, thereby forming a three dimensional (3-D) lattice-structure between the cellulose chains. Cellobiose, consisting of two glucose residues linked by β-1,4 glycosidic bonds, are the building blocks of each cellulose molecule (Fernandes et al. 2011). Plant cell walls generally consist of 35-50% cellulose, 20-35% hemicellulose, and 10-25% lignin, depending on the type of plant

species or cell type (Lynd et al. 2002; Pauly et al. 2008, Fry 2001). Enzymes such as hemicellulases, cellulases and other glycosyl hydrolases produced by certain bacteria and fungi aid in the degradation of the structural polysaccharides in biomass, synergistically.

1.11 Fermentation and ethanol synthesis

Alcohols (methanol, ethanol, butanol) may be synthesized by microbial fermentation of sugars under anaerobic conditions. In most Clostridia, the biochemical conversion of cellobiose to ethanol begins with glycolysis or Embden-Meyerhof-Parnas pathway, where cellobiose is converted to glucose (6-carbon sugar) and then into two 3-carbon pyruvate molecules along with adenosine tri phosphate (ATP) and nicotinamide adenine dinucleotide (NADH) (Figure 1.1). Pyruvate is a key metabolic branch-point, and under anaerobic conditions, leads to synthesis of alcohols like ethanol or butanol, and organic acids like lactate, acetate, or formate (Figure 1.2) (Desvaux et al. 2005).

Some Clostridia have the capacity to convert sugars derived from hydrolysis of cellulose, and/or hemicellulose into ethanol. Alcohol dehydrogenase (ADH) is the key ethanol synthesis enzyme in most species, including the solvent-producing Clostridia which can produce ethanol, butanol, and isopropanol (Chen 1995). The ADHs can be classified into three or four types based on their specificity in their primary structures. Ethanol or butanol producing Clostridia possess primary/secondary ADHs with Type 1 ADH zinc-binding domains, as well as Type 3 ADH domains (Reid and Fewson 1994). Coenzyme specificity, NAD(H) or NADP(H), are essential factors for proper understanding of the roles of different ADHs in microbial metabolism. NAD(H)-dependent enzyme catalyzes oxidative reactions for energy conservation, where as NADP(H)-dependent enzymes catalyze reductive biosynthetic reactions. In some

Clostridia, pyruvate is converted to acetyl-CoA in the presence of pyruvate ferredoxin oxidoreductase (PFOR) (Figure 1.2).

The detection of ADH and aldehyde dehydrogenase (AldH) activity can be difficult due to the fact that their activities are often linked through the catalysis of consecutive reactions during ethanol synthesis (Yan and Chen 1990). However, six distinct ADHs were identified in different species and the NAD(H)- and NADP(H)-dependent activities under specific conditions was determined (Chen 1995; Johnson and Chen 1995). The six major primary ADHs include: the butanol dehydrogenases BDH I (BDH-B- product of the *bdhB* gene), BDH II (BDH-A) from *C. acetobutylicum* ATCC 824; NAD(P)H-dependent enzymes ADH-1, ADH-2, and ADH-3 from *C. beijerinckii* NRRL B592; and NADPH-dependent ADH-1 (product of *adh-1* gene) from *Clostridium* sp. NCP 262 (Chen 1995).

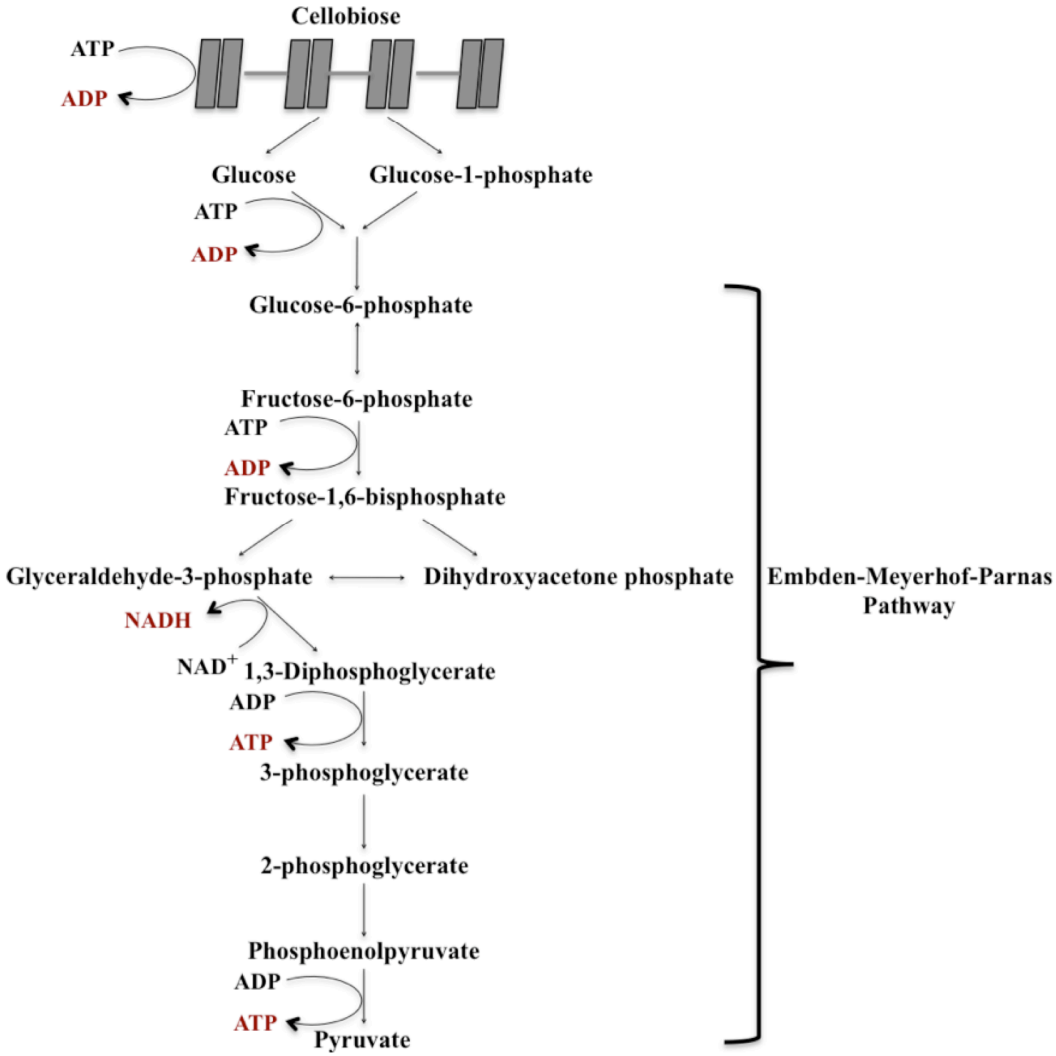

Figure 1.1 A schematic representation of glycolysis indicating the conversion of glucose to pyruvate (adapted from Levin et al. 2011).

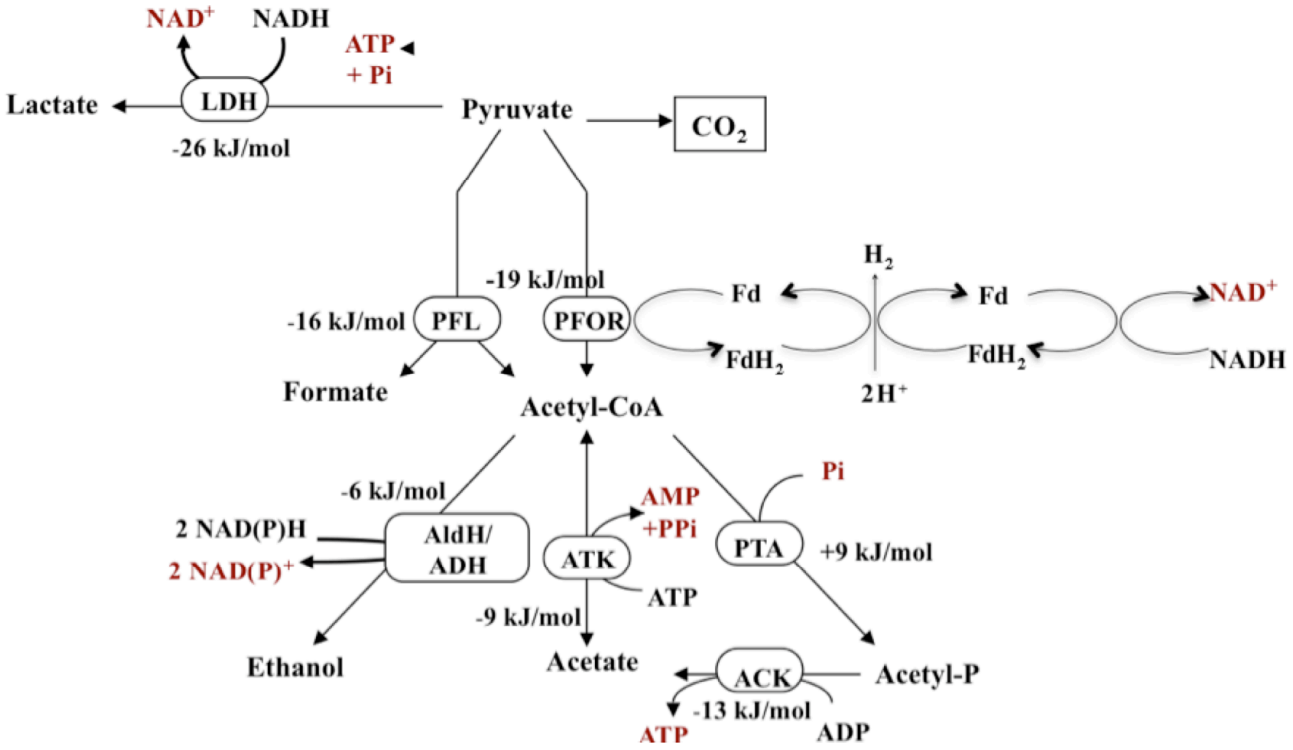

Figure 1.2 Metabolic pathways with corresponding standard free energies and end-products produced during anaerobic fermentation in Clostridia. The following enzymes are defined as: lactate dehydrogenase (LDH); pyruvate ferredoxin oxido-reductase (PFOR); aldehyde/acetaldehyde dehydrogenase (Aldh); alcohol dehydrogenase (Adh); phosphotransacetylase (PTA); acetate kinase (ACK); pyruvate formate-lyase (PFL) (adapted from Rydzak et al. 2009).

Bioinformatic analyses of these enzymes revealed amino acid sequence similarities between the ADH domain of the alcohol/aldehyde dehydrogenase (ADH-E, product of *adhE*/*aad* gene) identified for butanol production (Nair et al. 1994) and all the major ADHs characterized from solvent-producing Clostridia, suggesting a similar function (Chen 1995). *C. acetobutylicum* ATCC 824/DSM 792 *aad* or *adhE* gene showed higher amino acid sequence similarity to the *E. coli adhE* gene that encodes a multifunctional protein with pyruvate formate-lyase deactivase (PFL deactivase) and acetyl-CoA reductase (ethanol and acetaldehyde dehydrogenase) properties (Kessler et al. 1991).

C. beijerinckii NRRL B592 possesses three ADH isozymes that have high sequence similarity to *Clostridium* sp. NCP 262 (initially named as *C. acetobutylicum* P262) ADH-1 and to the alcohol/aldehyde dehydrogenase ADH domain of *C. acetobutylicum* ATCC 824/DSM 792 (Chen 1995). The type-3 ADH-1 of *Clostridium* sp. NCP 262 showed sequence similarity with type-3 iron-activated ADH-2 of *Zymomonas mobilis* and zinc-activated ADH-4 of *S. cerevisiae* (Conway et al. 1987; Reid and Fewson 1994). pH acts as an essential factor affecting the NADH-dependent activity of the ADHs from *C. beijerinckii* NRRL B592 and the BDHs from *C. acetobutylicum* ATCC 824. Most of the solvent forming enzymes, including primary ADH, aldehyde dehydrogenase, and 3-hydroxybutyryl-CoA dehydrogenase show sequence similarity between various *Clostridium* sp. such as *C. beijerinckii*, *Clostrdium* sp. NCP2662 and NRRLS B643 (Chen 1995).

1.12 'Omic technologies and advancements

Microorganisms act as efficient cell factories consisting of complete machineries for bioconversions from simpler source molecules to several biochemical substances along with degradation potential for the breakdown of complex compounds. Genomics refers to the functional and structural analysis of the whole "genome" of an organism using state-of-art sequencing technologies. Proteomics refers to a detailed analysis of the "proteome" in an organism to study the structure and functions of proteins expressed by a genome. Where as, "metabolome" is the complete set of metabolites expressed within an organism and "transcriptome" refers to the collection of all the mRNA transcripts of a gene present in a given cell (Adams 2008). In order to study and understand the relationship between gene and gene function, the products of the genome, especially proteins and expressed RNAs are studied extensively. At times, its difficult to obtain a best snapshot of the proteome, due to the interacting and changeable nature of the proteins. Also, proteomics demands several technical challenges due to nature of certain proteins that undergo many post-translational modifications in higher organisms. In such cases, transcriptomics connects the gap between the genetic code and functional molecules in a cell (Adams 2008).

Metabolomics has exciting applications in bioenergy, environmental interactions, functional genomics and gene discovery, secondary metabolism, genome-wide association mapping, systems biology and metabolic modeling in plant, algal, and microbial systems (Arita 2009). However, the scientific promise of metabolomics currently faces multiple challenges that need to be addressed. These challenges include: how to define the metabolome, metabolite annotation, standardization of spatially and

temporally resolved sampling, measurement of metabolite flux, dynamic range and depth-of-coverage, instrumentation and infrastructure, informatics and databases (Arita 2009).

All bioconversions in cells derive from metabolism. Metabolism is a set of biochemical reactions made feasible by enzymes (Stryer 1995), which in turn are encoded by genes. Thus, the whole potential of metabolism of an organism is encoded in its genome, the complement of all genes. At present, the metabolic potential of an organism can usually be efficiently modified or engineered, with the variety of molecular biology tools available today. Metabolic engineering is, as stated by Stephanopoulos already in 1990's, "directed improvement of product formation or cellular properties through the modification of specific biochemical reaction(s) or the introduction of new one(s) with the use of recombinant DNA technology"(Stephanopoulos 1998).

Unicellular organisms comprise catabolism of substrates and anabolic pathways for synthesis of biomass components in a single cell. Pathways for metabolization of various carbon sources unite and a range of biosynthetic pathways initiate in central carbon metabolism, which is a common node for catabolism and anabolism (Ma and Zeng 2003). Source molecules are broken down and energy and precursors for biosynthetic pathways are produced in the central carbon metabolism. Metabolic flux is a time-dependent quantity of the rate of consumption or production of compounds in a metabolic reaction (Nielsen et al. 2003; Stephanopoulos 1998).

Further, the 'omic technologies coupled with metabolic flux analysis (MFA) aids in the construction of a model of metabolism providing better knowledge of internal reaction nodes. However, in the absence of genome information, the metabolic models

are limited to mass-balanced and charge-balanced reactions and may be unable to identify thermodynamic bottlenecks in a reaction pathway, alternative reaction pathways, or incorporate, proteomic and transcriptomic regulatory data. One such example is the production of formate in *C. cellulolyticum*, which is illustrative of how the modeling of metabolism, in the absence of a genome, may overlook alternative reaction pathways. Earlier, the end-products detected of *C. cellulolyticum* cultured on cellulose were H_2, CO_2, ethanol, acetate, lactate and formate (Petitdemange et al. 1984). Whole genome analysis of *C. cellulolyticum* (http://genome.ornl.gov/microbial/ccel/) provided a strong evidence to support the production of each of these end-products, along with the presence of two putatively identified open reading frames encoding pyruvate-formate lyase (Ccel_2582, Ccel_2224). Further investigations, however, failed to detect formate as an end-product (Desvaux 2005, 2006; Desvaux et al. 2000, 2001a,b; Guedon et al. 2002; Guedon et al. 1999). By integrating genome information and experimental evidences (end-product synthesis pattern, enzyme activity assays) and comparing with previously constructed metabolic model to elucidate the flux distribution in *E. coli* (Holms 1996), the first stoichiometric model of *C. cellulolyticum* was first developed in the year 2001 (Desvaux et al. 2001a,b). Further, this model was used to study flux distribution in *C. cellulolyticum* cultures in synthetic and chemically defined media containing cellobiose and cellulose, both in batch and continuous modes.

A comparative genomics study of thermophilic and mesophilic cellulolytic *Clostridium* sp. and multiple strains of saccharolytic *Thermoanaerobacter* sp., related to biofuels production and biomass conversion were performed (Hemme et al. 2011; Xue et al. 2001). *Thermoanaerobacter sp. X514* has an ability to ferment a wide variety of C_5

and C_6 sugars to ethanol and few other metabolites under thermophilic conditions (Feng et al. 2009). Genome annotation and isotopic analysis of amino acids showed three essential observations with respect to the central metabolic pathway of *Thermoanaerobacter sp. X514*: 1) oxidative pentose phosphate pathway is not functional and the TCA cycle is incomplete under fermentative growth conditions; 2) Presence of (*Re*)-type citrate synthase activity, although no gene homologous to the recently characterized (*Re*)-type citrate synthase of *C. kluyveri* was found; and 3) synthesis of isoleucine from pyruvate and acetyl CoA through the citramalate pathway, instead of derived from threonine via threonine ammonia-lyase (Feng et al. 2009). Transcriptional profiles of *Thermoanaerobacter sp. X514* with different carbon substrates had been conducted (Hemme et al. 2011).

Experimental studies showed that *Thermoanaerobacter sp.* X514 was able to utilize hexose (glucose, galactose, ribose, fructose etc.), pentose sugars (including xylose), and some complex carbohydrates (sucrose, cellobiose, starch). When *Thermoanaerobacter sp. X514* was grown in glucose, fructose, xylose, and cellobiose, the specific genes in the carbon uptake systems were more highly expressed. Embden-Meyerhof-Parnas (EMP) and pentose phosphate (PPP) pathways were used to metabolize these four sugars. Carbohydrate active enzymes were encoded by *Thermoanaerobacter sp. X514* for the catabolism of fructose, xylose and cellobiose.

During growth on fructose, xylose, and cellobiose, the carbohydrate metabolism genes were significantly up-regulated, and shifted carbon fluxes towards ribose. Thus, the results obtained indicate that more ribose should be synthesized as the substrate of nucleotide and amino acid metabolism, when *Thermoanaerobacter sp. X514* was grown

on fructose, xylose and cellobiose. Also, energy metabolism of *Thermoanaerobacter sp. X514* grown on fructose was more active than other sugars, with increased production of ethanol, acetate and lactate. Further, up-regulation of V-type ATPase genes and genes specific for inorganic ion transport and metabolism (such as sodium-translocating decarboxylase enzyme genes, Na+/ H+ antiporter and sodium/hydrogen exchanger genes) were observed. When grown on fructose, a more active electrochemical ion gradient was generated at the plasma membrane than when grown on other sugars, suggesting the synthesis of more ATP. Three characterized *adh* genes were expressed at similar levels when grown on these four sugars during ethanol synthesis. Except for the additional six lineage-specific *adh* genes, the expression levels significantly changed under different growth conditions, showing differential expression of the *adh* genes in *Thermoanaerobacter sp. X514* under various growth conditions (Hemme et al. 2011).

The Gram-positive anaerobic, extremely thermophilic bacterium, *Caldicellulosiruptor saccharolyticus* has the ability to ferment cellulose, hemicellulose, pectin-containing biomass to H_2, CO_2, and acetate. Whole genome analysis depict that *C. saccharolyticus* possess necessary enzymes that can extensively hydrolyze polysaccharides present in cellulose, hemicellulose, starch, and pectin, along with many ABC transporters for monomeric and oligomeric sugar uptake. *In silico* analyses also showed the presence of components of both Embden-Meyerhof-Parnas and nonoxidative pentose phosphate pathways, whereas no components of Entner-Doudoroff pathway were evident.

Metabolic pathways for other varieties of sugars, such as arabinose, glucoronate, fructose, galactose, fucose, and rhamnose were also identified and these catabolic

pathways result in the production of NADH and reduced ferredoxin. Further, two distinct hydrogenases use the generated NADH and ferredoxin to synthesize H_2. When cultured on glucose and xylose, significant upregulation of the glycolytic pathway and an ABC-type sugar transporter was observed based on whole-genome trancriptome analysis. This shows that *C. saccharolyticus* co-ferments these sugars unrestricted by glucose-based catabolite repression (van de Werken et al. 2008). Higher yields of H_2 were observed on a wide range of carbon sources utilized by *C. saccharolyticus*, except for the production lactate that significantly affected the H_2 yields (Willquist and van Niel 2010). As a result of the initiation of low lactate flux, the cells enter stationary phase, which further coincides with a significant decrease in the glucose consumption and acetate production fluxes. Significant reductions in the growth rate coincided with the sudden increase and then decrease in NADH levels.

Kinetic analysis showed that LDH activity was regulated by competitive inhibition of pyrophosphate and NAD, and allosteric activation by fructose 1,6-bisphosphate (300%), ATP (160%) and ADP (140%). LDH activation by ATP shows that *C. saccharolyticus* uses LDH to maintain its flux of ATP and NADH production. Hence, pyrophosphate was observed as an effector as the sensitivity of LDH with respect to NADH/NAD ratio was influenced by different concentrations of pyrophosphate (Willquist and van Niel 2010). Further investigation of the role of inorganic pyrophosphate as a significant energy carrier in the hydrogen-producing pathways of *C. saccharolyticus* showed significant pyrophosphate-dependent phosphofructokinase and pyruvate phosphate dikinase activity. No significant cytosolic pyrophosphatase activity was detected, whereas, membrane-bound pyrophosphatase activity was observed. Also, it

was observed that pyrophosphate allosterically regulated the activity of pyruvate kinase enzyme (Bielen et al. 2010).

Metabolic fluxes are process streams of a cell factory. Therefore, a common aim of metabolic engineering is to generate changes in pathway fluxes. The essential biocatalysts, i.e. enzymes, can be amplified, deleted, and modified with versatile molecular biology tools. However, metabolic homeostasis prevails in cells that are highly balanced systems. A flux through a pathway depends on various factors in addition to the enzymes. The complement of fluxes in a cell, namely the "fluxome", is cell's ultimate response to genetic and environmental conditions (Sauer 2004). The flux response emerges from an integrated function of complex and dynamic interaction networks (metabolic, signal transduction, regulatory, protein-protein interaction networks etc). Many of the components of the biochemical interaction networks such as concentrations of enzymes, other proteins, metabolites, and genome-wide gene expression levels are at present directly measurable with high-throughput systems. Since the fluxes are dependent of time, they cannot be directly measured but have to be inferred from other, measurable, quantities through a model based computational analysis.

1.13 Cellulolytic Clostridia and metabolism

The major focus of this research is to characterize bacteria that can efficiently convert lignocellulosic substrate and aid in the enhanced production of H_2 and ethanol. Very little is known about mesophilic, cellulolytic, and anaerobic bacterium, *Clostridium termitidis*, isolated from the gut of a wood-feeding termite, *Nasutitermes lujae*. The naming of the bacterium was based on the fact that it was isolated from a termite (Hethener et al. 1992). Among different types of mesophilic Clostridia, the metabolism of

C. cellulolyticum has been extensively studied by Guedon, Desvaux and Petitdemange (Desvaux et al. 2001a,b; Guedon et al. 2000, 2002; Guedon et al. 1999; Petitdemange et al. 1984) and research efforts on other related Clostridia including *C. termitidis* have been modeled on the work on *C. cellulolyticum*. Based on the literature available for *C. cellulolyticum* metabolism, it can be stated that the natural habitat of the bacteria does not necessarily correspond with the physiological conditions under which the bacterium was completely characterized. *Clostridium cellulolyticum*'s metabolism has evolved to actively utilize a limited ecological niche and involve in the development of a diverse microbial system. Such metabolic studies would aid in the development of industrial applications such as cellulose degradation, biofuels (H_2 and ethanol) production rather than not exclusively directed towards existing in its natural habitat. Early metabolic studies focused on the examination of nutritional requirements of *C. cellulolyticum* in batch containers without agitation or pH control. Later, experiments were conducted in bioreactors/chemostats under batch conditions to study the effect of mineral-salt versus complex mediums, the negative effects of acidification, as well as to develop a continuous culture system and determine the effect on growth/metabolism.

In Clostridia with branched fermentation pathways, there are different branch-points that significantly affect the thermodynamics of pathways involving specific end-products of interest. Branch-points formed by metabolites that act as substrates or products of more than one enzyme interconnect most of the metabolic pathways. In general, there are four essential branch-points in the central metabolism of clostridial bacteria: glucose-1-phosphate, glucose-6-phosphate, pyruvate, and acetyl-CoA (Desvaux

et al. 2006; Guedon et al. 2000). The role of glucose-6-phosphate and pyruvate branch-points in central metabolism will be discussed in detail below (Figure 1.2).

1.13.1 The glucose-1-phosphate and glucose-6-phosphate branch-points

Isomerization of glucose-6-phosphate to fructose-6-phosphate regulates glycolysis resulting in the formation of pyruvate and ATP. Further oxidation of glucose-6-phosphate results in 6-phosphogluconate, which is used as substrate in the pentose phosphate pathway, mediating the synthesis of NADPH (used as reducing agent for biosynthetic pathways) and pentose phosphates (used for nucleotide synthesis). Moreover, glucose-6-phosphate can be synthesized using gluconeogenesis or glycogenolysis. In *C. cellulolyticum*, the glucose-1-phosphate and glucose-6-phosphate are connected by the phosphoglucomutase reaction, which was shown to be essential for the regulation of carbon flux both through glycolysis and carbon uptake from outside the cell during steady-state growth in continuous cultures (Guedon et al. 2000). Chemostat cultures of *C. cellulolyticum* with ammonia as growth-limiting nutrient showed that as much as 30% of cellobiose being consumed was converted to cellotriose, polysaccharides, and glycogen, irrespective of the specific growth rates. Further, kinetic analysis showed that the carbon flux through phosphoglucomutase significantly reduced with the increase in the cellobiose consumption rate and carbon flux through glycolysis. The increase in carbon flux through glycolysis resulted in reduced pool of glucose-6-phosphate, whereas increased accumulation of glucose-1-phosphate (a key precursor for glycogen, cellotriose, and exopolysaccharides) was observed (Guedon et al. 2000; Desvaux 2006). Hence, the glucose-1-phoshapte/glucoe-6-phosphate branch-points may appear to control the excess carbon flow and dissipate excess energy.

1.13.2 The pyruvate-acetyl coenzyme A branch-points

Pyruvate acts as an essential branch-point during lignocellulosic substrate fermentation using anaerobic bacteria (Figure 1.2). Pyruvate can be obtained from glucose, lactate, alanine, and other glucogenic amino acids. Under anaerobic conditions, pyruvate is reduced to lactate regenerating NAD^+ and allowing further ATP synthesis via glycolysis (Lengler et al. 1999).

Chemostat cultures of *C. cellulolyticum* grown under cellobiose-limited conditions, showed a shift from acetate-ethanol fermentation to a partial ethanol-lactate fermentation, due to an increase in the dilution rate. This condition resulted in the accumulation of pyruvate, since the specific production rate of lactate paralleled the increase of catabolic rate associated with increasing dilution rate. This phenomenon indicated that the anabolic and catabolic pathways downstream of pyruvate were not able to accommodate the carbon flowing through glycolysis, resulting in pyruvate overflow. Based on H_2/CO_2 ratios, Desvaux and co-workers (Desvaux 2006; Guedon et al. 1999) reveal that the redox balance was principally maintained via NADH-ferredoxin oxidoreductase and associated hydrogenase activities at a low dilution rate. Further, electron flow was balanced through the production of reduced products, such as ethanol and lactate (Desvaux 2006; Guedon et al. 1999). This kind of carbon flux distribution was not observed in cultures grown on cellulose, which suggested that pyrutate:ferredoxin oxidoreductase (PFOR) and lactate dehydrogenase did not compete for carbon flowing through glycolysis. Moreover, the true growth yield (Y^{max}) determined on cellobiose was significantly lower than cellulose suggesting that growth on cellulose could reach a higher biomass for the same quantity of carbon consumed as cellobiose.

Extensive studies on *C. cellulolyticum* indicate that the metabolism of this

bacterium has been modeled by the rate of carbon flowing from cellulosomal activity, generating a bacterium that is accustomed to a cellulolytic environment in which carbon flow is limited. It has been observed that in *C. thermocellum*, cellulase production is decreased by the increase in the cellobiose concentration in the medium (Brener and Johnson 1984). Cellulosome activity, however, could be increased by 10-fold by the addition of exogenous β-glucosidase in the medium, which reduced cellulase inhibition during co-cultures (Maki et al. 2009). Also, the lower growth rate exhibited by other anaerobic cellulolytic bacteria such as *C. termitidis* and *C. thermocellum* can be exploited as a merit due to the fact that it aids in higher ethanol production and reduces end-product inhibition to the hydrolytic enzymes because of a lack of overgrowth (Maki et al. 2009).

Most of the anaerobic cellulolytic bacteria characterized have limited carbon consumption rates associated with limited growth capabilities. In *C. cellulolyticum*, limited growth during early log phase was observed due to inefficiently regulated carbon flow entering glycolysis (Guedon et al. 1999). Studies on *C. cellulolyticum* metabolism also illustrates the mechanism by which bottlenecks in core metabolic pathways may shift the carbon flux towards "overflow" pathways resulting in the production of undesirable metabolites. One such example that has been discussed above is the production of extracellular pyruvate in cultures grown on higher concentrations of cellobiose. Recent advances using metabolic engineering as a valuable tool has resulted in the development of genetically modified strains of biofuels producing cellulolytic bacteria such as, *C. cellulolyticum*, via the incorporation of a heterologous catabolic pathway branched on pyruvate metabolic node. *Zymomonas mobilis* genes encoding Pyruvate decarboxylase (*pdc*) and acetaldehyde dehydrogenase (*adhII*) were expressed using ferredoxin promoter

from *Clostridium pasteurianum*. The recombinant strain of *C. cellulolyticum* cultured on cellulose exhibited higher cell density, enhanced cellulose degradation and increased concentrations of H_2, acetate, CO_2 and ethanol, when compared to the wild-type. Apart from introducing an alternative ethanol producing pathway, the major end-products obtained were H_2, acetate, CO_2, but not ethanol (Guedon et al. 2002). Hence, pyruvate-acetyl-CoA act as essential branch-points as altering carbon flux at this node will reveal the extent to which metabolism is restricted by pyruvate ferredoxin oxidoreductase (PFOR).

In most of the Clostridia, ATP is generated using substrate-level phosphorylation and the organic molecules act as final electron acceptors. NADH is generated during the formation of 1,3-diphosphoglycerate from glyceraldehyde-3-phosphate and a second oxidation occurs during the synthesis of acetyl-CoA from pyruvate in the presence of PFOR. This biochemical reaction results in the formation of reduced ferredoxin, during which, electrons are transferred to a Fd-dependent hydrogenase responsible for H_2 synthesis (Desvaux 2005). The fresh reducing equivalents are generated by the oxidation of NADH (generated during glycolysis) in the presence of NADH:Fd reductase.

The regulation of flux through PFOR is significant as the removal of PFL and LDH pathways may overcome the flux through PFOR causing extracellular pyruvate production or synthesis of other metabolites such as cellodextrins, glycogen, exopolysaccharides or amino acids. In *C. cellulolyticum*, during high carbon flux, pyruvate overflow results in the oxidation of reducing equivalents through the formation of ethanol and lactate (less-reduced metabolites) (Desvaux et al. 2001b). This indicates the incapability of PFOR to sustain the carbon flux at the pyruvate branch-point from

cellobiose hydrolysis. During these conditions, the electron flow from glycolysis was balanced by the synthesis of ethanol and lactate (Guedon et al. 1999). Hence, it could be inferrd that lactate and acetyl-CoA synthesis pathways did not compete with each other as lactate production was only observed during high carbon flux in *C. cellulolyticum*.

If PFOR does not represent an essential bottleneck favoring lactate or formate producing pathways, increased production of H_2/acetate or ethanol will be observed. In order to overcome the bottleneck at acetaldehyde dehydrogenase, overexpression of an acetaldehyde dehydrogenase under the influence of a constitutively active promoter could be effective (Maicas et al. 2002). This, however, might result in the creation of other bottlenecks, especially at alcohol dehydrogenase and thus may not always result in increased ethanol production.

In some Clostridia, alcohol production could be obtained by a bifunctional acetaldehyde/alcohol dehydrogenase, encoded by *adhE* (Carere et al. 2012). During carbohydrate catabolism, energy requirements and the availability of oxidized reducing equivalents within the cell are basically associated with the relative yields of metabolites like lactate, ethanol and acetate produced. Reoxidization of reducing co-enzymes like NAD(P)H-$NAD(P)^+$ through either lactate to pyruvate switch or through the conversion of acetyl phosphate to ethanol. In order to enhance the carbon flow towards ethanol, recycling of NAD(P)H-$NAD(P)^+$ is necessary apart from the energetic requirement of the cell.

1.14 Pathway regulation and flux balance necessary for efficient biofuel synthesis

1.14.1 Peripheral pathways channeling into central degradation pathways in hexose catabolism

There are several pathways that are responsible for the oxidation of carbohydrates. The peripheral reactions channel the catabolism of hexoses, pentoses (aldose, ketose), glucosides, amino sugars, hexuronides, hexuronates, hexonates, and polyols into the central degradation pathways (Lengler et al. 1999). Peripheral reactions may be defined as a set of interconversion reactions that are necessary for proper channeling of low-molecular-weight carbohydrates into the central catabolic pathways (Lim 2003). The different mechanisms of sugar interconversions include oxidation or reduction, phosphorylation, phosphorolysis of glycosides, keto-enol isomerization, and aldol cleavage (Lengler et al. 1999).

In most cellulolytic bacteria, cellulose hydrolysis occurs in two steps: 1) Cellulose is first cleaved to the disaccharide cellobiose by endoglucanases and exoglucanases; and 2) cellobiose is either transported across the plasma membrane using permeases or further hydrolyzed by cellobiohydrolase to glucose (Desvaux 2005; Lynd et al. 2002; Boisset et al. 1999). Within the cell, glucose is metabolized via Embden-Meyerhof pathway or other metabolic pathways. Other complex carbohydrates such as starch and glycogen consist of D-glucose subunits linked by α-1,4-glycosidic linkages. Glycogen acts as an essential storage molecule and occurs in the form of storage granules in bacteria such as *E. coli* (Lim 2003).

Bacteria metabolize endogenous glycogen as a carbon and energy source by phosphorylysis of glycogen to glucose-6-phosphate in a two-step process: 1)

Phosphorylysis of glycogen in the presence of phosphorylase to glucose-1-phosphate; and 2) further catalyzed by phosphoglucomutase to glucose-6-phosphate. Glucose-6-phosphate can then enter Embden-Meyerhof-Parnas pathway for further degradation. This process of glycogen catabolism does not require the expenditure of ATP hydrolysis, unlike conventional phosphorylation of glucose to glucose-6-phosphate in the Emden-Meyerhof-Parnas (glycolysis) pathway (Gottschalk 1986; Lengler et al. 1999; Lim 2003).

1.14.2 Channeling hexose intermediates in the central degradation pathways

In general, hexoses produced by the enzymatic hydrolysis of disaccharides and polysaccharides are converted to glucose or its isomers. In cellular metabolism, glucose plays a vital role and acts as the starting point into various metabolic pathways for several carbohydrates. Hexose metabolism usually occurs via Embden-Meyerhof-Parnas pathway, but this is not always the scenario. One of these other pathways called the phosphoketolase pathway results in the formation of xylulose-5-phosphate that acts as an essential intermediate of pentose metabolism. In *Lactobacilli* and some enteric bacteria, pentose sugars like xylose, ribose and arabinose are phosphorylated to xylulose-5-phosphate. Further, xylulose-5-phosphate is oxidized to lactate and acetate by the formation of glyceraldehyde-3-phosphate and acetyl-phosphate intermediates, with a net yield of two moles of ATP per mole of pentose (Lengler et al. 1999; Lim 2003).

1.14.3 Channeling pentose intermediates in the central degradation pathways

Pentoses are synthesized from hexoses through the pentose phosphate pathway (PPP) or hexose monophosphate pathway (HMP), also referred to as the hexose monophosphate shunt. In most bacteria, pentose sugars play an essential part in the cellular metabolism as they are the principal component of nucleoside, act as precursors

for the synthesis of aromatic amino acids like phenylalanine, tryptophan and tyrosine, and take part in the dark reactions of photosynthesis.

Pathways involving the interconversion of pentose and hexose sugars allow microorganisms to merge important metabolic pathways with photosynthesis and nucleic acid synthesis. Firstly, glucose is phosphorylated to glucose-6-phosphate, followed by oxidation to 6-phosphogluconate with 6-phosphogluconolactone as an intermediate. Further decarboxylation and oxidation of 6-phosphogluconate, results in the formation of a pentose, ribulose-5-phosphate.

Reduced NADP (NADPH) is necessary for anabolic reactions. Ribulose-5-phosphate is interconvertible with other two pentose sugars, namely ribose-5-phosphate and xylulose-5-phosphate, that act as precursors for nucleotides and production of other important intermediates such as glyceraldehyde-3-phosphate, erythrose-4-phosphate, fructose-6-phosphate, and pseudoheptulose-7-phosphate. These intermediates act as precursors for other metabolic pathaways. Generally, xylulose-5-phosphate and ribose-5-phosphate are converted to fructose-6-phosphate and glyceraldehyde-3-phosphate in the presence of transaldolase and transketolase, respectively, further proceeding to the Emden-Meyerhof-Parnas pathway (Figure 1.1). Methylpentoses such as rhamnose and fucose are also obtained from hexose sugars and are transported in to the cell via permeases. These sugars are converted to the 1-phosphoketulase form and catabolized by specific aldolases to dihydroxyacetone phosphate and lactaldehyde; the latter is oxidized through lactate to pyruvate reaction (Lengler et al. 1999; Lim 2003).

In most bacteria, the pentose phosphate pathway is normally used in a non-cyclic way for pentose and NADPH synthesis by oxidizing C1 of hexoses to CO_2. These sugar

phosphates play an essential role in pentose catabolism via conversion into hexoses and in gluconate metabolism. The interconversion reactions are called as non-oxidative branch of the pentose phosphate cycle. The oxidative branch includes hexose phosphate oxidation to pentose phosphate along with CO_2 and the non-oxidative branch includes pentose phosphate interconversion to hexose phosphate.

Combining these two branches results in the oxidation of hexose-6-phosphate to CO_2 and triose phosphate, plus the reduction of NADP to NADPH. Hence, the oxidative pentose phosphate cycle aids in the complete oxidation of glucose without entering the Embden-Meyerhof-Parnas or Entner-Doudoroff pathways. This kind of metabolism is observed in Cyanobacteria, and some acetic acid bacteria, such as *Gluconobacter sp*. that oxidize triose phosphate to acetate, followed by excretion of acetate out of the cell. In *Thiobacillus novellus* and *Brucella abortus*, oxidative pentose phosphate cycle replaces the Embden-Meyerhof-Parnas, or Entner-Doudoroff pathway. Some anaerobic bacteria are able to degrade pentose sugars, converting hexoses and pentoses into xylulose-5-phosphate, catabolized by a transketolase like enzyme (phosphoketolase) catalyzing an internal redox reaction, resulting in the formation of energy-rich intermediate acetyl phosphate (Gottschalk 1986; Lengler et al. 1999).

1.14.4 Channeling hexose-related compounds into intermediates of degradation pathways

Hexauronides (glycosides of glucuronic acid), hexauronates (glucoronic acid), and hexonates (gluconate) are metabolized by some bacteria into 2-keto-3-deoxy-gluconate-6-phosphate, which is an essential intermediate of the Entner-Doudoroff pathway of hexose catabolism. Moreover, polyols (sugar alcohols such as sorbitol,

mannitol or galactitol) are generally transported by phosphotransferase system (PTS) and converted into their corresponding 6-phosphates. Further oxidation and phosphorylation results in the formation of fructose-6-phosphate and ketose-1-6-bisphosphate respectively. Ribitol, arabinitol and xylitol are oxidized by NAD^+-dependent dehydrogenases to the respective pentuloses and further activated by ATP-dependent kinases.

In Archaea, many variants of the main pathways occur. Two major modifications of the Entner-Doudoroff pathway are found: 1) In eubacteria and halophilic archaebacteria, glucose is first oxidized to gluconate, then dehydrated to 2-keto-3-deoxy-gluconate, followed by phosphorylation into 2-keto-3-deoxy-phosphogluconate and aldol cleavage generating pyruvate and glyceraldehyde-3-phosphate; 2) In some arachaebacteria, like *Thermoplasma* and *Sulfolobus*, non-phosphorylated Entner-Doudoroff pathway occur, causing aldol cleavage of 2-keto-3-deoxy-gluconate, resulting in the formation of pyruvate and glyceraldehyde. Oxidation of glyceraldehyde to glycerate, followed by phosphorylation to 2-phosphoglycerate, results in the formation pyruvate via phosphoenol pyruvate. The ATP molecule that is gained in pyruvate kinase reaction is used for glycerate activation. Hence, in this modified Entner-Doudoroff pathway, utilizing $NAD(P)^+$-linked dehydrogenases, there is no net gain of ATP during the oxidation of glucose to pyruvate (Gottschalk 1986; Lim 2003).

Gluconeogenesis acts as a ubiquitous pathway for synthesis of hexoses (glucose) from non-carbohydrate precursors. Gluconeogenesis occurs only when the microbial cells require hexoses for structural purposes or when they have surplus energy, with additional energy stored in the form of reduced compounds. Gluconeogenesis is not simply the

reversal of Embden-Meyerhof-Parnas (glycolysis) pathway, although these two pathways have seven enzymes common. It involves three essential reactions that are irreversible and must be bypassed in glycolysis: 1) Conversion of pyruvate to phosphoenol pyruvate; 2) conversion of fructose-1,6-bisphosphate to fructose-6-phosphate by hydrolysis of C-1 phosphate; and 3) conversion of glucose-6-phosphate to free glucose.

The conversion of pyruvate to phosphoenol pyruvate (PEP) occurs in two possible ways: 1) pyruvate is converted to PEP in the presence of PEP synthase, as this reaction requires two high energy phosphate bonds; and 2) Carboxylation of pyruvate to oxaloacetate occurs, followed by the decarboxylation to produce PEP. These reactions are catalyzed by pyruvate carboxylase and phosphoenolpyruvate carboxykinase. The synthesis of glucose is a energy-intense process, and gluconeogenesis and glycolysis are reciprocally regulated to avoid futile cycling in cells (Lengler et al. 1999).

1.14.5 Pathway and flux regulation (thermodynamics)

Direct conversion of glycogen to glucose-1-phosphate is thermodynamically unfavorable. Using an alternate pathway, glycogen is synthesized in which ADP-glucose pyrophosphorylase catalyzes the conversion of glucose-1-phosphate to ADP-glucose. Glycogen synthetase unites all the glucose monomers with the existing glycogen molecule. The Emden-Meyerhof-Parnas pathway is a best example for an amphibolic pathway that functions in dual roles of both catabolism and anabolism. In most of the bacteria, the Emden-Meyerhof-Parnas pathway and TCA Cycle are amphibolic.

Another essential aspect is that the metabolic intermediates that are obtained through anabolic pathways must be replenished through anaplerotic reactions for the continuity of the primary pathways. Although, these intermediates are necessary for both

carbohydrate anabolism and catabolism, different enzymes normally control the direction of their flow. Co-enzymes such as NAD^+ and $NADP^+$ are mostly involved in the oxidation/reduction reactions, but co-enzyme NAD^+ is often used in catabolic reactions, whereas, $NADP^+$ is normally used in anabolic reactions (Lengler et al. 1999; Thauer et al. 1977).

The process of oxidative phosphorylation provides maximum number of ATP molecules formed during respiration. In the presence of oxygen, NADH + H^+ synthesized during glycolysis and NADH + H^+ and $FADH_2$ produced in the TCA Cycle, can be shunted into the electron transport chain. In most bacteria, fermentation and aerobic respiration are the two energy-deriving processes. The total amount of free energy obtained from the oxidation of glucose to CO_2 and water is -688 kcal/mol. Theoretically, 38 ATP molecules are generated from oxidation of one molecule of glucose in aerobic respiration in bacteria. Considering each ATP molecule accounts for -7.3 Kcal/mole of free energy in its terminal phosphate bond, approximately 40% of the total available energy is released as a result of glucose oxidation in the aerobic respiration process is mostly conserved in the form of ATP. In comparison, fermentation of glucose to ethanol and CO_2 accounts for 57 kcal/mol of free energy, out of which only 26% or 14.6 Kcal/mol of free energy is conserved in the 2 ATP molecules obtained.

Higher yield of ATP and higher efficiency of aerobic respiration is evident from the growth of facultative anaerobes, where high cell density is obtained during aerobic conditions. The Gibb's free energy (ΔG_R) changes of the reactions are normally dependent on the concentrations of reactants and products. ΔG_R values are defined at concentrations of 1mol/L of all reactants and products including H^+ (i.e., for pH= 0). As

for biological systems, the ΔG_R value is corrected at pH 7 [(H^+) is 10^{-7}]. Also, the redox potential of any reaction is very important as it provides an estimate of the feasibility and magnitude of a specific redox half-reaction. In general, oxidation of inorganic compounds have a low Gibb's free energy change, hence, low concentrations of either the substrate or its products may influence the magnitude and sign (+ or -) of the ΔG. Even if a microorganism carries out a specific reaction that is thermodynamically possible, it does not necessarily result in the production of biologically useful energy. For this reaction to be possible, not only the organism must possess specific enzymes, but it should also have a way of coupling the reaction to the conservation of chemical energy. This process normally requires a proton motive force or proton potential (electrochemical gradient) or a high-energy chemical compound like ATP. In most of the oxidation/reduction reactions, simulataneous occurrence of proton pumping and scalar consumption/production is observed.

Another essential mechanism that is necessary for the production of biochemically/biologically useful energy in chemolithotrophic bacteria such as *Thiobacillus thioparus* and *T. denitrificans* is substrate level phosphorylation. Whereas, in facultative anaerobic bacteria, pathways with high ATP yield are preferred. In *E. coli*, the catabolic pathways are normally determined by the electron acceptors, hence, O_2 represses all anaerobic pathways, and nitrate represses fumarate respiration and fermentation. The hierarchial rank is related to the ΔG values of the corresponding pathways and net ATP gain. In *E. coli,*, the transcriptional regulation of metabolism with respect to O_2 is controlled by three O_2 responsive regulators: 1) Arc (aerobic respiratory control); 2) Fnr (fumarate nitrate reductase regulation for anaerobic fermentation); and 3)

FhlA (formate hydrogen lyase regulation for formate/H_2 metabolism (Gottschalk 1986; Lengler et al. 1999).

As already mentioned, pyruvate acts as an essential branch-point and one of the important intermediate products of hexose metabolism. For the efficient conversion of cellulosic substrate using anaerobic Clostridia into biofuels (H_2 or ethanol), it is very important to understand the fate of pyruvate and thermodynamics involved in the reactions promoting the carbon flux towards acetate/H_2 synthesis and ethanol synthesis pathways.

To summarize, there are at least four essential pathways to oxidize sugar phosphates to either pyruvate or to acetyl phosphate through the following enzymes: 1) Fructose-1-6-bisphosphate aldolase (Embden-Meyerhof-Parnas and its variant in archaebacteria); 2) 2-dehydro-3-deoxy-6-phosphogluconate aldolase (KDPG-aldolase, Entner-Doudoroff pathway); 3) xylulose-5-phosphate phosphoketolase (phosphoketolase pathway); or 4) a combination of transaldolase and ketolase reactions (*Bifidobacterium bifidium* pathway) (Devries and Stoutham 1967; Tzortzis et al. 2005). Pyruvate is formed in the pyruvate-kinase reaction via the Embden-Meyerhof-Parnas pathway.

Whereas, in Gram-positive anaerobic bacteria, anaerobic unicellular eukaryotic parasites and archaea, pyruvate is converted to acetyl-SCoA, 2 reduced ferredoxin$^-$ and CO_2 in the presence of pyruvate ferredoxin oxidoreductase (pyruate synthase). In Lactobacilli, Enterobacteria, and some Clostridia under only strict anoxic conditions, pyruvate is converted to acetyl-CoA and formate in the presence of pyruvate formate lyase and CoASH. Heterolactic fermentation involves the oxidation of hexoses to pentose-5-phosphates and finally to lactate, CO_2, and ethanol or acetate, whereas pentose

sugars do not require oxidation. Most of the sugars are converted to xylulose-5-phosphate, which is further cleaved to pyruvate and acetyl phosphate. In case of hexose sugars, the excess NADH is utilized to reduce acetyl phosphate to ethanol through acetyl-CoA with the release of CO_2. The net ATP gain of oxidative phase of pentose phosphate pathway is 2 when compared with the non-oxidative branch.

In Clostridia, lactic acid bacteria and enterobacteria, acetaldehyde is produced by the reduction of acetyl-CoA, whereas in *Saccharomyces* and *Zymomonas*, acetaldehyde is formed by the decarboxylation of pyruvate. Pyruvate is formed in *S. cerevisiae* and *Z. mobilis* via the Embden-Meyerhof-Parnas (2 ATP) and Entner-Doudoroff pathways (1 ATP), respectively (Neveling et al. 1998; Stoops et al. 1997; Tzortzis et al. 2005). In *C. pasteurianum*, butyrate is synthesized via the Embden-Meyerhof-Parnas pathway, where pyruvate is oxidized to acetyl-CoA and CO_2 by pyruvate:ferredoxin oxidoreductase (PFOR). The reduced ferredoxin due to low redox potential (E_0= -420 mV), is able to reduce protons resulting in the evolution of molecular H_2 with acetyl-CoA acting as electron acceptor for NADH produced in the Embden-Meyerhof-Parnas pathway (Biebl 2001; Heyndrickx et al. 1991). In general, the products of fermentation are CO_2, molecular H_2, formate, acetate and other short-chain fatty acids. Some organisms have the capacity to convert these end-products further as we discussed earlier.

The synthesis of molecular H_2 deserves more attention. Molecular H_2 is synthesized via the reduction of two protons by two electrons catalyzed by hydrogenase enzyme. In this case, the electron acceptor is a proton rather than an organic substrate of fermentation. Hence, H_2 synthesis conserves substrates for oxidation resulting in the net yield of 1 mole of ATP per mol of substrate utilized. However, the removal of reducing

equivalents as molecular H_2 is thermodynamically less favourable (E_0= -420 mV) when compared to the reduction of substrates that have a positive redox potential (Lengler et al. 1999). Hence, it is essential to characterize the desired microorganisms for biofuels production and elucidate their metabolic pathways. Knowing their specific end-product synthesis patterns will help us to understand the strategies for efficient substrate conversion and improving H_2/ethanol yields.

1.15 Structure and Objectives of Thesis

1.15.1 Objectives of the Thesis

The **long-term objective** of this research is to develop biocatalysts for conversion of lignocellulosic biomass via consolidated bioprocessing. The **short-term objectives** of the research presented in this thesis are: 1) to perform a complete metabolic and growth characterization of the mesophilic, cellulolytic bacterium, *Clostridium termitidis*; 2) to perform a metabolic characterization in scale-up experiments in a bioreactor under different physiological conditions; 3) to perform a deep compositional and quantitative proteomic analyses of *Clostridium termitidis* grown on hexoses (cellobiose versus cellulose); and 4) to characterize the pentose utilization abilities based on hexose proteomics and whole genome analysis of *C. termitidis*.

1.15.2 Hypotheses

Hypothesis 1: Rates of growth and synthesis patterns of H_2 and ethanol by *C. termitidis* cultured on cellobiose versus cellulose will be different. As stated in section 1.14.2 of the literature review, carbon/electron flux at the pyruvate-acetyl coenzyme A branch-points and the rate of production of reducing equivalents greatly affect certain key enzymes involved in H_2 and ethanol synthesis pathways.

Hypothesis 2: Growth of *C. termitidis*, and synthesis of H_2 and ethanol on cellobiose (high carbon flux) versus cellulose (low carbon flux) will reveal the same kinds of metabolic bottlenecks observed for *C. cellulolyticum*. Detailed characterization of the mesophilic, cellulolytic bacterium, *C. cellulolyticum*, revealed that growth and end-product synthesis patterns of *C. cellulolyticum* are significantly influenced by carbon loading as under higher cellobiose concentrations, and extracellular pyruvate was observed in the medium with cellobiose catabolism exceeding the rate of pyruvate catabolism. This indicates that the the oxidation of pyruvate using PFOR is the rate limiting step in the glycolytic pathway. Also, in *C. cellulolyticum*, pyruvate overflow was coupled with growth arrest (Guedon et al. 1999).

Hypothesis 3: Maintaining different physiological conditions such as continuous gas sparging, pH control, and constant agitation could result in metabolic shifts in the H_2 and ethanol synthesis pathways in *C. termitidis*. Studies in *C. cellulolyticum* (sections 1.14, 1.14.2) have shown that metabolic flux could be affected by continuous sparging with N_2 or H_2 gas in a bioreactor. Also, pH control can also change end-product profiles and could result in shifting metabolic pathways accordingly.

Hypothesis 4: Based on preliminary findings (Hethener et al. 1992), sequential fermentation of hexose and pentose is possible in *C. termitidis*. Initial biochemical characterization revealed the ability of *C. termitidis* to ferment glucose/cellobiose and xylose. A complete understanding of central carbon metabolism involving glycolysis, pyruvate catabolism, pentose/glucoronate interconversion and the pentose phosphate pathway is necessary for identifying key enzymes for hexose and pentose catabolism.

1.15.3 Structure of the Thesis

Chapter 1 has presented an overview of the literature on consolidated bioprocessing and the use of cellulolytic bacteria for conversion of lignocellulosic biomass to H_2 and ethanol. Chapter 2 presents the results of experiments designed to characterize synthesis of hydrogen, ethanol, and other end-products by *C. termitidis* strain CT1112 in batch cultures containing 2 g L^{-1} cellobiose and α-cellulose. Cell growth, biomass accumulation (as measured by protein concentration), organic acid synthesis, changes in pH profiles, ethanol and H_2 yields were measured and compared with those of *C. cellulolyticum*, a mesophilic, cellulolytic, obligate anaerobe that has been characterized and studied extensively. Chapter 3 presents data on the growth and end-product synthesis patterns of *C. termitidis* cultured on cellobiose versus α-cellulose in pH-controlled bioractors with different physiological conditions. Chapter 4 presents genomic and proteomic analyses of *C. termitidis* in mid-exponential phase versus stationary phase when cultured on cellobiose versus α-cellulose. Chapter 5 presents the sequential fermentation of hexose and pentose sugars based on proteomic and genomic analyses of *C. termitidis* cells grown on cellulose and cellobiose. Also, this hypothesis was verified using a putative functional pentose phosphate pathway model and metabolic characterization of *C. termitidis* cultured on xylose and xylan, versus xylose plus cellobiose for the first time. Chapter 6 presents highlights and conclusions of the thesis in the context of the research hypotheses, and suggests future research directions.

Chapter 2: Hydrogen Production and end-product sysnthesis patterns by *C. termitidis* strain CT1112 in batch fermentation cultures with cellobiose or α-cellulose

This Chapter is based, in-part, on the following publication: "Ramachandran, U., Wrana, N., Cicek, N., Sparling, R., and Levin, D.B. 2008. Hydrogen production and end-product synthesis patterns by *Clostridium termitidis* strain CT1112 in batch fermentation cultures with cellobiose or alpha-cellulose. International Journal of Hydrogen Energy 33(23): 7."

2.1 Abstract

Hydrogen (H_2) production and end-product synthesis were characterized in a novel, mesophilic, cellulolytic, anaerobic bacterium, *Clostridium termitidis* strain CT1112, isolated from the gut of the termite, *Nasutitermes lujae*. Growth curves, pH patterns, protein content, organic acid synthesis, and H_2 production were determined. When grown on 2 g l^{-1} cellobiose and 2 g l^{-1} α-cellulose, *C. termitidis* displayed a cell generation time of 6.5 h and 18.9 h respectively. The major end-products synthesized on cellobiose included acetate, hydrogen, CO_2, lactate, formate and ethanol, where as on cellulose, the major end-products included hydrogen, acetate, CO_2 and ethanol. The concentrations of acetate were greater than ethanol, formate and lactate on both cellobiose and α-cellulose throughout the entire growth phase. Maximum yields of acetate, ethanol, hydrogen and formate on cellobiose were 5.9, 3.7, 4.6 and 4.2 mmol l^{-1} culture respectively, where as on cellulose, the yields were 7.2, 3.1, 7.7 and 2.9 mmol l^{-1} culture respectively. Hydrogen and ethanol production rates were slightly higher in *C. termitidis* cultured on cellobiose when compared to α-cellulose. Although, the generation time on α- cellulose was higher than on cellobiose, H_2 production was favored corresponding to acetate synthesis, thereby restricting the carbon flowing to ethanol.

During log phase, H_2, CO_2 and ethanol were produced at a specific rate of 4.28, 5.32, and 2.99 mmoles h^{-1} g dry $weight^{-1}$of cells on cellobiose and 2.79, 2.59, and 1.1 mmoles h^{-1} g dry $weight^{-1}$ of cells on α-cellulose respectively.

2.2 Introduction

There is great interest in the use of cellulosic biomass as a renewable source of energy (Demain et al. 2005). Microorganisms that produce cellulose and lignocellulose degrading enzymes can be used to hydrolyze this biomass and convert the bulk of the substrate into various fermentation end products, including hydrogen (H_2) (Levin et al. 2006; Lynd et al. 2002). Cellulose fibers are embedded in a complex, intertwined matrix of other structural biopolymers, primarily hemicelluloses and lignin, which account for 20 to 35% and 5 to 30% of plant dry weight respectively (Lynd et al. 2002). Because of its diverse architecture and complex nature, cellulose hydrolysis has become the rate-limiting step in the conversion of cellulose to fuels. Biochemical analyses have been conducted on the cellulase systems of aerobic and anaerobic bacteria and fungi (Levin et al. 2006). Some cellulolytic bacteria expresses a suite of cellulolytic enzymes that are assembled into a complex structure on the cell surface called a cellulosome (Demain et al. 2005; Desvaux et al. 2000; Lynd et al. 2002). The bacteria attach to cellulose particles via the cellulosome. Cellulases within the cellulosome act in a coordinated manner to efficiently hydrolyze cellulose to cellobiose and other soluble cellulodextrans (Zhang and Lynd 2005). The cellulases and cellulosome of *Clostridium thermocellum*, a thermophilic, cellulolytic, obligate anaerobe have been studied extensively (Demain et al. 2005; Lynd et al. 2002; Zhang and Lynd 2005). Also, *C. thermocellum* is known to possess some interesting fermentative properties cultured with different substrates like cellulose and hence, it has been evaluated for its ability to produce biofuels (ethanol and hydrogen) during fermentation of cellulosic substrates (Levin et al. 2006; Lynd et al. 2002).

In this chapter, we describe the fermentative properties of a novel anaerobic, mesophilic, cellulose-degrading bacterium, *Clostridium termitidis* strain CT1112 (Hethener et al. 1992). *C. termitidis* was isolated from the gut of the wood-feeding termite *Nasutitermes lujae*, found in the Mayombe tropical rainforest in Congo, Central Africa. It is a mesophilic, obligate anaerobe, that can utilize cellulose, cellobiose, glucose, fructose, and many other sugar monomers, as a sole carbon source.

In the initial characterization of the species, the fermentation end-products: H_2, carbon dioxide (CO_2), acetate, and ethanol reported on cellulose or cellobiose were stated (Hethener et al. 1992), but growth characteristics on these substrates were not described. The objectives of this study were to characterize H_2 production and end-product formation by *C. termitidis* strain CT1112 cultured in batch cultures containing cellobiose and α-cellulose. Cell growth, biomass accumulation (as measured by protein concentration), organic acid synthesis, changes in pH profiles, ethanol and H_2 yields were measured and compared with those of *C. cellulolyticum*, a mesophilic, cellulolytic, obligate anaerobe that has been characterized and studied extensively.

2.3 Materials and Methods

2.3.1 Microbial source and media

Clostridium termitidis CT1112 obtained from the American Type Culture Collection (ATCC 51846), was cultured in 1191 medium (Islam et al. 2006) with cellobiose and α-cellulose at 37°C. All chemicals and reagents for media and substrates were obtained from Fisher Scientific with the exception of Bacto™ yeast extract, which was obtained form Becton, Dickinson and Company. To maintain fresh cells, *C. termitidis* was serially subcultured by transferring 10% (v/v) inoculum into 1191 media

containing 2 g L^{-1} cellobiose and α-cellulose. This complex medium contained (per liter of milliQ water): KH_2PO_4, 1.5 g; Na_2HPO_4, 3.35 g; NH_4Cl, 0.5 g; $MgCl_2.6H_2O$, 0.18 g; yeast extract (BD 212750), 2.0 g; resazurin (0.25 mg/ml), 2.0 ml; 10x vitamin solution, 0.50 ml; 10x mineral solution, 1.00 ml. Vitamin supplement and mineral elixir solutions were prepared according to Islam et al. (2006). Sodium disulfide (Na_2S) at a concentration of 200 mM was used as a reducing agent.

2.3.2 Experimental Procedures

Balch tubes (Bellco Glass Co.) with a working volume of 27 ml were used for all tests. To maintain an anaerobic and sterile environment, tubes containing 9 ml fresh 1191 medium were air-sealed with butyl-rubber stoppers, crimped with aluminum seals, and gassed and degassed (1:4 min) four times with 100% nitrogen (N_2). 0.1 mL of sterile Na_2S (200 mM) reducing solution was added and each tube was autoclaved (Daniels et al. 1986). Sterile, anaerobic cellobiose was added to a final concentration of 2.0 g L^{-1}. Two grams per litre α-cellulose powder was added to the Balch tubes containing 1191 medium, followed by gassing and degassing with the addition of 0.1 ml of sterile Na_2S (200 mM) solution and the tubes were autoclaved. Tubes were inoculated (10% v/v) with fresh, mid-late exponential phase cultures (18-20 h on cellobiose and 60-65 h on α-cellulose) that had been serially subcultured twice prior to the initiation of the experiments. Balch tubes inoculated with *C. termitidis* were incubated for 39 h at 37°C with cellobiose and 93 h at 37°C with α-cellulose. During exponential phase, samples (1.0 mL) were taken every 2 h, based on an expected cell-doubling rate of approximately 6.5 h on cellobiose. During the late log and stationary phase, samples were taken every 5

h. The samples were taken every 8 h throughout the experiment on α-cellulose. Three independent replicate samples were taken at each time point.

2.3.3 Cell growth and pH measurements

For the cellobiose experiment, cell growth rates were determined by monitoring changes in optical densities at 600 nm (OD_{600}) using spectrophotometrical analysis (Biochrom, Novaspec II). The tubes were vortexed briefly and the values were measured within 3 seconds while cells remained in suspension. All results were blanked against an environmental control that contained only 1191 medium with same concentration of reducing agent and cellobiose. For the α-cellulose experiment, the growth rate was determined based on the protein analysis done using a modification of the Bradford method (Bradford 1976). Aliquots of cultures were dispensed into microcentrifuge tubes (Fisher Scientific) and centrifuged (IEC Micro-MB, International Equipment Company) at 10,000 *g* for 10 min to separate the pellets from the supernatants. The supernatants were transferred to new microcentrifuge tubes and stored at -20°C for further end-product analysis. The pellets were re-suspended with 0.9% (wt/vol) sodium chloride (NaCl) and centrifuged for 10 min. The supernatant was discarded and 1 mL of 0.2 M sodium hydroxide (NaOH) was added to re-suspend the pellets. Samples were incubated at 100°C in a water bath for 10 min, and after cooling down, the supernatants were collected for Bradford analysis. Optical densities at 595 nm (PowerWave XS, BIO-TEK) were measured until results stabilized, and then recorded. The pH of each tube was measured using a Sension2 pH ISE meter (Hach) outfitted with a ThermoOrion triode probe.

2.3.4 End-product analysis

The supernatants were used for analyzing soluble end-products. A high-performance liquid chromatograph equipped with an anion-exchange IonPac-AS11 analytical column (4 x 250 mm) was used to measure acetate, lactate, and formate production (Dionex Corporation, Sunnyvale, CA, USA). Ethanol and glucose concentrations in the supernatants were measured using the UV-Test kit (R-Biopharm AG, Darmstadt, Germany). The ethanol content was based on the amount of NADH produced by alcohol dehydrogenase, measured by spectrophotometry at 340 nm. The glucose concentrations were measured based on the amount of NADPH produced by hexokinase and glucose-6-phosphate dehydrogenase, measured by spectrophotometry at 340 nm. All end-product yields were determined as described in Islam et al. (2006).

2.3.5 Gas measurements

Gas (H_2 and CO_2) concentrations were measured using a gas chromatograph (SRI Instruments, Model 8610C) capable of detecting concentrations between 200-500 ppm and equipped with a Thermal Conductivity Detector (TCD). H_2 analysis was conducted using a stainless steel (3.2 mm x 1.8 m) column packed with a 13x molecular sieve while CO_2 was analyzed using a stainless steel (3.2 mm x 1.8 m) column packed with silica gel. Gases were collected and quantified according to Islam et al. (2006). Gas phase and aqueous phase concentrations (Sander 1999) were determined for both gases, including the fraction of bicarbonate found in CO_2 analysis (Darrett and Grisham 1995).

2.4 Results

2.4.1 Growth characteristics

Cell growth (based on OD_{600} values) and protein concentration of *C. termitidis* on 1191 medium containing 2 g L^{-1} cellobiose are shown in Figure 2.1 A. *C. termitidis* remained in exponential growth for 25 h based on increase in protein despite a significant drop in pH below 7.0 within the first 5 h of the experiment (see Figure 2.2). There was no initial lag observed in the cellobiose grown cultures. Maximum cell concentration reached an OD_{600} of approximately 0.6 during late exponential phase. The doubling time for *C. termitidis* during exponential phase was found to be 6.5 hours based on optical density values, with all R^2 values exceeding 0.99. The protein concentration of *C. termitidis* on 1191 medium containing 2 g L^{-1} α-cellulose is shown in Figure 2.1 B. The cells were in the exponential phase for a period of 75 h. The growth curve was assessed and the generation time during exponential phase was calculated as 18.9 hours, with all R^2 values exceeding 0.98.

A)

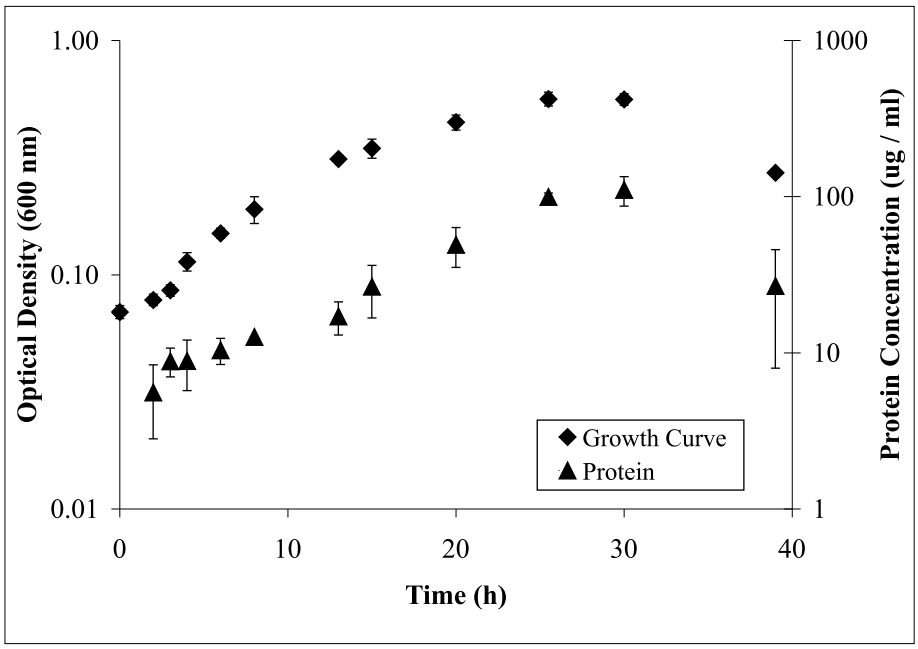
1.00
0.10
0.01
1000
100
10
1
0
10
20
30
40
Optical Density (600 nm)
Protein Concentration (ug / ml)
Time (h)
Growth Curve
Protein

B)

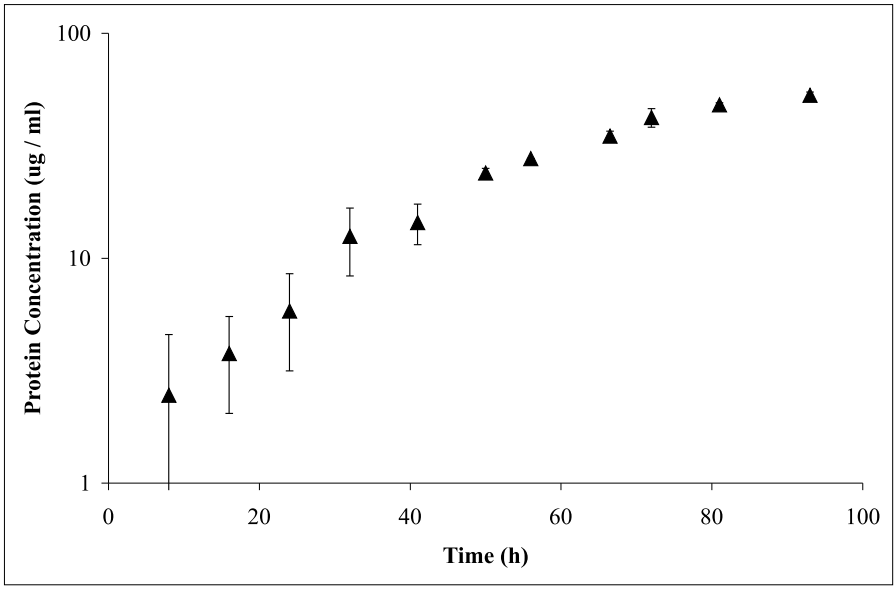
100
10
1
0
20
40
60
80
100
Protein Concentration (ug / ml)
Time (h)

Figure 2.1 Growth kinetics of *C. termitidis*. A) Optical density and protein concentration of *C. termitidis* cultured in 1191 medium containing 2 g L^{-1} cellobiose and B) protein concentration of *C. termitidis* cultured in 1191 medium containing 2 g L^{-1} α-cellulose. Data points represent the means of 3 independent replicates; bars above and below the means represent the standard deviation (SD). OD could not be measured in α-cellulose experiments due to the insoluble nature of the substrate.

2.4.2 Gas production

Plots of H_2 and CO_2 production by *C. termitidis* cultured on 2 g L^{-1} cellobiose and α- cellulose, and corresponding changes in pH with respect to cultivation time, are shown in Figures 2.2 A and 2.2 B. *C. termitidis* rapidly produced H_2 within the first 10 h of the experiment on cellobiose, where as on α-cellulose, H_2 production was lower within the first 10 h relative to cellobiose. This is due to the fact that *C. termitidis* has a faster doubling time when cultured on cellobiose when compared to α-cellulose. Significantly reduced rate of H_2 production on cellobiose, however, coincided with a drop in pH below 7.0. A second shift in H_2 production occurred when the pH fell below 6.2. The rate of H_2 production on cellobiose and α-cellulose during exponential phase was 0.26 and 0.14 mmoles h^{-1} L culture $^{-1}$ respectively. The maximum volumetric production rates were calculated based on the sum of the average individual rates obtained from four consecutive time points obtained during the mid and late exponential phase of growth. The rate of CO_2 production was lower than H_2, but the overall pattern of CO_2 production was similar to that of H_2 production. H_2 and CO_2 were synthesized even after the cells entered stationary phase, but the rates of synthesis were much lower. The rate of CO_2 production on cellobiose during exponential phase was higher (0.33 mmoles h^{-1} L culture $^{-1}$) than on α-cellulose (0.13 mmoles h^{-1} L $culture^{-1}$).

The maximum concentrations of H_2 and CO_2 during exponential phase were calculated based on the highest value of the average of the concentrations of individual triplicates measured at each time point. H_2 and CO_2 synthesis corresponded to cell growth. The growth pattern was characterized by a high production rates in early exponential phase that gradually decreased as it entered late exponential phase. The final

concentrations of total H_2 and CO_2 produced on cellobiose were 4.6 and 5.6 mmoles L culture^{-1} respectively, whereas, on α-cellulose, the final concentrations were 7.7 and 6.9 mmoles L^{-1} culture^{-1} respectively (Table 2.1).

A)

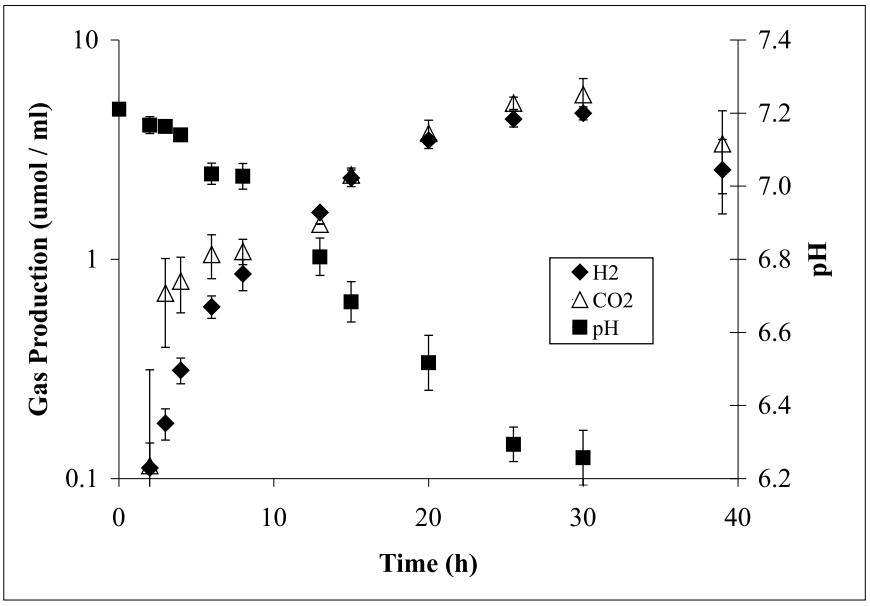
10
1
0.1
Gas Production (umol / ml)
7.4
7.2
7.0
6.8
6.6
6.4
6.2
pH
H2
CO2
pH
0
10
20
30
40
Time (h)

B)

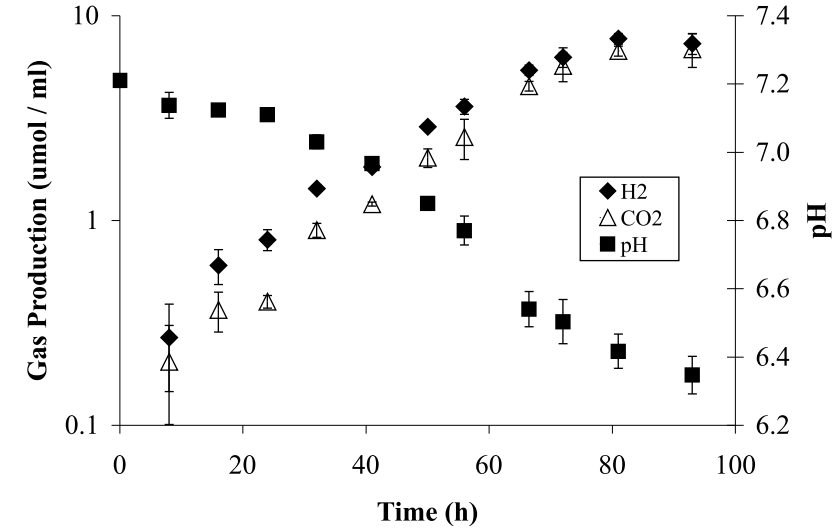
10
1
0.1
Gas Production (umol / ml)
7.4
7.2
7.0
6.8
6.6
6.4
6.2
pH
H2
CO2
pH
0
20
40
60
80
100
Time (h)

Figure 2.2 H_2 and CO_2 production and corresponding changes in pH in *C. termitidis* cultures. *C. termitidis* was cultured in 1191 medium containing 2 g L^{-1} A) cellobiose and B) α-cellulose. Data points represent the means of 3 independent replicates. Bars above and below the means represent SD.

2.4.3 Production of soluble end-products

The major end-products synthesized by *C. termitidis* during fermentation of cellobiose and α-cellulose were acetate, formate, ethanol and lactate. Figure 2.3 A and 2.3 B plots the concentrations of end-product synthesized versus time. Acetate production was greater than formate, ethanol and lactate throughout the entire growth on both substrates. The rates and concentrations of acetate, formate, ethanol and lactate production from cellobiose were significantly higher during the logarithmic phase of growth and then plateaued after 25-30 h when the cells reached the stationary phase. On α- cellulose, the rates and concentrations were consistently higher until 70-75 h of log phase and then plateaued after 75 h as soon as the cells reached the stationary phase.

Lactate production followed a different pattern, when compared to other end-products synthesis. During the initial exponential growth, there was a significant lag in lactate production, which subsequently significantly peaked up after 8-10 h on cellobiose and after 40 h on α- cellulose. This metabolic shift in organic acids and ethanol production coincided with a drop in pH below 7.0, correspondingly affecting the rates of H_2 production on both the substrates. Acetate, formate and ethanol concentrations plateaued when the cells entered the stationary phase on both the substrates, the pH observed at this point was 6.5. As the pH neared 6.2, organic acid and ethanol production declined substantially. Organic acid synthesis appeared to follow the same curve as cell growth during the exponential growth phase, and began to plateau as the cells entered stationary phase at 25-30 h on cellobiose and 70-75 h on α-cellulose. Lactate was produced throughout the latter stages of the experiment, its synthesis remained constant

during the exponential phase of growth but began to decline after the cells reached stationary phase.

Although, the maximum concentrations of ethanol were similar on both the substrates, the volumetric rate of ethanol production on cellobiose (0.18 mmoles h^{-1} L^{-1} culture) was much higher than the rates obtained on α- cellulose (0.06 mmoles h^{-1} L^{-1} culture), as expected from the differences in growth rate. The maximum concentrations of acetate, formate, lactate and ethanol from cellobiose were 5.9, 4.2, 2.0 and 3.7 mmoles L^{-1} culture, respectively, whereas the maximum concentrations from α-cellulose were 7.2, 2.9, 0.5 and 3.1 mmoles L^{-1} culture, respectively. Production of organic acids increased at similar rate despite higher initial concentrations of acetate. Fermentation continued after 25-30 h on cellobiose and 70-75 h on α-cellulose because both acetate and formate synthesis continued at a constant rate until the stationary phase. Ethanol concentrations increased during log-phase, but was synthesized at lower concentrations than acetate and formate, and declined during stationary phase on both the substrates.

A)

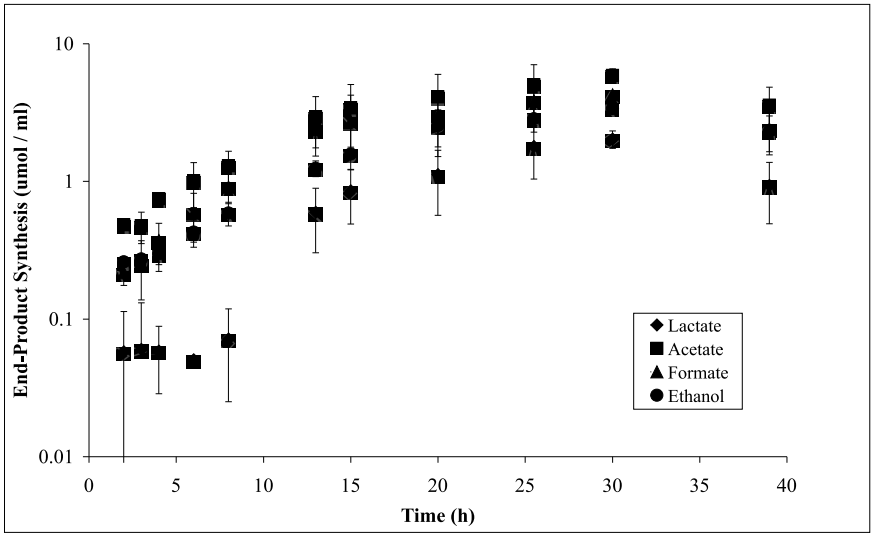
End-Product Synthesis (umol / ml)
10
1
0.1
0.01
0
5
10
15
20
25
30
35
40
Time (h)
Lactate
Acetate
Formate
Ethanol

B)

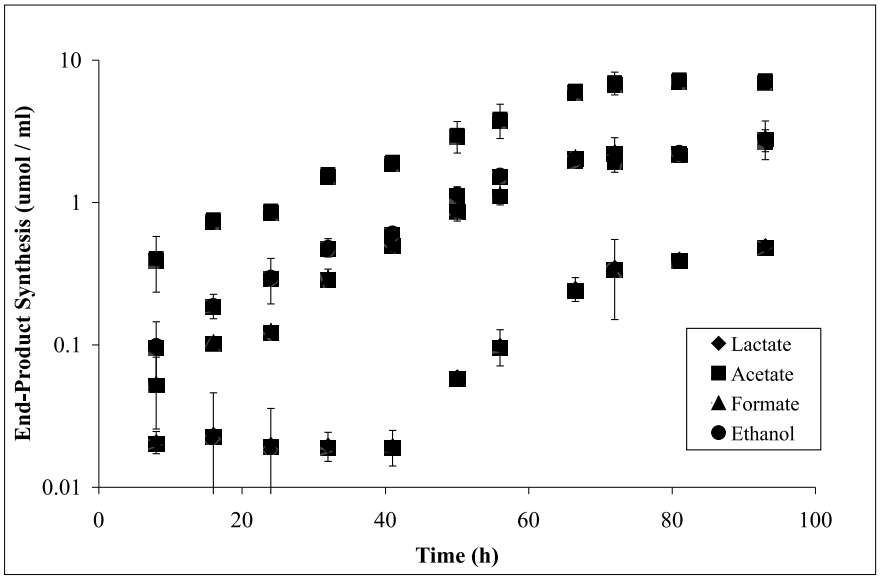
End-Product Synthesis (umol / ml)
10
1
0.1
0.01
0
20
40
60
80
100
Time (h)
Lactate
Acetate
Formate
Ethanol

Figure 2.3 End-product synthesis patterns in cultures of *C. termitidis*. Lactate, acetate, formate, and ethanol synthesis by *C.termitidis* cultured in 1191 medium containing 2 g L^{-1} A) cellobiose and B) α-cellulose. Data points represent the means of 3 independent replicates. Bars above and below the means represent SD.

The maximum specific production rates were calculated based on the amount of end-products produced per hour between four consecutive time points and corresponding cell dry weight during mid to late exponential phase. The maximum specific production rates of H_2, CO_2 and ethanol production obtained during fermentation of cellobiose by *C. termitidis* were 4.28, 5.32, and 2.99 mmoles h^{-1} g^{-1} dry weight of cells, whereas, on α-cellulose, the rates were 2.79, 2.59, and 1.1 mmoles h^{-1} g^{-1} dry weight of cells, respectively. The specific production rates of *C. cellulolyticum* on cellobiose were 1.59, 0.52, 1.0 mmoles h^{-1} g^{-1} dry weight of cells and on α-cellulose (3.9 g L^{-1}) were 1.73, 1.23, 1.43 mmoles h^{-1} g^{-1} dry weight of cells respectively. The specific production rates of H_2, CO_2 and ethanol production (Table 2.3) in *C. termitidis* is higher than *C. cellulolyticum* on both the susbstrates (Desvaux et al. 2000; Guedon et al. 1999).

The maximum volumetric production rates of H_2, CO_2 and ethanol production obtained during fermentation of cellobiose by *C. termitidis* were 0.26, 0.33 and 0.18 mmoles h^{-1} L^{-1} culture, whereas, on α-cellulose, the rates were 0.14, 0.13 and 0.06 mmoles h^{-1} L^{-1} culture, respectively. End-product volumetric production and rates are summarized in Tables 2.1 and 2.2. Carbon balance during anaerobic fermentation of cellobiose and α-cellulose was calculated based on the concentrations of the end-products obtained, cell mass and substrates. The residual glucose levels measured during the initial and late exponential phase were minimal on both the substrates, indicating the complete utilization of the substrate (2 g L^{-1}). The overall oxidation/reduction (O/R) ratios during the exponential phase with time points showing maximum yields were 1.29 and 1.36 on cellobiose and α-cellulose, respectively. The overall carbon recovery of cellobiose fermentation by *C. termiditis* during the entire growth phase was 86.8%.

Table 2.1 Maximum concentration of biofuels and end-products by *C. termitidis*.

Substrate	Generation Time	H_2	CO_2	Acetate	Lactate	Formate	Ethanol
	hours	*mmoles / litre of culture*					
Cellobiose	6.9	4.6	5.6	5.9	2.0	4.2	3.7
α-Cellulose	18.9	7.7	6.9	7.2	0.5	2.9	3.1

Table 2.2 Maximum volumetric production rates of *C. termitidis* on cellobiose and a-cellulose.

Substrate	H_2	CO_2	Ethanol
	mmoles / litre of culture / hour		
Cellobiose	0.26	0.33	0.18
α-Cellulose	0.14	0.13	0.06

Table 2.3 Comparison of maximum specific production rates between different strains of *Clostridia*.

Microorganisms	Substrate	H_2	CO_2	Ethanol
		mmoles / gram dry weight of cells / hour		
C. termitidis	Cellobiose	4.28	5.32	2.99
	α-Cellulose	2.79	2.59	1.1
C. cellulolyticum	Cellobiose[*a]	1.59	0.52	1.0
	α-Cellulose[*b]	1.73	1.23	1.43

[*a] maximum rate calculated based on time points during log phase with 17.54 mM cellobiose (Guedon et al. 1999);

[*b] maximum rate calculated based on time points during log phase with 3.9 g L^{-1} α-cellulose (Desvaux et al. 2005)

2.5 Discussion

C. termitidis is a novel mesophilic bacterium that can produce H_2 at a rate that is comparable to those of the mesophilc cellulolytic bacterium *Clostridium cellulolyticum* (Desvaux et al. 2000). *C. cellulolyticum* had a higher doubling time of 7 h (Giallo et al. 1983) and 24 h (Giallo et al. 1985) on cellobiose and α-cellulose respectively, when compared to *C. termiditis* (Table 2.1).

C. cellulolyticum produced similar end-products as *C. termiditis* during both cellulose and cellobiose fermentations, except that formate synthesis by *C. cellulolyticum* was not observed, and extracellular pyruvate synthesis was observed (Desvaux et al. 2000; Guedon et al. 1999). The synthesis of lactate and ethanol compete against H_2 synthesis (Levin et al. 2006). Lactate production was significantly higher in *C. cellulolyticum* (Desvaux et al. 2000) and ethanol production considerably lower than *C. termiditis* on both the substrates. Growth on cellulose resulted in the linear increase in the levels of the end-products formed during the anaerobic fermentation in *C. cellulolyticum*. Also, a first metabolic shift occurred below pH 7.0 when lactate started being produced forcing the carbon flow towards acetate and ethanol, followed by a second metabolic shift from ethanol to acetate formation (Desvaux et al. 2000). In *C. termiditis*, a second metabolic shift was observed with the drop in pH below 6.2 with ethanol to acetate formation and a downward trend of H_2 to CO_2 ratio, as the cells entered into stationary phase. The H_2-synthesis by *C. termiditis*, however, appears to be more sensitive to pH change than *C. thermocellum*, a thermophilic bacterium that is extensively studied (Islam et al. 2006; Sparling et al. 2006). *C. termitidis* sensitivity to pH seems to trigger a shift to lactate production at a much higher pH than *C. thermocellum*.

On cellobiose, *C. cellulolyticum* produced extracellular pyruvate, acetate and ethanol within 5-10 h after inoculation, followed by lactate synthesis that corresponded with the maximum extracellular pyruvate production. Moreover, increase in the specific rate of lactate synthesis coincided with reduced acetate, pyruvate and ethanol levels observed (Guedon et al. 1999). Pyruvate synthesis was not observed during the anaerobic fermentation of cellobiose by *C. termiditis*, instead formate was produced along with acetate, ethanol and lactate within 5-10 h of growth and further end-product synthesis were similar to that of cellulose fermentation.

During initial exponential phase, *C. termitidis* synthesized H_2 and acetate at high rates on both the substrates. The concentration of H_2 synthesized decreased as the pH dropped below 7.0, and then declined again as the pH dropped below 6.2. The concentration of acetate synthesis followed a similar trend and declined as the pH first dropped below 7.0 and then again as the pH dropped below 6.2. These results suggest that metabolic flux responses in *C. termitidis* are influenced by changes in pH. *C. termiditis* produces more CO_2 than H_2 on cellobiose, which corresponds to the maximum production of ethanol during the late log phase. On α-cellulose, the H_2 production is greater than CO_2, which corresponds to the increased acetate and reduced ethanol production.

C. termitidis prefers producing H_2 on α-cellulose irrespective of the substrate complexity (longer doubling time than on cellobiose) without shifting the carbon flow towards ethanol synthesis, whereas on cellobiose, although the specific rate of H_2 production is higher during log phase, the metabolism is shifted towards ethanol synthesis (Table 2.3). Whereas, on α-cellulose, *C. cellulolyticum* has a higher doubling

time of 24 h (Giallo et al. 1985) and produces more ethanol (Desvaux et al. 2000), when compared to *C. termitidis* and the ratio of H_2 and ethanol is similar (Table 2.3). This characteristic feature in *C. termitidis* is significant and could be used for further investigation of continous culture experiments of *C. termitidis* on α-cellulose to stabilize the production of H_2 by controlling metabolism towards acetate rather than ethanol synthesis. The production of lactate already in mid-log phase of growth decreases the amounts of carbon available for synthesis of other end-products. The extent to which pH change and lactate synthesis affect H_2-synthesis and whether these negative effects can be mitigated to increase H_2-production by *C. termitidis* remain to be elucidated.

2.6 Conclusions

H_2 and CO_2 synthesis and soluble end-product production (acetate, formate, lactate, and ethanol) in *C. termitidis* strain CT1112, cultured in 1191 medium containing 2 g l^{-1} cellobiose and α-cellulose was measured using batch experiments. Cell growth, pH patterns, organic acid and ethanol synthesis, and H_2 and CO_2 production were determined. *C. termitidis* had a doubling rate of 6.5 h on cellobiose compared to 18.9 h on α-cellulose. In *C. termitidis*, H_2 synthesis was greatly reduced as pH dropped below 6.2. Acetate, formate and ethanol concentrations also decreased as the pH dropped below 6.2. Reduced acetate and H_2 synthesis coincided with increased CO_2 and ethanol production on cellobiose. Increased H_2 and acetate synthesis coincided with decreased CO_2 and ethanol production on α-cellulose. Although *C. termitidis* grows more slowly on α-cellulose when compared to cellobiose, it prefers synthesizing H_2 three times more than ethanol by following acetate synthesis, which is characteristically distinct from *C. cellulolyticum*, that had higher generation time on both the substrates, and produced less

H_2 and more ethanol during the cellulose metabolism. More work has to be done to elucidate the cellulase activities of *C. termitidis*, effect of substrate loading on hydrogen production and determine the presence and structural characteristics of a cellulosome.

Chapter 3: Cellulose fermentation by *Clostridium termitidis* in pH-controlled bioreactors

This Chapter is based, in-part, on the following publication: "Ramachandran, U., Blunt, W., Cicek, N., Sparling, R., and Levin, D.B. 2013. Cellulose fermentation by *C. termitidis* in pH-controlled bioreactors. Bioresource Technology (submitted)".

3.1 Abstract

Growth and end-product synthesis patterns of *Clostridium termitidi*s, an anaerobic, cellulolytic, mesophilic bacterium, in controlled bioreactor conditions were reported in this chapter for the first time. pH-controlled batch fermentation reactions were conducted at 37°C in 7 L bioreactors (with a 3 L working volume) containing 1191 medium with 2 g L^{-1} cellobiose or 2 g L^{-1} α-cellulose as carbon sources. The reactors were sparged continuously with nitrogen at 3 mL min^{-1}. During incubation, the liquid samples were collected every 4 hours from the cellobiose fermentations and every 24 h from the α-cellulose fermentations. The major end-products of *C. termitidis* grown on 2 g L^{-1} cellobiose and α-cellulose were H_2, CO_2, acetate, formate, lactate, and ethanol. The maximum volumetric production of H_2 and ethanol obtained during α-cellulose fermentation were 16.54 ± 0.62 mmol L^{-1} and 2.34 ± 0.49 mmol L^{-1}, respectively, where as, on cellobiose, the maximum volumetric yields were 11.98 ± 0.06 and 3.37 ± 0.48, respectively. The specific production rates of H_2 and ethanol during exponential phase on α-cellulose were 1.50 ± 0.02 and 0.24 ± 0.14 mmol product g^{-1} protein h^{-1}, respectively. During exponential phase, cellobiose cultures exhibited specific production rates of 3.30 ± 0.28 and 1.38 ± 0.38 mmol product g^{-1} protein h^{-1} for H_2 and ethanol, respectively. H_2 and ethanol production concomitant with synthesis of acetate and CO_2, and a trace

amount of lactate was observed as the cells entered late exponential and stationary phases. The substrate-specific yields of H_2 and ethanol on cellobiose were calculated as 1.03 ± 0.01 and 0.29 ± 0.04 mol product per mol hexose equivalent added, where as on α-cellulose, the yields were 1.34 ± 0.05 and 0.22 ± 0.04 mol product per mol hexose equivalent added, respectively. The maximum volumetric yields of H_2 were significantly higher in pH-controlled batch reactors compared with previous reports of non-pH controlled batch reactions conducted in Balch tubes.

3.2 Introduction

Although the fermentative properties of *C. termitidis* strain CT1112 have been studied at the bench scale (Hethener et al. 1992; Ramachandran et al. 2008), there are no reports of larger-scale production for this species. In this chapter, we present the results of scaled-up fermentation reactions using *C. termitidis* cultured in 1191 medium containing cellobiose versus α-cellulose. Growth characteristics, cell mass accumulation, and fermentation end-product synthesis patterns, along with their yields and rates, were determined. The main objective of this study was to compare how reactor environments and batch bottles compare and evaluate the potential of *C. termitidis* to be industrially relevant for biofuels production. This chapter provides an initial characterization of *C. termitidis*, establishing benchmarks for subsequent optimization.

3.3 Materials and Methods

3.3.1 Microorganism, substrates and media preparation

Clostridium termitidis CT1112 was obtained from the American Type Culture Collection (ATCC 51846). All the chemicals, reagents, substrates, stock cultures, anaerobic cellobiose stock solution, gasing/degassing and inoculation procedures are same as that described in the materials and methods section in chapter 2 (section 2.3.1).

3.3.2 Bioreactor fermentation experiments

The stock cultures of *C. termitidis* were obtained after two passages in 500 mL Corning bottles containing specific substrates at 37°C as described previously (chapter 2). A 7 L Applikon Biotechnology bioreactor (Foster city, CA), with a working volume of 3 L, was used for the scale-up fermentation experiments. The 1191 medium containing 2 g L^{-1} α-cellulose was added in to the bioreactor and autoclaved. In the case of

cellobiose experiments, anaerobic and sterile cellobiose (2 g L^{-1}) was added 1191 medium after autoclaving. Anaerobiosis (removal of O_2) was achieved through overnight purging of the autoclaved bioreactor containing 1191 medium with 100% nitrogen (Welder's Supplies, Winnipeg, MB) continuously at a flow rate of 3 mL min^{-1} before inoculation. The carrier gas flow was regulated using a two-stage regulator (Winnipeg Fluid Systems, Winnipeg, MB) and was passed through a 0.2 μm filter prior to being introduced into the reactor. After setting up the bioreactor in the fume-hood and overnight sparging, 20 mL of Na_2S (200 mM) was added to reduce the medium to an Eh suitable for growth. Batch fermentations were carried out at 37°C and the pH was controlled automatically at 7.2 by the addition of 1 N potassium hydroxide (KOH). The culture was mixed during the addition of KOH at a speed of 50 rpm. Two independent biological replicates of each fermentation with the different carbon sources were conducted, each with a runtime of 55 hours (h) for the culture containing 2 g L^{-1} cellobiose and 214 h for the culture containing 2 g L^{-1} α-cellulose. Liquid samples were collected every 4 h for the cellobiose experiments and every 24 h for the α-cellulose experiments.

3.3.3 Growth characteristics and pH

For both cellobiose and α-cellulose experiments, the growth rate was measured based on total protein analyses using Bradford method (Bradford 1976) as described in chapter 2. For α-cellulose samples, the residual cellulose pellets were washed with 0.9% (w/v) NaCl and 0.2 M NaOH, then filtered using Whatman No. 1 filter paper, and finally dried overnight in a hot-air oven at 100°C. After, drying, the cellulose pellet was weighed and further used for calculating carbon balance and carbon recovery. For the entire

fermentation experiments including all the biological replicates, pH was maintained at 7.2 continuously so that the carbonate buffer system could be adequately accounted via the Henderson-Hasselbach equation (Darrett and Grisham 1995; Sander 1999) (chapter 2).

3.3.4 End-product analysis

Soluble end-products were analyzed using the supernatants obtained from the different time points during the fermentation process using HPLC analysis as described earlier (chapter 2).

3.3.5 Gas measurements

Concentrations of gaseous end-products (H_2 and CO_2) were measured using gas chromatography with the sampling methods and procedures described previously (chapter 2). Vented H_2 and CO_2 in the off-gas from the open system were accounted for by means of a gas phase mass balance, based off the sparging rate, and assuming a uniformly mixed headspace. Henry's Law was used to relate the concentrations of H_2 and CO_2 remaining in the solution with respect to the headspace gas composition (Sander 1999). CO_2 is associated with various dissolved carbonate species, including carbonic acid, bicarbonate, and carbonate. The bicarbonate fraction was calculated based on the Hendersen-Hasslebach equation (Darrett and Grisham 1995; Sander 1999) (chapter 2). A single technical replicate was used for the GC samples across the biological replicates, whereas triplicate samples were used for HPLC analysis.

3.3.6 Carbon recovery and mass balances

Carbon recovery index was used to verify the obtained results by accounting all carbon consumed in the substrate present and being accounted for in the end-products

synthesized, including biomass. In addition, the O/R index was calculated to balance the oxidized end-products over the reduced end-products, as in a typical biochemical reaction, reducing equivalents have to be regenerated (Gottschalk 1986). Further calculation of C1/C2 ratio depicts the mass balance regarding the acetyl-CoA branch-point.

3.4 Results

3.4.1 Growth characteristics

On 2 g L^{-1} cellobiose, *C. termitidis* entered an exponential (log-) growth phase with a 5-6 h lag time (post-inoculation of the reactor) and the log-phase growth continued up to 18-20 h, after which the cells entered stationary phase (Figure 3.1 A). The maximum protein concentration reached in the cellobiose cultures was 77 ± 3 μg mL^{-1}. This value was calculated for two biological replicates as the arithmetic average between time points 28 h to 40 h. The standard deviation represents the deviation from the mean of the two biological replicates for this set of time points. Compared with growth on cellobiose, a 50 h lag time was observed in the *C. termitidis* cultures containing 2 g L^{-1} α-cellulose. The increase in cell mass is shown in Figure 3.1 B. After inoculation, biosynthesis continued in a consistent manner and the cells reached stationary after 160 h. The average maximum protein content, taken as the average value between time points 160 h to 214 h, was found to be concentration of 97 ± 29 μg mL^{-1} was observed. Standard deviation represents the deviations between two biological replicates.

3.4.2 Gas production

Hydrogen and CO_2 were the only gas phase end-products synthesized by *C. termitidis* with both cellobiose and α-cellulose as carbon sources. This is consistent with

previous studies of *C. termitidis* on similar substrates (chapter 2), and also consistent with *C. cellulolyticum* (Desvaux et al. 2000; Guedon et al. 1999, 2000). Gas production on 2 g L^{-1} cellobiose correlated with the growth pattern. Hydrogen production was observed as soon as the onset of exponential phase after 6 h, and there was no significant increase in the volumetric production after 25 h (Figure 3.2 A). From Table 3.2, it can be seen that at stationary phase, the maximum concentration of H_2 from the two biological replicates of *C. termitidis* grown on 2 g L^{-1} cellobiose was 11.98 ± 0.06 mmol L^{-1} culture. The corresponding total CO_2 production was 8.25 ± 1.0 mmol L^{-1} culture. For the cultures grown on 2 g L^{-1} α-cellulose, the rate of gas production was much slower (Figure 3.2 B), but the maximum concentration of both H_2 and CO_2 produced was higher when compared to 2 g L^{-1} cellobiose (Table 3.1). The maximum concentrations of H_2 and CO_2 from *C. termitidis* grown on 2 g L^{-1} α-cellulose were 16.54 ± 0.62 and 9.1± 0.25 mmol L^{-1} culture, respectively.

A)

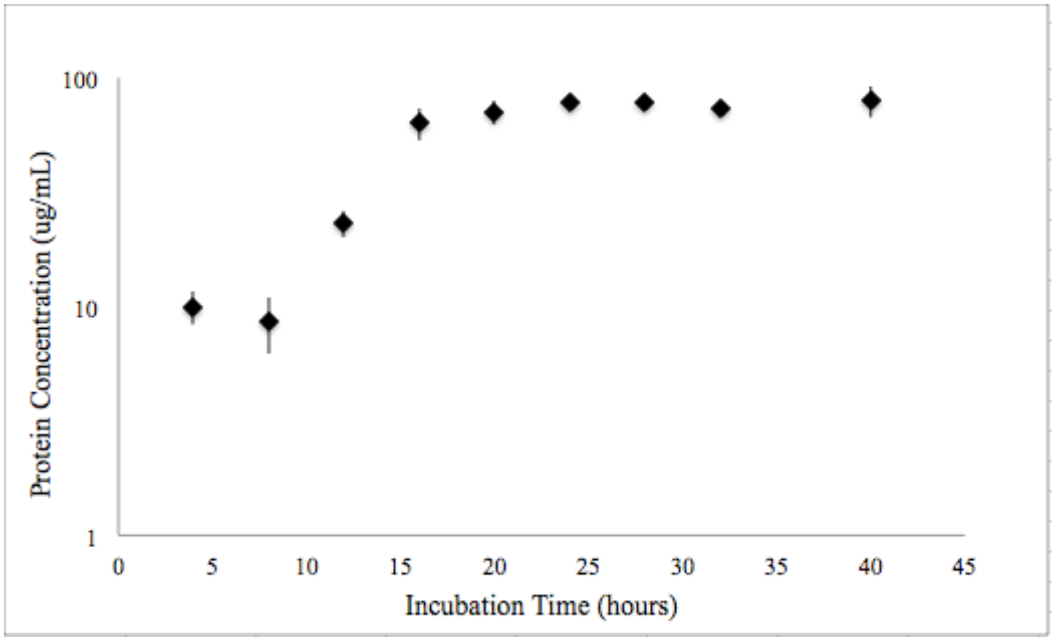
100
10
1
Protein Concentration (ug/mL)
0
5
10
15
20
25
30
35
40
45
Incubation Time (hours)

B)

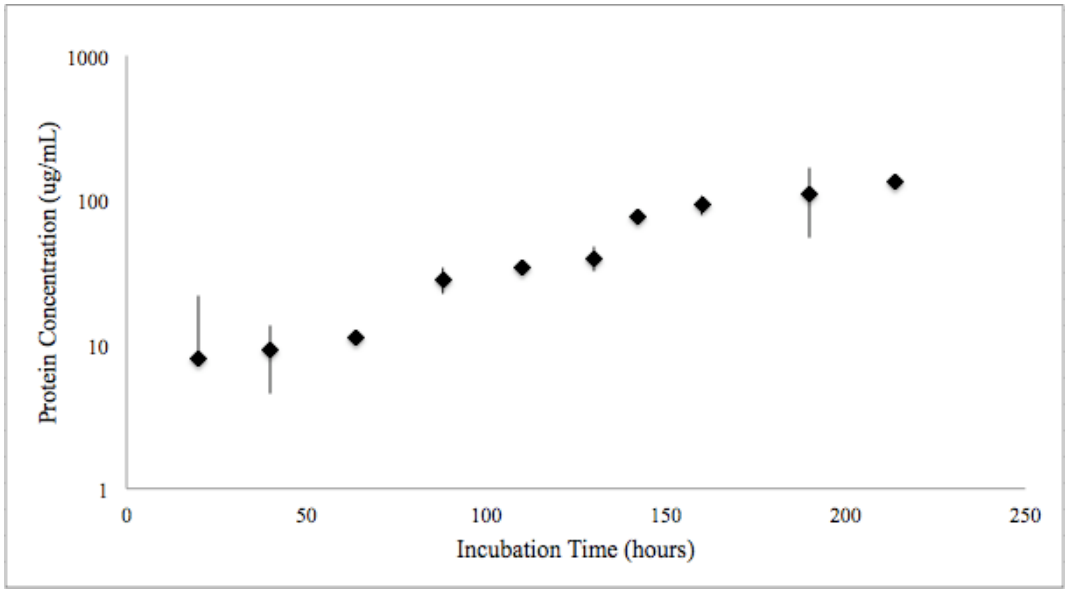
1000
100
10
1
Protein Concentration (ug/mL)
0
50
100
150
200
250
Incubation Time (hours)

Figure 3.1 Growth kinetics of *C. termitidis* cultured in an open, pH controlled bioreactor. A) Protein concentration from growth of *C. termitidis* cultured in a 7 L reactor (3 L working volume) containing 1191 media and 2 g L^{-1} celloboise. B) Protein concentration from growth of *C. termitidis* cultured in a 7 L reactor (3 L working volume) containing 1191 media containing and 2 g L^{-1} α-cellulose.

A)

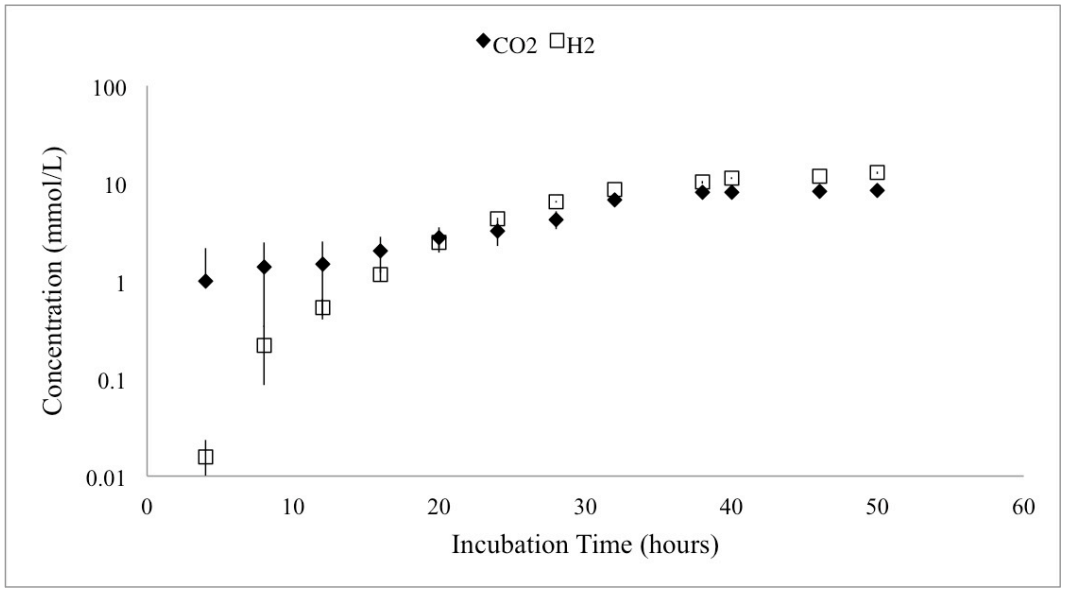
CO2
H2
100
10
1
0.1
0.01
Concentration (mmol/L)
0
10
20
30
40
50
60
Incubation Time (hours)

B)

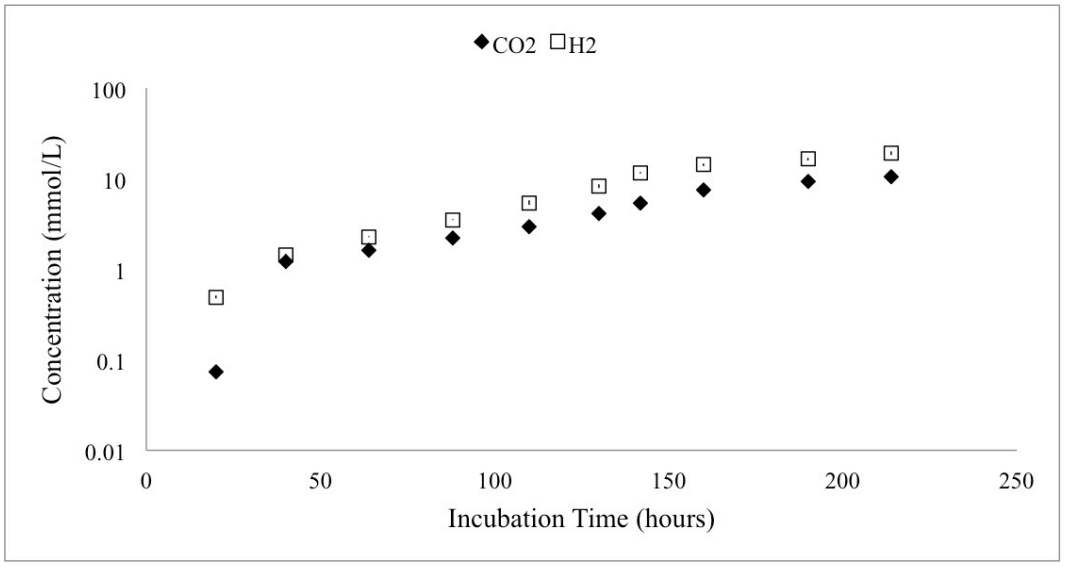
CO2
H2
100
10
1
0.1
0.01
Concentration (mmol/L)
0
50
100
150
200
250
Incubation Time (hours)

Figure 3.2 Gas-phase end-product synthesis by *C. termitidis.* A) Production of H_2 and CO_2 by *C. termitidis* cultured in a 7 L reactor (3 L working volume) containing 1191 media containing and 2 g L^{-1} celloboise. B) Production of H_2 and CO_2 by *C. termitidis* cultured in a 7 L reactor (3 L working volume) containing 1191 media and 2 g L^{-1} α-cellulose.

Table 3.1 Substrate-specific yields and volumetric production of major end-products synthesized by *C. termitidis* in a in an open, pH-controlled bioreactor. These values were calculated from the maximum concentration observed between time points 160-214 h for α-cellulose and 28-40 h for cellobiose, respectively.

		Yield and Volumetric Production of Product					
		Lactate	Formate	Acetate	Ethanol	H_2	CO_2
Cellobiose	Yield[a]	0.43 ± 0.07	0.57 ± 0.02	1.13 ± 0.13	0.29 ± 0.04	1.03 ± 0.01	0.71 ± 0.09
	Production[b]	4.98 ± 0.84	6.66 ± 0.25	13.17 ±1.53	3.37 ± 0.48	11.98 ± 0.06	8.25 ± 1.0
α-cellulose	Yield[a]	0.05 ± 0.01	0.18 ± 0.12	0.58 ± 0.04	0.22 ± 0.04	1.34 ± 0.05	0.74 ± 0.02
	Production[b]	0.66 ± 0.18	2.24 ± 1.46	7.09 ± 0.50	2.34 ± 0.49	16.54 ± 0.62	9.10± 0.25

[a] units are in mol product per mol hexose equivalent added

[b] units are in mmol L^{-1} culture

Table 3.2 Maximal volumetric production rates and specific production rates of the major end-products for *C. termitidis* grown with 2 g L^{-1} α-cellulose and 2 g L^{-1} cellobiose in an open, pH-controlled bioreactor. All rates for α-cellulose were taken between time points 64-160 h of growth and all rates for cellobiose were taken between time points 8-24 h of growth.

		Production Rates					
Substrate	Rate	Lactate	Formate	Acetate	Ethanol	H_2	CO_2
Cellobiose	Volumetric[a]	0.22 ± 0.01	0.33 ± 0.04	0.54 ± 0.06	0.13 ± 0.07	0.22 ± 0.01	0.15 ± 0.04
	Specific[b]	3.90 ± 1.04	3.54 ± 0.98	6.36 ± 0.94	1.38 ± 0.38	3.30 ± 0.28	2.10 ± 0.26
α-cellulose	Volumetric[a]	0.00 ± 0.00	0.03± 0.00	0.07 ± 0.02	0.02 ± 0.01	0.12 ± 0.03	0.07 ± 0.01
	Specific[b]	0.06 ± 0.00	0.32 ± 0.10	1.08 ± 0.32	0.24± 0.14	1.50 ± 0.02	0.84 ± 0.04

[a] volumetric rates reported in mmol product L^{-1} culture h^{-1}

[b] specific production rates reported in mmol product g^{-1} protein h^{-1}

3.4.3 Production of soluble end-products

The major soluble end-products for *C. termitidis* cultures grown on 2 g L^{-1} cellobiose were acetate, formate, and ethanol, and lactate, in order of decreasing carbon flux. Acetate production followed the cell growth pattern. Acetate was detected in the cultures by 5-6 h post-inoculation (pi) and concentrations of acetate leveled-off (ceased to increase) by 25 h (Figure 3.3 A). Acetate reached a maximum concentration of 13.2 ± 1.5 mmol L^{-1} culture (Table 3.1). Formate and lactate production also reflected the growth pattern, and both were detected in the culture by 5-6 h pi and concentrations ceased to increase by 25 h. However, the maximum concentration of formate and lactate were lower than acetate, reaching a maximum concentration of 6.66 ± 0.25 and 4.98 ± 0.84 mmol L^{-1} culture, respectively (Table 3.1). The maximum concentration of ethanol was 3.37 ± 0.48 mmol L^{-1} culture and the substrate-specific yield obtained was 0.29 ± 0.04 mol product per mol hexose equivalent added (Table 3.1). The specific production rate was 1.38 ± 0.38 mmol product g^{-1} protein h^{-1} (Table 3.2).

The major soluble end-products for *C. termitidis* cultures grown on 2 g L^{-1} α-cellulose similar to those observed on cellobiose, except that more acetate was produced, at the expense of lactate and ethanol, when compared with cellobiose cultures. Acetate, formate, and ethanol followed the trend of the growth curve. Their production rates were most rapid after the onset of exponential phase growth (60 h), and continued until up to 160 h (Figure 3.3 B). Similar to the cellobiose cultures, acetate was the major aqueous phase end-product, with a maximum concentration of 7.09 ± 0.5 mmol L^{-1} culture. The maximum concentration of formate was 2.24 ± 1.46 mmol L^{-1} culture (Table 3.1). Lower

amounts of ethanol, 2.34 ± 0.49 mmol L^{-1}, were detected in the α-cellulose cultures compared with the cellobiose cultures (Table 3.1).

Contrary to lactate production on cellobiose, which occurred during exponential phase, lactate production was minimal on α-cellulose, and was not observed until the cells entered stationary phase after 160 h (Figure 3.3 B) The maximum concentration of lactate was 0.66± 0.18 mmol L^{-1} culture (Table 3.1). The carbon recovery, OR index, and C1/C2 index are presented in Table 3.3. These values are close to the theoretical value of 1, indicating that all major end-products have been accounted for.

A)

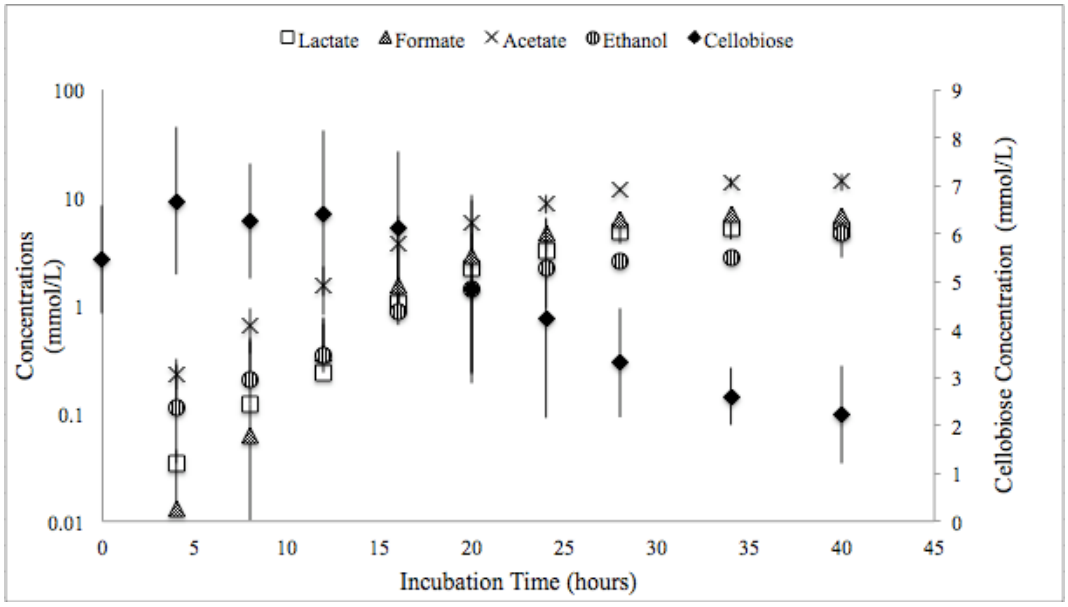
Lactate
Formate
Acetate
Ethanol
Cellobiose
Concentrations (mmol/L)
Cellobiose Concentration (mmol/L)
Incubation Time (hours)
100
10
1
0.1
0.01
0
5
10
15
20
25
30
35
40
45
9
8
7
6
5
4
3
2
1
0

B)

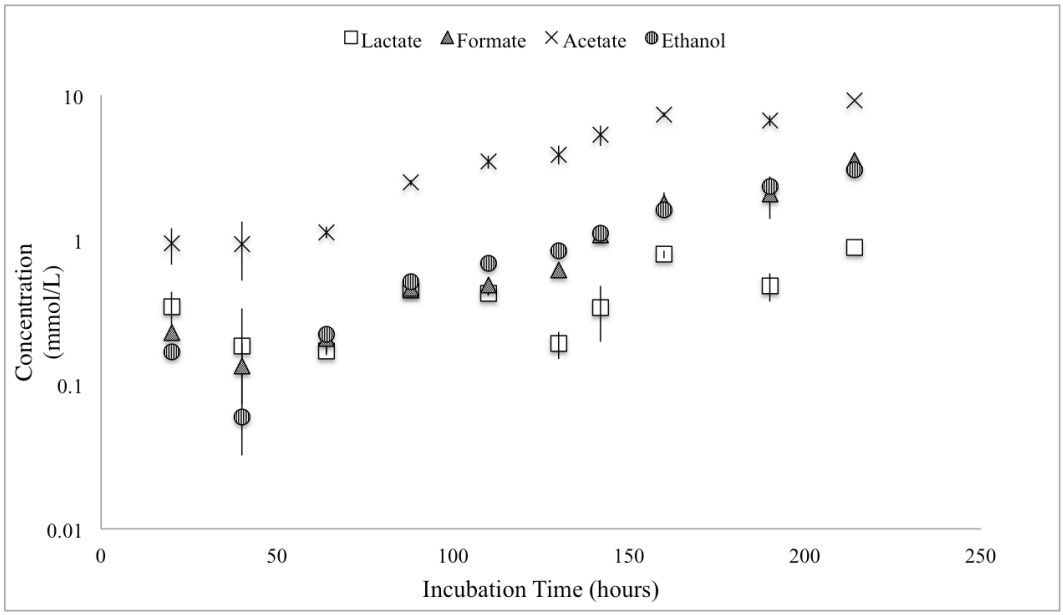
Lactate
Formate
Acetate
Ethanol
Concentration (mmol/L)
Incubation Time (hours)
10
1
0.1
0.01
0
50
100
150
200
250

Figure 3.3 Liquid-phase end-product synthesis by *C. termitidis.* A) Production of soluble end- products by *C. termitidis* cultured in a 7 L reactor (3 L working volume) containing 1191 media and 2 g L^{-1} celloboise. B) Production of soluble end-products by *C. termitidis* cultured in a 7 L reactor (3 L working volume) containing 1191 media and 2 g L^{-1} α-cellulose.

Table 3.3 Carbon recovery, OR, and C1/C2 indices from *C. termitidis* cultures grown on 2 g L^{-1} α-cellulose or cellobiose, when sampled in stationary phase.

Substrate	Carbon Recovery (%)	OR	C1/C2
Cellobiose[a]	1.35± 0.11	1.36 ± 0.13	0.81± 0.12
α-cellulose [b]	0.86 ± 0.08	0.94± 0.09	0.98 ± 0.22

[a] cellobiose values were calculated during 20-40 h

[b] α-cellulose values were calculated from 88-190 h

Table 3.4 Comparison of volumetric production rates and maximum concentrations with *C. termitidis* closed (Balch tube) versus open, pH-controlled, batch fermentation studies.

	Open System in this study			Batch Conditions (Ramachandran et al. 2008)		
	H_2	CO_2	Ethanol	H_2	CO_2	Ethanol
Volumetric Production Rate (mmol L^{-1} h^{-1})						
Cellobiose	0.22 ± 0.01	0.15 ± 0.04	0.13 ± 0.07	0.26	0.33	0.18
α-cellulose	0.12 ± 0.03	0.07 ± 0.01	0.02 ± 0.01	0.14	0.13	0.06
Volumetric Yield (mmol L^{-1} culture)						
Cellobiose	11.98 ± 0.06	8.25 ± 1.0	3.37 ± 0.48	4.6	5.6	3.7
α-cellulose	16.54 ± 0.62	9.10 ± 0.25	2.34 ± 0.49	7.7	6.9	3.1

3.5 Discussion

In contrast to the earlier closed batch experiments of *C. termitidis* in Balch tubes without pH control (chapter 2), this study employed the same carbon loading conditions, but the transition to stationary phase occurred at approximately after 60 h on α-cellulose. This difference was likely due to the use of pH control (at pH 7.2) and continuous N_2 sparging, which prevented a build up of H_2 and CO_2. The generation time of *C. termitidis* during exponential phase growth was assessed using total protein content as a metric for bacterial growth. It is important to note, however, the large deviations in protein concentrations extracted from the two replicates of 2 g L^{-1} α-cellulose. Given this deviation, it cannot be claimed that there is any significant difference in maximum protein concentration between cellobiose and α-cellulose cultures.

In the current study, the doubling-time of *C. termitidis* cultures grown on 2 g L^{-1} cellobiose was 5.5 ± 1.4 h $generation^{-1}$ (or 0.2 ± 0.0 generations per h), where as, 2 g L^{-1} α-cellulose grown cultures showed a doubling-time of 39.7 ± 8.1 h $generation^{-1}$ (or 0.03 ± 0.0 generations per h). A closely related extensively studied mesophilic, cellulolytic, bacterium, *Clostridium cellulolyticum*, was shown to have a doubling-time of 24 h $generation^{-1}$ (Giallo et al. 1985), in sealed, 250 mL flasks containing 1 g L^{-1} hexose equivalent and a starting pH of 7.0. Desvaux et al. (2000) studied growth of *C. cellulolyticum* in a 2 L bioreactor (1.5 L working volume) with pH-controlled at 7.2, and found that *C. cellulolyticum* displayed a generation time of 12.4 h on cellulose concentrations less than 6.7 g L^{-1}. *Clostridium phytofermentans*, a mesophilic, anaerobic, cellulolytic bacterium showed linear rates of cellulose degradation with stable cell densities of 10^7-10^8 CFU mL^{-1} at 32°C in cultures containing 10 g L^{-1} cellulose (0.5 x 5

cm strips of Whatman # 1 filter paper, cellulose content higher than 98%) (Tolonen et al. 2011). The growth on cellulose was measured using the dry mass of residual cellulose in the cultures. Batch experiments on cellulose indicated that a concentration of 3 g L^{-1} cellulose was consumed in 15 days (360 h) after inoculation and a maximum concentration of just over 6 g L^{-1} was consumed in 29 days (696 h) (Tolonen et al. 2011). The generation time for *C. thermocellum* growth on cellulose was determined to be 6.6 h generation^{-1} in cultures containing 1 g L^{-1} α-cellulose and 4.5 h generation^{-1} for 5 g L^{-1} in batch fermentations within bioreactors with pH control (Islam et al. 2009).

Gas production on both substrates correlated with the growth pattern, with the volumetric and specific production rates being higher in cellobiose cultures, compared with α-cellulose cultures (Table 3.2), while the maximum concentration of H_2 and CO_2 obtained during fermentation were higher on α-cellulose, compared with those observed in cellobiose cultures (Table 3.1). Similar results for total gas production were reported earlier for *C. termitidis* in batch fermentation studies in Balch tubes (Table 3.4) containing 2 g L^{-1} α-cellulose and cellobiose (chapter 2).

Increased H_2 production on 2 g L^{-1} α-cellulose cultures coincided with increased acetate production and decreased ethanol production. In contrast, the cellobiose cultures showed lower H_2 concentrations, and increased ethanol concentrations. The ratios of H_2:CO_2 for cellobiose and α-cellulose cultures were obtained as 1.45 and 1.82, respectively. The total H_2 production in this study was 11.98 ± 0.06 mmol L^{-1} culture for cellobiose cultures and 16.54 ± 0.62 mmol L^{-1} in α-cellulose cultures (Table 3.1). These far exceed the volumetric H_2 production values of 4.6 mmol L^{-1} culture (same as μmol mL^{-1}) in cellobiose and 7.7 mmol L^{-1} culture in α-cellulose, previously reported for *C.*

termitidis in batch conditions (in Balch tubes) (chapter 2). This may be due to pH-controlled conditions during fermentation: the lack of low pH-induced 1) growth arrest enables a higher degree of substrate utilization; and 2) pyruvate diversion to lactate formation in the case of α-cellulose. The increased H_2 and lower ethanol yields in the open bioreactor system of *C. termitidis,* when compared with the batch experiments, may be also due to continuous N_2 sparging along with agitation apart from the fact that the pH is controlled at 7.2. The comparison of maximum concentration and volumetric production rates for H_2, CO_2, and ethanol between open, pH-controlled/N_2 sparged systems and batch fermentations are summarized in Table 3.4.

The H_2:acetate ratios for *C. termitidis* growth on cellobiose were 0.98 ± 0.16 and 0.71 ± 0.10 for the two replicate fermentations. These ratios were calculated from the start of the experiment until stationary phase. For α-cellulose, the H_2:acetate ratios for both replicates were and 1.04 ± 0.25, and 1.61 ± 0.42. All H_2:acetate ratios were found to be consistent throughout the growth phase of a single biological replicate, rather than between the two replicates. It seems that with the exception of the second cellobiose replicate, the H_2:acetate ratios are in agreement with literature, so it is reasonable to assume robust H_2 production, and under-estimation of CO_2 in this study. Previous work with *C. termitidis* suggested that the ratios for both substrates should be closer to unity. However, Desvaux et al. (2000) reported H_2:CO_2 ratios consistently greater than 1 for *C. cellulolyticum* across a wide range of initial substrate concentrations.

The soluble end-products produced for both cellobiose and α-cellulose cultures were lactate, formate, acetate, and ethanol, consistent with previous work with *C. termitidis* (see chapter 2). From Table 3.1, it can be seen that fermentation of 2 g L^{-1}

cellobiose produced more lactate and less ethanol. Previous studies indicated that for growth on α-cellulose, the end-product distribution changed somewhat, with formate being produced in lesser amounts than ethanol, minimal lactate production, and greater acetate production (chapter 2).

The most marked difference in the distribution of these end-products is the presence of relatively high lactate concentrations in the cellobiose cultures, whereas on the insoluble substrate, lactate was hardly detected until stationary phase. A possible explanation is that while lactate fermentation is more thermodynamically favorable, it yields less conserved energy, which is why, in most Clostridia, its activity is very tightly allosterically regulated (Rydzak et al. 2009). Because of this, it is only used in carbon-excess conditions (Gottschalk 1986; Islam et al. 2006). This finding is in agreement with earlier batch experiments done with *C. termitidis,* as in that work it was reported that lactate concentrations were four-fold greater on 2 g L^{-1} cellobiose than on 2 g L^{-1} α-cellulose (chapter 2).

The higher production of formate on cellobiose is consistent with the previous findings (chapter 2), which reports 4.2 mmol L^{-1} culture of formate for cellobiose, but only 2.9 mmol L^{-1} culture for α-cellulose. No significant difference was found in ethanol production between the two substrates. This is again consistent with the reported values of 3.7 and 3.1 mmol L^{-1} of ethanol for cellobiose and α-cellulose, respectively, reported in (chapter 2).

The profile of acetate production corresponds quite well with H_2 production. The H_2:acetate ratio found in this work for growth on cellobiose was 0.92 ± 0.10. For α-cellulose, the H_2:acetate ratios for both replicates were and 2.34 ± 0.08. In contrast, the

Balch tube batch studies shown earlier implies that the H_2:acetate ratio is 0.77 for cellobiose and 1.07 for α-cellulose (chapter 2).

The maximum concentration of acetate from growth on cellobiose in the open system was two-fold greater than the value reported in the previous batch study (chapter 2), but production was comparable for the α-cellulose cultures. However, it is noteworthy that the acetate production was greater in cellobiose cultures than α-cellulose cultures, whereas under Balch tube batch conditions, acetate production was greater in α-cellulose cultures (chapter 2).

The acetate:ethanol (A/E) ratios found in this study were 3.91 ± 0.10 in cellobiose cultures and 3.03 ± 0.22 in α-cellulose cultures. This is much higher than the findings for *C. termitidis* in previous Balch tube batch experiments (chapter 2). Desvaux et al. (2000) reported that A/E ratios were consistently greater than 1 for cultures with substrate loadings of less than 6.7 g L^{-1} cellulose for *C. cellulolyticum*.

The average specific rate of cellobiose utilization found during log-phase growth of *C. termitidis* was 4.17 mmol g dcw^{-1} hr^{-1}. For α-cellulose cultures, *C. termitidis* consumed only 77% of the substrate over a growth period of 160 h. In contrast, *C. cellulolyticum* consumed cellobiose at much lower rates on both a synthetic medium (2.13 mmol g dcw^{-1} h^{-1}) and a complex medium (0.67 mmol g dcw $^{-1}$ h^{-1}) (Guedon et al. 1999). On the presence of cellulose, *C. cellulolyticum* consumed 85% of the substrate in 120 hours of growth for all initial substrate concentrations of less than 6.7 g L^{-1} (Desvaux et al. 2000). However, the result for *C. cellulolyticum* was found after the culture had ceased growth, and had been re-inoculated. In another study of *C. cellulolyticum* growth on cellulose, Giallo et al. (1985) concluded that *C. cellulolyticum* was not able to degrade

more than 70% of the substrate at initial concentrations less than 7.6 g L^{-1}. Soluble sugars were also not detected in the liquid phase via HPLC. The incomplete cellulose utilization indicates carbon excess, but it was not substrate depletion that caused the cells to enter stationary phase in *C. termitidis*.

Extracellular pyruvate was not detected in *C. termitidis* cultures grown on either cellulose or cellobiose during any time throughout the growth phase. This finding indicates that *C. termitidis* does not suffer from pyruvate overflow from cellulose catabolism exceeding pyruvate flux to acetyl-CoA, as it has been observed for *C. cellulolyticum* when growing on cellulose (Desvaux et al. 2000). In *C. termitidis*, given the pH of the process was held constant at 7.2, this is indicative that growth may have ceased due to end-product inhibition, nitrogen or phosphorus limitations, or limitations due to sulfur or vitamins in the growth medium.

3.6 Conclusion

This chapter demonstrates scale-up experiments of *C. termitidis* in a bioreactor under different physiological conditions. Higher specific and volumetric yields of H_2 during fermentation with cellobiose and α-cellulose were observed in the open fermenter systems relative to batch cultures on 2 g L^{-1} cellobiose and α-cellulose (chapter 2), while corresponding yields of ethanol production decreased somewhat. These increased yields of H_2 production from scale-up experiments involving 1) an open system, 2) pH control, 3) different mode of agitation, and 4) continuous N_2 sparging, reveal the possibility of using *C. termitidis* as a potential candidate for exploitation in the future for enhanced biohydrogen production and is consistent with increased H_2 production at a lower concentrations of H_2 in the environment.

Chapter 4: Shotgun proteomic analysis of hexose grown cultures of mesophilic cellulolytic *C. termitidis*

This Chapter is based, in-part, on the following publication: "Ramachandran, U., Shamshurin, D., Spicer, V., Ezzati, P., McQueen, P.D., Krokhin, O.V., Wilkins, J.A., Sparling, R., and Levin, D.B. 2013. Shotgun proteomic analysis of hexose grown cultures of mesophilic cellulolytic *C. termitidis*. Applied and environmental Microbiology (in preparation)."

4.1 Abstract

Differential shotgun proteome analysis of a mesophilic, hydrogen and ethanol producing cellulolytic bacterium *C. termitidis*, isolated from the gut of the wood-feeding termite *Nasutitermes lujae*, was performed between two growth substrates, 2 g/L α-cellulose and cellobiose. End-product characterization of *C. termitidis* have shown the production of H_2, ethanol, CO_2, acetate, formate, and lactate on both α-cellulose and cellobiose. Optimization of end-product yields and the rate of production is imperative for economic feasibility of biofuels production. Relative protein expression profiles provide insights in understanding central carbon metabolism and protein expressional changes in response to growth phase, substrate, pH, and carbon limitation. The peptides from both the biological replicates were labeled using isobaric tags for Relative/Absolute Quantitation (iTRAQ), and subjected to 2D LC/MS/MS analysis using an AB SCIEX QSTAR® Elite Hybrid TOF-MS system. An in-house GPU-based search engine scanned the fragment ion spectra against a *C. termitidis* derived peptide database to report observed peptide sequences and their corresponding iTRAQ reporter-ion intensity values. Approximately, 1370 proteins were identified with replicate-correlated protein level Z-score values, yielding relative protein expression levels of α-cellulose versus cellobiose

grown cultures. A majority of the core metabolic proteins did not change across the two growth phases, although there were some exceptions. The relative abundance and differential expression profiles of the proteins identified were determined by calculating $\log_2$TIC and overall Znet score values.

4.2 Introduction

Bacteria capable of hydrolyzing and catabolizing the polymeric constituents of lignocellulosic biomass are extensively studied as biocatalysts for CBP in recent times (Peralta-Yahya and Keasling 2010). High throughput "Omic technologies" such as next generation sequencing of the genome followed by bioinformatics data mining provide insights into the metabolic potential of the organism. The data obtained are further verified using fuctional proteomics analysis, which supports an in-depth understanding of central carbon metabolism in bacteria for the production of desired end-products (Rydzak et al. 2012; Lee et al. 2008). Initial studies in thermophilic, celluloytic, and biofuels producing bacteria *C. thermocellum* have shown the expressional analysis of 17 genes encoding proteins involved in fermentation end-product formation, catabolite repression, intracellular phosphorylation and cellulose degradation with respect to substrate specificity and growth rate (Stevenson and Weimer 2005).

In this chapter, based on the initial metabolic characterization of *C. termitidis* (Hethener et al. 1992; Ramachandran et al. 2008), a deep compositional and quantitative proteomic analysis was performed on cultures grown on the two hexose substrates, cellobiose and α-cellulose for the first time. iTRAQ relative quantitation analysis of mid-exponential and stationary phase cultures on the two substrates showed certain essential proteins involved in glycolysis, pyruvate metabolism, H_2 and ethanol synthesis pathways at high levels that could be related to the end-product synthesis patterns observed on 2 g/L α-cellulose and cellobiose (chapter 2).

4.3 Materials and Methods

4.3.1 Microorganism and Media

The type strain of *Clostridium termitidis* CT1112 was obtained from American Type Culture Collection (ATCC 51846). Most of the reagents and chemicals for media and substrates were obtained from Fisher Scientific, with the exception of Bacto^{TM} yeast extract, which was obtained form Becton, Dickinson and Company. Active cultures of *C. termitidis* were made by two consecutive passages on 1191 medium as previously described in chapter 2 containing specific substrates (α-cellulose and cellobiose) correspondingly, with 10% v/v inoculation. Cellobiose stock solution was prepared as per protocols described by Ramachandran et al. (2008, 2011). The initial pH of the medium for all the experiments was set to 7.2.

For the shotgun proteome analyses, the cells were prepared from batch experiments in duplicate serum bottles (50 mL) containing 1191 media with 2 g L^{-1} cellobiose and α-cellulose substrates at 37^0C. Liquid samples were collected during the mid-exponential and stationary phase as previously described (chapter 2), and the pellets were separated by centrifugation at 4,700 rpm using Sorvall SH BK-3000 rotor and processed accordingly.

4.3.2 Cell growth and pH measurements

Optical density measurements at 600 nm (OD_{600}) using spectrophotometrical analysis (Biochrom, Novaspec II) and pH measurements were perfomed as per the methods desribed in chapter 2. The cell pellets were subjected to Bradford assay for protein measurements as previously described (Ramachandran et al. 2008, 2011; Bradford 1976).

4.3.3 Soluble and gaseous end-products analysis

The supernatants obtained for cellobiose and α-cellulose culture across both growth condtions for proteomic analyses were processed based on the protocols described previously (chapter 2) using a high-performance liquid chromatograph equipped with an anion-exchange IonPac-AS11 analytical column (4 x 250 mm). A conductivity detector was used to measure the organic acids (Dionex Corporation, Sunnyvale, CA, USA). Ethanol concentrations in the supernatants were measured using the same ion-chromatography system (Dionex ICS-3000) using an Aminex HPX 87H (300 x 7.8 mm) ion exclusion column (Bio-Rad Laboratories, Ontario) fitted with Cation-H, micro-guard cartridge (40 x 4.6 mm) and a refractive index detector having a mobile phase of 0.004 N H_2SO_4 (flow rate: 0.75 mL min^{-1}).

Head space gas concentrations for hydrogen (H_2) and carbon dioxide (CO_2) were measured using a gas chromatograph (SRI Instruments, Model 8610C) with a detectable range of 200-500 ppm in the presence of a Thermal Conductivity Detector (TCD) as described in chapter 2. Based on the CO_2 analysis (Sander 1999), bicarbonate fraction was determined along with aqueous and gas phases of both H_2 and CO_2 (Ramachandran et al. 2008; Sander 1999; Darrett and Grisham 1995).

4.3.4 Protein isolation, purification, and quantitation

From the proteomic batch experiments, liquid samples (20 mL) were collected during the mid-log phase, and the pellets were separated by centrifugation at 4,700 rpm at 4 °C for 10 min using Sorvall SH BK-3000 rotor. A modified filter-aided sample preparation (FASP) method (Wisniewski et al. 2009) was used to isolate proteins from the cell pellets from both α-cellulose and cellobiose cultures. The pellets were washed

thoroughly 3 times with 500 μL of 1X PBS (pH 7.4) and stored at -80 °C, if the lysis was planned to perform later. The pellets were resuspended in SDT-lysis buffer (4%(w/v) SDS; 100 mM Tris-HCl, pH 7.6; 0.1 M freshly prepared DTT) and boiled for 15 min. The samples were sonicated continuously for 2 min, followed by centrifugation at 13,500 rpm for 5 min to remove cell debris. The protein concentration in the supernatants was determined by Bicinchoninic Acid (BCA) Protein Assay Kit (Thermo Scientific Pierce, Rockford, IL) and the methodology used as described by the manufacturer.

Protein samples were prepared for proteomic analyses as follows. To 1.5 mL of supernatant from protein-extracted portion, 10 mL of UA solution (8 M Urea in 0.1 M Tris-HCl, pH 8.5, filter sterilized before use) was added in to 50 mL ultrafiltration unit (Amicon Ultra-15 cetrifugal unit with Ultracel-10, Thermo Scientific) and centrifuged for 20-25 min. After discarding the flow-through, 5 ml of iodoacetamide (50 mM) was added for protein alkylation and incubated in dark for 5-10 min. The samples were centrifuged for 20-25 min and washed with 5 mL of UA twice. All centrifugation steps were carried out at room temperature at 4000 rpm for 20-25 min. An aliquot of 200 μL of the protein sample was stored at -80 °C for BCA analysis. After discarding the flow-through, 7 mL of ammonium bicarbonate (500 mM) was added and centrifuged for 20-25 min. The protein samples were digested using a 1:50 trypsin/protein ratio overnight at room temperature. The filtration units containing the digested peptides were transferred in to fresh 50 mL falcon tubes (Thermo Scientific) and washed with 200 μL of sodium chloride (0.5 M) twice, by centrifugation at 4000 rpm for 20-25 min.

Based on the concentrations obtained from the Nanodrop, the peptide samples were acidified by adding 10 μL of triflouroacetic acid to obtain a final concentration of 1

% and stored at -80 °C. For desalting and purification of the peptide samples were loaded on an Agilent 1100 series HPLC (Agilent Technologies, Wilmington, DE) with C18 X-Terra column (1x 100 mm, 5 μm, 100 Å, Waters Corporation, Milford, MA, USA) using 0.1 % TFA, and were eluted with 50 % acetonitrile. The purified peptides were stored at -80 °C for further 2D LC/MS/MS analysis. For compositional proteomic analysis of mid-exponential and stationary samples from cellulose versus cellobiose cultures of *C. termitidis*, 100 μg of total peptides from both the biological replicates were labeled using isobaric tags for Relative and Absolute Quantitation (iTRAQ) reagent (Applied Biosystems, Foster City, CA, USA) as outlined by the manufacturer and subjected to deep 2D LC/MS/MS analysis (Aggarwal et al. 2006; Zieske 2006).

4.3.5 2-D Liquid chromatography-mass spectrometry analysis

After iTRAQ labeling, desalted peptides were separated in the first dimension using an Agilent 1100 series HPLC system (Agilent Technologies, Wilmington, DE) equipped with C18 X-Terra column (1x 100 mm, 5 μm, 100 Å, Waters Corporation, Milford, MA, USA). The samples were eluted with a water-acetonitrile gradient (20 mM ammonium formate, pH 10, 1 % acetonitrile per min, 150 μL/min flow rate). Ammonium formate (200 mM) solution (Gilar et al. 2005) was prepared followed by buffers A and B for ID separation using 1/10 dilution of this concentrated buffer with water and acetonitrile. Fractionation was performed and approximately 60 fractions (5.5 μg/fraction) were collected. The peptide samples were pairwise concatenated as shown by Dwivedi et al. (2008) (1 and 28, 2 and 29 etc.) into a total of 29 fractions. Each fraction was lyophilized and re-suspended in 100 μL of formic acid (0.1 %). The online LC-MS analysis was performed using a nanoflow Tempo LC system (Eksigent, Dublin, CA, USA) with 20 μL

sample volume through a 300 μm × 5 mm PepMap100 precolumn and a 100 μm × 150 mm analytical column packed with 5 μm Luna C18(2) (Phenomenex, Torrance, CA). Formic acid (0.1 %) was used as ion-pairing modifier along with eluent A (2 % acetonitrile in water) and eluent B (98 % acetonitrile). For each fraction, a 2 hour run-time per fraction was used with 0.33 % acetonitrile/min linear gradient (0-30 % B) for the elution of peptides.

4.3.6 Protein identification and statistical analysis

Deep 2-D LC/MS/MS analysis was performed using an AB SCIEX QSTAR® Elite Hybrid TOF-MS system (Applied Biosystems, Foster City, CA) equipped with a Nano-electro spray ionization source. Before performing the 2-D LC/MS/MS analysis, a 1-D run with the same conditions were performed to test the consistency and accuracy of the iTRAQ labelling procedure (see appendix, supplementary Tables 2 and 3). A collection time of 1 s survey MS spectra (*m/Z* 400- 1500) was used with three MS/MS measurements on the most intense parent ions (80 counts/s threshold, +2 to +4 charge state, m/z 100–1500 mass range for MS/MS) with iTRAQ and "smart exit" settings as described by the manufacturer.

The resulting raw WIFF files were processed using a standard conversion script bundled with Analyst QS 2.0 into Mascot Generic File format (MGF) (Perkins et al. 1999); for each run collection these files were concatenated into a single MGF file for peptide identification and quantification using both Global Proteome Machine's (GPM) X!Tandem (Craig et al. 2004) cyclone (2012.10.01.1) and an in-house GPU-based peptide identification engine (McQueen et al. 2012). These systems used identical search parameters that utilize the 50 most intense fragment peaks, 100 ppm tolerance on the

parent mass, 0.2 Da bin for CID fragments, fixed PTM's of C+57.021 (cystine protection carboxamidomethyl) and +144.102 on N-terminal and lysine (for iTRAQ) with a +-0.1 Da integration window on iTRAQ reporter ion intensities. Only tryptic peptides with up to one permitted missed cleavage from a putative annotation of *C. termitidis* on DDBJ/EMBL/GenBank under the accession AORV00000000 were pursued for identification.

The protein total ion counts (TIC) were used as a relative measure of protein expression within an experimental run: the sum of the MS/MS fragment ion intensities for every identified member peptide. This value is expressed in a $\log_2$ scale.

For both experimental run collections, the two search engines (GPU and X!tandem) gave results that agreed well on a protein level, with $\log_2$ TIC values correlating to an $R^2 > 0.90$. The number of engine-unique non-redundant peptides with peptide log(e) values <-1.5 were approximately equal, with an overlap of ~ 90%, showing that algorithm-level biases don't favor either tool; however our GPU system is typically 5-30x faster than X!tandem. The XML results from the X!tandem searches are archived at the Proteomics Centre's GPM site (http://140.193.59.2) under the filenames GPM02M00007937 for the exponential experiment and GPM02M00007938 for the stationary experiment. Additionally, the MGF files have been modified from their converted originals to permit easier iTRAQ analysis. The TITLE field of each MGF fragment spectrum entry now contains a run-unique four-number identifier *Locus:XX.XX.XX.XX*. As with the GPU search, values obtained by integrating the iTRAQ reporter intensities within a +-0.1 Da window of (114.102, 115.102, 116.102, 117.102)

can then be linked to their X!tandem XML identified peptides by matching the Locus: field values.

The iTRAQ labels encoded biological replicates of the same state in adjacent channel pairs (114,115) and (116,117). Reporter ion intensities for each tryptic peptide with identified expectation values log(e)<-1.5 were histogrammed by the $\log_2$ of the following ratios (R0=116/114, R1=117/115, R2=115/114 and R3=117/116) to build roughly Gaussian peptide differential expression distributions. The intra-replicate populations were extremely narrow, <1/3 the width of the cross-condition populations. Histogram standard deviations (in $\log_2$) for the stationary-phase experiment were (1.63, 1.62 / 0.52, 0.54) and for the exponential-phase experiment were (1.87,1.82 / 0.45,0.56).

For each peptide in the four populations, its ratio was normalized to a Z-score: the distance from the population mean in units of standard deviation. These were then averaged into member proteins, yielding protein-level normalized values of (Z0,Z1,Z2,Z3). An in-house simple algorithm was devised to combine these values into a ”Znet”, expressed as the absolute value of the difference between the magnitudes of vectors from the origin to points (Z0,Z1) and (Z2,Z3), scaled by the widths of their respective peptide difference histograms. The sign of Znet is determined by the angle subtended from the X-axis to the point (Z0,Z1); angles between 315 and 135 degrees are positive, otherwise negative (see appendix, supplementary Figures 3 and 4 for Z-limits).

The values are themselves normalized into final protein-level Znet values. The resulting distributions are again roughly Gaussian, with ~ 33% of the population with Z-scores of an absolute value >1, 10% of the population with Z-scores of an absolute value >1.65, and 5% of the population with Z-scores of an absolute value >1.96.

Protein level Z-scores and their supporting peptide data are mapped onto KEGG pathways (Ogata et al. 1999; Kanehisa et al. 2000) as shown in supplementary Figures 1 and 2 (see appendix). The peptide sequence results were searched against the 2013 release of the *C. termitidis* genome available at DDBJ/EMBL/GenBank under the accession AORV00000000 (Lal et al. 2013).

4.4 Results and Discussion

4.4.1 Proteomic analyses- overall findings

Deep 2-D liquid chromatography-tandem mass spectrometry revealed a total of 1368 out of 2032 and 1377 out of 2034 proteins identified during mid-exponential and stationary phase samples of *C. termitidis* respectively, with a minimum peptide detection threshold of 2 and a confidence score of 99.9%. Figure 4.1 A-B indicates the two time-points (mid-exponential and stationary phases) of growth on 2 g L^{-1} cellobiose and α-cellulose during which samples were collected for proteomic analysis. An overview of the iTRAQ experimental design is illustrated in Table 4.1. Table 4.2 indicates similar numbers of CID fragment spectra and identified peptides for both experimental growth conditions. The primary focus was on the core metabolic proteins that are involved in the regulation of carbon and electron flux from cellulose and cellobiose hydrolysis. Hence, in this chapter, putative proteins involved in a) glycolysis; b) carbohydrates hydrolysis; c) Pyruvate catabolism; and d) H_2/ethanol and other end-product synthesis are examined and discussed below.

Comparison of 4-plex 2D-HPLC/MS/MS analysis of the two growth conditions (mid-exponential and stationary phases) between the two biological replicates of cellulose versus cellobiose grown cultures are shown in Figure 4.2. These correlation

plots illustrate the consistency of the experimental sample preparation, purification, and labeling procedures. A perfect correlation is represented by coordinates 0,0. Most of the proteins showed very good correlation between the biological replicates (Figure 4.3), except for a few proteins, Hence, statistical analysis was perfomed to identify significant differences between the protein expression ratios while factoring the deviations between the biological replicates across both growth conditions (see methods, section 4.3.6). The Z-scores for corresponding proteins were converted into vector differences (see methods, section 4.3.6). The correlation plot based on derived Total ion count (log_2 TIC) values and Z-scores are shown in Figures 4.2 A-B. The log_2 TIC value represents the relative high abundance of the corresponding proteins in the proteome, where as Z-scores indicate the relative expression (either up- or down-regulated) profiles. Table 4.3 shows an overview of the identified proteins with Z-score> 1.65 (outermost 10%) from both the iTRAQ experiments that are mapped on a coarse functional level COG categories using an in-house developed software (see methods, section 4.3.6). The maximum number of proteins that were identified belonged to the COG categories “G” and “J” across both growth conditions in cellulose versus cellobiose cultures of *C. termitidis*. COG category “G” (involved in carbohydrate transport and metabolism) included 23 proteins that were up-regulated in mid-exponential samples, where as 25 proteins were found to be down-regulated in the stationary phase samples. Functional group “J”(required for translation ribosomal structure and biogenesis) included 13 proteins that were down-regulated in both mid-exponential and stationary phase samples. The iTRAQ 2D HPLC/MS/MS analysis resulted in approximately 33% of proteins with Z-scores of an absolute value greater than 1, 10% of the protein population greater than 1.65, and 5% of the population

greater than 1.96 across both growth conditions of mid-exponential and staionary phase samples (see methods, section 4.3.6 for calculation).

Table 4.1 An overview of the iTRAQ experimental design.

iTRAQ labels/ experiments	114	115	116	117
P1	ML_CB	ML_CB	ML_AC	ML_AC
P2	SP_CB	SP_CB	SP_AC	SP_AC

Table 4.2 An overview of the total detected CID fragment spectra and identified peptides/proteins using two-dimensional iTRAQ analysis of *C. termitidis* mid-exponential and stationary phase samples cultured on 1191 medium containing either 2g/L α-cellulose or cellobiose.

Experiment state	Proteins log(e)<-10	Proteins log(e)<-3	Proteins log(e)<-1	Total proteins	NR peptides	Total peptides	MS-MS spectra
Mid-Exponential	1368	1609	2017	2032	10351	20154	104571
Stationary	1377	1627	2018	2034	11382	20505	99296

A)

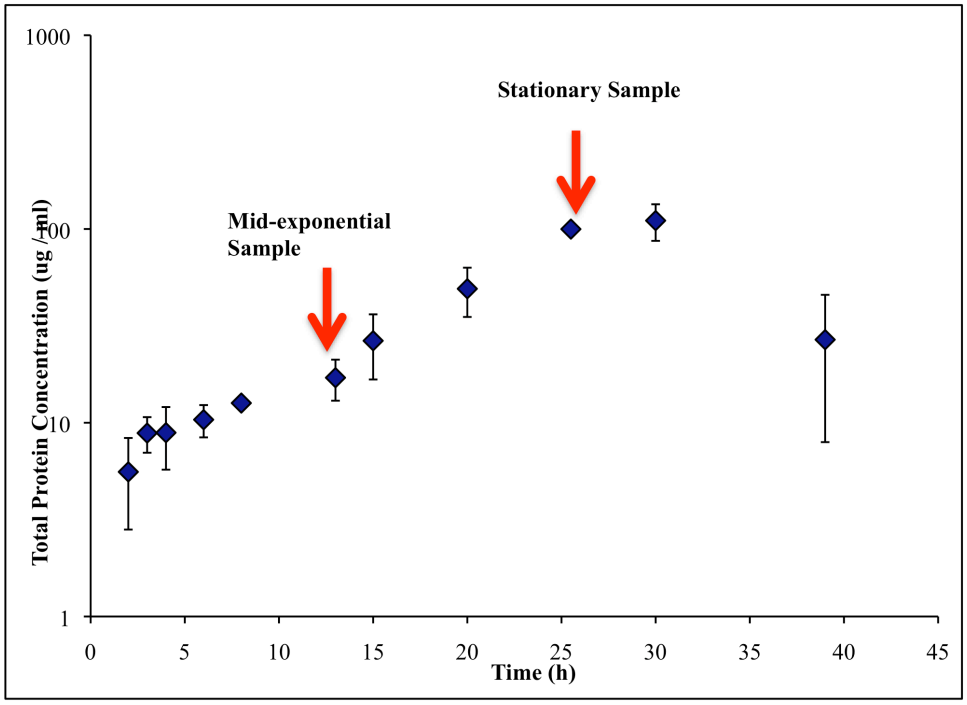
1000
100
10
1
Total Protein Concentration (ug /ml)
Stationary Sample
Mid-exponential Sample
0
5
10
15
20
25
30
35
40
45
Time (h)

B)

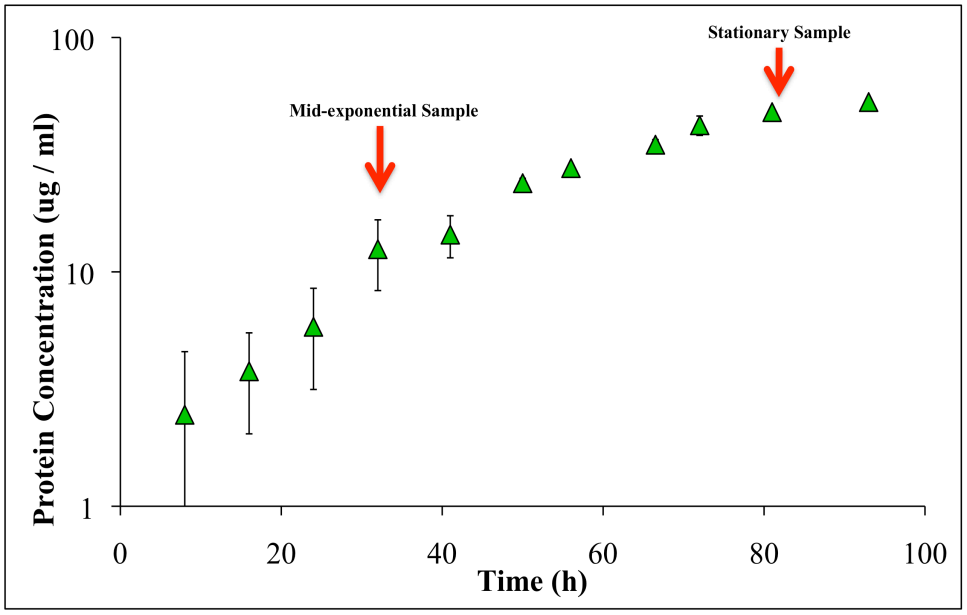
100
10
1
Protein Concentration (ug / ml)
Stationary Sample
Mid-exponential Sample
0
20
40
60
80
100
Time (h)

Figure 4.1 Growth and protein characterization of *C. termitidis* on 1191 medium containing A) 2 g L^{-1} cellobiose B) 2 g L^{-1} α-cellulose. The arrows indicate the two time-points (mid-exponential and stationary phase) during growth on both the substrates that were used for proteomic analysis. The mid-exponential and stationary phase samples on cellobiose were collected after 12 h and 28 h, respectively, whereas on α-cellulose, the mid-exponential and stationary phase samples were collected after 36 h and 80 hours, respectively.

A)

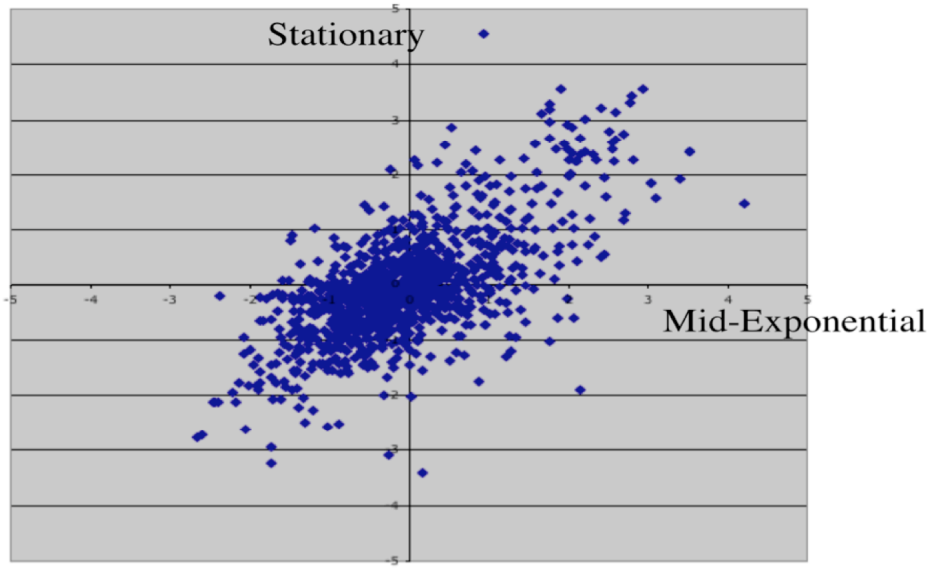
Stationary
Mid-Exponential

B)

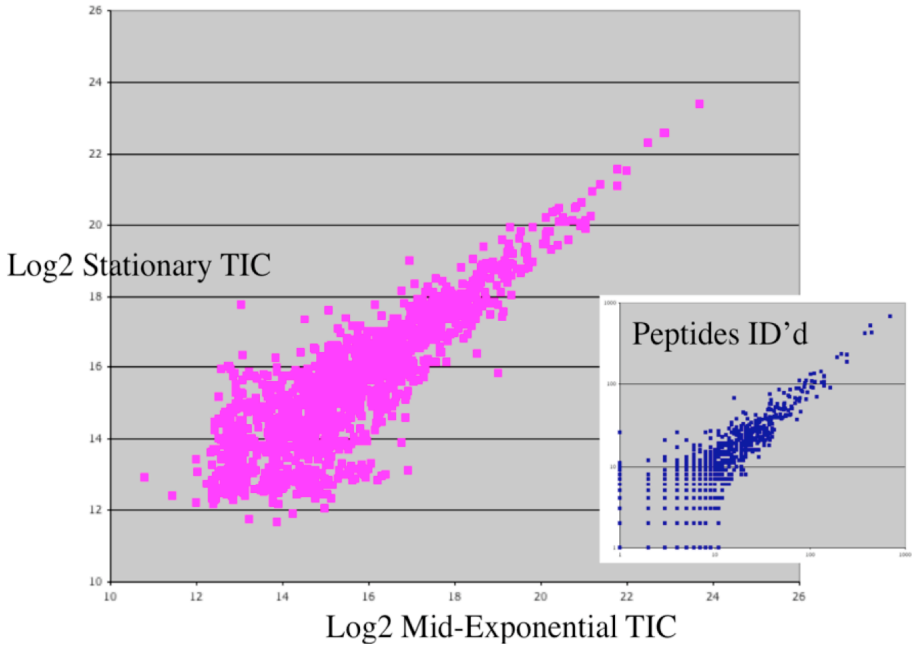
Log2 Stationary TIC
Peptides ID'd
Log2 Mid-Exponential TIC

Figure 4.2 A) Correlation of protein Z-scores comparison between mid-exponential and stationary phases. B) Correlation of total ion count (TIC) between proteins identified in mid-exponential and stationary phase samples.

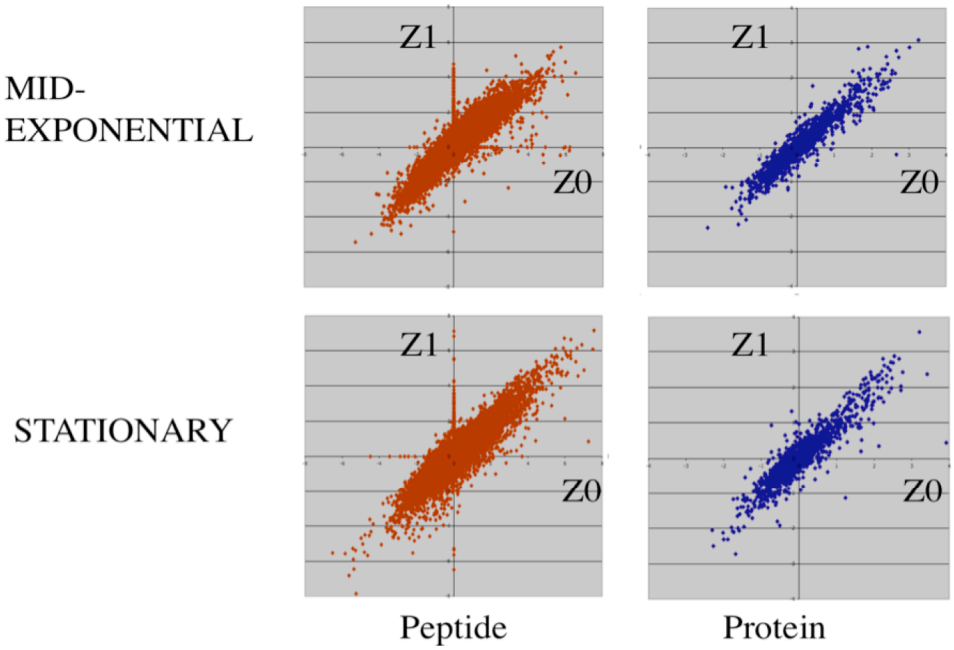

Figure 4.3 Correlation of protein and peptide Z-scores between the biological replicates in the iTRAQ experiment.

Table 4.3 An overview of the COG mapping of identified proteins with Z-score greater than 1.65 (the outermost 10% of the population). The highlighted categories indicate maximum number proteins classified under functional groups G (up-regulated) and J (down-regulated) in both mid-exponential and stationary phase samples.

.

FUNCTION	DESCRIPTION	EXPONENTIAL UP	EXPONENTIAL DOWN	STATIONARY UP	STATIONARY DOWN
J	Translation, ribosomal structure and biogenesis	2	13	1	13
K	Transcription	2	3	1	0
L	Replication, recombination and repair	0	1	1	0
B	Chromatin struture and dynamics	0	0	0	0
D	Cell cycle control, cell divison, chromosome partitioning	0	0	3	0
V	Defense mechanisms	1	0	2	0
T	Signal transduction	4	3	5	4
M	Cell wall/membrane/envelope biogenesis	7	3	7	3
N	Cell motility	2	3	1	6
Z	Cytoskeleton	0	0	0	0
U	Intracellular trafficing, secretion and vesicular transport	3	0	1	3
O	Posttranslation modification, protein turnover, chaperones	1	3	2	1
C	Energy Production and conversion	2	2	4	3
G	Carbohydrate transport and metabolism	23	1	25	4
E	Amino acid transport and metabolism	5	1	0	1
F	Nucleotide transport and metabolism	0	0	2	0
H	Coenzyme transport and metabolism	2	0	4	2
I	Lipid transport and metabolism	3	1	1	1
P	Inorganic ion transport and metabolism	0	2	1	2
Q	Secondary metabolites biosynthesis, transport and catabolism	3	1	1	0
R	General function prediction only	4	2	7	2
S	Function unknown	4	2	4	3
X	Not in COGs	32	4	33	3
TOTALS		**100**	**45**	**106**	**51**

4.4.2 Proteins involved in glycolysis, pyruvate formation, and malate transhydrogenase pathways

Two dimensional iTRAQ RP-HPLC/MS/MS analysis showed a high abundance of most of the glycolytic proteins in both mid-exponential and stationary phase samples across both α-cellulose and cellobiose grown cultures of *C. termitidis* (Table 4.4). In *C. termitidis*, conversion of glucose to phosphoenol pyruvate, and then pyruvate occurs via Embden-Meyerhof-Parnas pathway (see Figure 1.1, chapter 1). The log_2TIC values (ranging between 11.0-22.0) indicate the relative abundance of the proteins identified across both conditions, where as the Znet scores indicate significant protein expression (up-regulation or down-regulation) on α-cellulose, when compared with cellobiose cultures. Multiple genes were identified in the *C. termitidis* genome, that encode for proteins belonging to the same enzyme class across both the iTRAQ experiments (Tables 4.4, 4.5, and 4.6). In both mid-exponential and stationary phase experiments, glyceraldehyde-3-phosphate dehydrogenase (EC:1.2.1.12; CTER_4809 gene) was the most abundant protein identified with an overall log_2TIC value of 22.0 in the hexose proteome, where as 6-phosphofructokinase (EC:2.7.1.11; CTER_4719), fructose-1,6-bisphosphate aldolase (EC 4.1.2.13; CTER_4718), GTP-dependent phosphoenol pyruvate carboxykinase (EC:4.1.1.32; CTER_1146), malic enzyme (EC:1.1.1.38; CTER_4718), malate dehydrogenase (EC:1.1.1.37; CTER_0412), pyruvate/oxaloacetate decarboxylase (EC:4.1.1.3; CTER_0730), and bifunctional phosphoglycerate kinase (EC:2.7.2.3; CTER_4786) showed an overall log_2TIC value of over 19.0 (Table 4.4). Recently, 4-plex iTRAQ analysis in the anaerobic, thermophilic, cellulolytic bacterium, *C. thermocellum* also showed glyceraldehyde-3-phosphate dehydrogenase as the most abundant of the all

the other proteins detected in glycolysis (Rydzak et al. 2012). In extremely thermophilic cellulolytic bacterium, *Caldicellulosiruptor obsidiansis*, label-free quantitative proteomic analyses of the whole cell lysates revealed glyceraldehyde-3-phosphate dehydrogenase as the most abundant protein with normalized spectral counts ranging between 800-1000 for all the four substrates tested, namely, cellobiose, avicel, filter paper, and switchgrass respectively (Lochner et al. 2011).

During glycolysis, all the enzymes catalyzing the biochemical conversion from glucose-1-phosphate to pyruvate were detected in the *C. termitidis* genome and proteome (across both growth conditions), with a few exceptions. Out of the three genes (CTER_0067, CTER_4719, CTER_5379) encoding 6-phosphofructokinase (EC:2.7.1.11) in the *C. termitidis* genome, CTER_5379 was not detected in the hexose proteome. In *C. termitidis*, the pyrophosphate (PPi)-dependent phosphofructokinase (CTER_4719) was detected at higher levels across both growth phases than the ATP-dependent 6-phosphofructokinase (CTER_0067). Similar results were observed in *C. thermocellum*, as the levels of ATP-dependent 6-phosphofructokinase (Cthe_1261, Cthe_0389) were lower than the pyrophosphate (PPi)-dependent phosphofructokinase (Rydzak et al. 2012). Although, studies have shown decreased mRNA expression levels of 6-phosphofructokinase (Cthe_1261, Cthe_0389) during stationary phase in *C. thermocellum* (Raman et al. 2011), protein level changes were undetected (Rydzal et al. 2012). Where as, in *C. termitidis*, there was no significant differences in the relative expression levels (see Znet scores, Table 4.4) of both CTER_4719 and CTER_0067 when the cells entered stationary phase on α-cellulose grown cultures, but yet, transcriptional studies have to be performed in the future for further verification. Triosephosphate

isomerase (EC:5.3.1.1; CTER_1845) was not detected in the hexose proteome across both growth phases. Among the three genes (CTER_4297, CTER_3439, CTER_5284) that encode enzymes classified as phosphomannomutase (EC:5.4.2.8), CTER_4297 gene product showed significantly lower expression levels in mid-exponential and stationary phases, when the cells grow on α-cellulose (Table 4.4). Also, CTER_5284 gene product was undetected during stationary phase. Unlike *C. thermocellum* (Rydzak et al. 2012), the bifunctional phosphoglycerate mutase observed in the hexose proteome of *C. termitidis* did not significantly change after the cells reached stationary phase. In *C. obsidiansis*, glyceraldehyde-3-phosphate and enolase showed higher expression (approximately 1.3 fold change) on cellulose (filterpaper) grown cultures than cellobiose during exponential phase (Lochner et al. 2011).

Apart from the most common mode of pyruvate synthesis from phosphoenol pyruvate via pyruvate kinase (producing ATP), the alternate pathways include the reversible conversion of phosphoenol pyruvate to pyruvate either using pyruvate phosphate dikinase that generates ATP and P_i from AMP and PP_i, or using pyruvate water dikinase (or otherwise called as phosphoenol pyruvate synthase) that generates ATP and water (H_2O) from AMP and P_i (Lengler et al. 1999; Sparling et al. 2012). In *C. termitidis*, pyruvate phosphate dikinase (EC:2.7.9.1; CTER_0809) was observed at high abundance than pyruvate kinase (EC:2.7.1.40; CTER_0649 in both mid-exponential and stationary phase samples. CTER_0809 was expressed relatively higher in mid-exponential phase, especially, when the cells were grown on cellulose. Pyruvate water dikinase or phosphoenol pyruvate synthase (EC:2.7.9.2; CTER_5054) was not detected in the hexose proteome across both the growth phases. In contrast, *C. thermocellum* does

not encode a pyruvate kinase, and pyruvate synthesis occurs via pyruvate phosphate dikinase (Carere et al. 2012). Proteomic analysis revealed up-regulation of pyruvate phosphate dikinase in exponential cultures of *C. thermocellum*, where as no significant change was observed with phosphoenol pyruvate synthase in the proteome (Rydzak et al. 2012). Where as, *C. obsidiansis* encoded a pyruvate phosphate dikinase (1145), which was detected at higher levels on both cellobiose and filter paper grown cultures during exponential phase (Lochner et al. 2011).

In *C. termitidis*, proteins belonging to the malate transhydrogenase pathway (Rydzak et al. 2012), that includes GTP-dependent phosphoenol pyruvate carboxykinase (EC:4.1.1.32; CTER_1146), malic enzyme (EC:1.1.1.38; CTER_4718), malate dehydrogenase (EC:1.1.1.37; CTER_0412), pyruvate/oxaloacetate carboxyltransferase (EC:4.1.1.3; CTER_0730), 3-isopropylmalate dehydrogenase (EC:1.1.1.85; CTER_0424), and phosphoenolpyruvate phosphotransferase (EC:2.7.3.9; CTER_1041) were detected in higher abundance in the hexose proteome during both growth phases (Table 4.4). Phosphoenol pyruvate carboxykinase (EC:4.1.1.32; CTER_1146) catalyzes the conversion of phosphoenol pyruvate to oxaloacetate, generating ATP, and further oxaloacetate can be biochemically converted to pyruvate via Pyruvate/oxaloacetate carboxyltransferase or oxaloacetate decarboxylase (EC:4.1.1.3; CTER_0730). Also, pyruvate formation from oxaloacetate can also happen via malate in the presence of malate dehydrogenase (EC:1.1.1.37; CTER_0412) first, and then, malic enzyme (EC:1.1.1.38; CTER_4718).

In *C. termitidis*, malic enzyme (EC:1.1.1.38; CTER_4718) and malate dehydrogenase (EC:1.1.1.37; CTER_0412) was significantly down-regulated during mid-

exponential cell growth on α-cellulose, and when the cells reached stationary phase, no significant change was detected in the protein expression levels (Table 4.4). Phosphoenol pyruvate carboxykinase (EC:4.1.1.32; CTER_1146) was expressed at higher levels during stationary phase cultures grown on α-cellulose. In contrast, phosphoenol pyruvate carboxykinase, malate dehydrogenase, and malic enzyme were significantly up-regulated during exponential phase in *C. thermocellum* (Rydzak et al. 2012). Recent studies have shown that transhydrogenation from NADH to $NADP^+$ could be possible in the presence of malate dehydrogenase/malic enzyme, resulting either in H_2 or ethanol synthesis or NADPH generation for biosynthesis (Rydzak et al. 2011). Also, reports have shown that malic enzyme is allosterically regulated by certain compunds such as ammonia, which acts as a regulator (Lamed and Zeikus 1986) and recently, PP_i which acts as an inhibitor in *Caldicellulosiruptor saccharolyticus* (Wilquist and van Neil 2010). Hence, the regulation of malate dehydrogenase/malic enzyme is dependent on pyruvate phosphate dikinase, which controls the levels of PP_i depending upon the availability of carbon and NADPH requirement for biosynthesis via glycolysis. This suggests that in *C. termitidis*, malate transhydrogenase pathway was not regulated during low carbon flux (on cellulose) versus cellobiose (high carbon flux). Faster growth and biosynthesis is observed on cellobiose compared to cellulose, during which, increased PP_i levels and NADPH demand is controlled by pyruvate phosphate dikinase (CTER_0809) via glycolysis, and the subsequent regulation using malate dehydrogenase/malic enzyme pathway.

Table 4.4 Proteins associated with glycolysis and malate trans dehydrogenase pathways in the Genome and Proteome in *C. termitidis*. This table shows log_2TIC and Znet scores of proteins involved in glycolysis and malate trans dehydrogenase pathways in both mid-exponential and stationary phases of α-cellulose versus cellobiose grown cultures of *C. termitidis*. The log_2TIC values in bold correspond to highly abundant proteins across both growth conditions.

Locus Tag	EC No.	log_2TIC	Znet	Name of the protein
		Mid-exponential phase		
CTER_3950	EC:2.7.1.1	**17.4**	-0.68	Hexokinase
CTER_3865	EC:5.3.1.9	**18.03**	-0.63	glucose-6-phosphate isomerase
CTER_5142	EC:5.4.2.2	**18**	-0.76	phosphoglucomutase
CTER_4297	EC:5.4.2.8	**18.6**	-2.46	phosphomannomutase
CTER_3439	EC:5.4.2.8	13.82	-0.53	phosphomannomutase
CTER_5284	EC:5.4.2.8	12.43	-0.97	phosphomannomutase
CTER_0067	EC:2.7.1.11	**18.44**	-0.41	ATP-dependent 6-phosphofructokinase
CTER_4719	EC:2.7.1.11	**20.39**	-0.41	pyrophosphate (PP_i)-dependent 6-phosphofructokinase
CTER_5379	EC:2.7.1.11	ND	ND	ATP-dependent 6-phosphofructokinase
CTER_4718	EC:4.1.2.13	**21.06**	-0.08	fructose-1,6-bisphosphate aldolase, class II
CTER_1264	EC:4.1.2.13	**18.09**	0.81	fructose-1,6-bisphosphate aldolase
CTER_4809	EC:1.2.1.12	**22**	0.56	glyceraldehyde-3-phosphate dehydrogenase
CTER_1092	EC:1.2.1.12	12.72	BD	glyceraldehyde-3-phosphate dehydrogenase

CTER_1845	EC:5.3.1.1	ND	ND	triosephosphate isomerase
CTER_4786	EC:2.7.2.3	**18.54**	-0.39	bifunctional phosphoglycerate kinase
CTER_4785	EC:5.4.2.1	**18.65**	-0.85	2,3-bisphosphoglycerate mutase
CTER_4779	EC:4.2.1.11	**18.5**	-0.34	phosphopyruvate hydratase/enolase
CTER_0649	EC:2.7.1.40	**17.64**	-0.89	pyruvate kinase
CTER_0809	EC:2.7.9.1	**19.03**	0.77	pyruvate, phosphate dikinase
CTER_5054	EC:2.7.9.2	ND	ND	pyruvate water, dikinase/phosphoenol pyruvate synthase
CTER_1146	EC:4.1.1.32	**20.92**	-0.31	phosphoenol pyruvate carboxykinase (GTP)
CTER_1041	EC:2.7.3.9	15.6	0.36	phosphoenolpyruvate-protein phosphotransferase
CTER_0730	EC:4.1.1.3	**20.27**	-0.48	pyruvate/oxaloacetate decarboxylase
CTER_4718	EC:1.1.1.38	**21.17**	-1.64	malic enzyme
CTER_0412	EC:1.1.1.37	**19**	-1.21	malate dehydrogenase
CTER_0424	EC:1.1.1.85	**17.82**	-0.4	3-isopropylmalate dehydrogenase
			Stationary phase	
CTER_3950	EC:2.7.1.1	16.21	-0.65	Hexokinase
CTER_3865	EC:5.3.1.9	**17.77**	-0.66	glucose-6-phosphate isomerase
CTER_5142	EC:5.4.2.2	**17.8**	-0.21	phosphoglucomutase
CTER_4297	EC:5.4.2.8	**18.6**	-2.12	phosphomannomutase
CTER_3439	EC:5.4.2.8	15.12	0.05	phosphomannomutase
CTER_5284	EC:5.4.2.8	ND	ND	phosphomannomutase
CTER_0067	EC:2.7.1.11	**18.09**	-0.77	ATP-dependent 6-phosphofructokinase
CTER_4719	EC:2.7.1.11	**19.42**	0.17	pyrophosphate (PP_i)-dependent 6-phosphofructokinase
CTER_5379	EC:2.7.1.11	ND	ND	ATP-dependent 6-phosphofructokinase

CTER_4718	EC:4.1.2.13	**19.88**	-0.01	fructose-1,6-bisphosphate aldolase, class II
CTER_1264	EC:4.1.2.13	**17.82**	0.12	fructose-1,6-bisphosphate aldolase
CTER_4809	EC:1.2.1.12	**22**	0.56	glyceraldehyde-3-phosphate dehydrogenase
CTER_1092	EC:1.2.1.12	16.01	BD	glyceraldehyde-3-phosphate dehydrogenase
CTER_1845	EC:5.3.1.1	ND	ND	triosephosphate isomerase
CTER_4786	EC:2.7.2.3	**21.1**	-0.09	bifunctional phosphoglycerate kinase
CTER_4785	EC:5.4.2.1	**17.7**	-0.27	2,3-bisphosphoglycerate mutase
CTER_4779	EC:4.2.1.11	**18.5**	-0.63	phosphopyruvate hydratase/enolase
CTER_0649	EC:2.7.1.40	**18**	-0.9	pyruvate kinase
CTER_0809	EC:2.7.9.1	**18.71**	0.38	pyruvate, phosphate dikinase
CTER_5054	EC:2.7.9.2	ND	ND	pyruvate water, dikinase/phosphoenol pyruvate synthase
CTER_1146	EC:4.1.1.32	**20.02**	0.18	phosphoenol pyruvate carboxykinase (GTP)
CTER_1041	EC:2.7.3.9	15.52	1.09	phosphoenolpyruvate-protein phosphotransferase
CTER_0730	EC:4.1.1.3	**20.32**	-0.26	pyruvate/oxaloacetate decarboxylase
CTER_4718	EC:1.1.1.38	**19.88**	-0.48	malic enzyme
CTER_0412	EC:1.1.1.37	**18.74**	-0.26	malate dehydrogenase
CTER_0424	EC:1.1.1.85	16.13	0.6	3-isopropylmalate dehydrogenase

BD: Below iTRAQ detectable range as only 1 peptide was detected for the protein, the minimum cutoff is atleast 2 peptides.
ND: Not detected in the proteome, but observed in the genome.
NA: Not available.

Table 4.5 Proteins associated with pyruvate metabolism in the Genome and Proteome in *C. termitidis*. This table shows log_2TIC and Znet scores of proteins involved in pyruvate catabolic pathways in both mid-exponential and stationary phases of α-cellulose versus cellobiose grown cultures of *C. termitidis*. The log_2TIC values in bold correspond to highly abundant proteins across both growth conditions.

Locus Tag	EC No.	log_2TIC	Znet	Name of the protein
		Mid-exponential phase		
CTER_2504	EC:1.1.1.27	**16.21**	-1.39	lactate dehydrogenase
CTER_4374	EC:1.2.4.1	ND	ND	pyruvate dehydrogenase, E1 component, alpha subunit
CTER_4373	EC:1.2.4.1	ND	ND	pyruvate dehydrogenase, E1 component, beta subunit
CTER_4054	EC:1.8.1.4	14.19	1.43	dihydrolipoamide dehydrogenase, E3 component
CTER_0038	EC:2.3.1.54	**19.24**	-1.44	formate acetyl transferase/pyruvate formate lyase
CTER_1187	EC:2.3.1.54	12.62	BD	pyruvate formate lyase
CTER_0232	EC:2.3.1.54	ND	ND	pyruvate formate lyase
CTER_3262	EC:2.3.1.54	ND	ND	pyruvate formate lyase
CTER_4126	EC:2.3.1.54	ND	ND	pyruvate formate lyase
CTER_4127	EC:2.3.1.54	ND	ND	pyruvate formate lyase
CTER_0037	EC:1.97.1.4	14.6	-1.71	pyruvate formate lyase-1-activating enzyme
CTER_2583	EC:1.97.1.4	ND	ND	pyruvate formate lyase-1-activating enzyme
CTER_1023	EC:1.2.7.1	**20.6**	-0.35	pyruvate:ferredoxin oxidoreductase, alpha subunit

CTER_1022	EC:1.2.7.1	**19.8**	-0.09	pyruvate:ferredoxin oxidoreductase, beta subunit
CTER_1024	EC:1.2.7.1	**18.73**	-1.63	pyruvate:ferredoxin oxidoreductase,delta subunit
CTER_1025	EC:1.2.7.1	**20.8**	-0.34	pyruvate:ferredoxin oxidoreductase, gamma subunit
CTER_2215	EC:1.2.7.8	**17.6**	-0.71	indole pyruvate oxidoreductase, alpha subunit
CTER_2214	EC:1.2.7.8	**17**	-0.26	indole pyruvate oxidoreductase, beta subunit
CTER_0199	EC:1.2.7.8	**16.34**	0.04	indole pyruvate oxidoreductase, alpha subunit
CTER_0198	EC:1.2.7.8	15.34	-0.17	indole pyruvate oxidoreductase, beta subunit
CTER_3763	EC:1.2.7.3	**16.5**	-1.36	2-oxoglutarate:ferredoxin oxidoreductase, alpha subunit
CTER_3762	EC:1.2.7.3	**16.7**	-1.36	2-oxoglutarate:ferredoxin oxidoreductase, beta subunit
CTER_3761	EC:1.2.7.3	**16.1**	0.62	2-oxoglutarate:ferredoxin oxidoreductase, gamma subunit
CTER_3589	EC:1.2.7.-	**17.71**	-0.5	putative pyruvate:flavodoxin oxidoreductase
CTER_3764	NA	ND	ND	4Fe-4S ferredoxin (dicluster domain)
CTER_4519	EC:2.3.1.8	**17.3**	-1.14	phosphate acetyltransferase (PTA)
CTER_4518	EC:2.7.2.1	**18.81**	-0.02	acetate kinase (ACK)
CTER_0993	EC:1.2.1.3	14.32	1.33	NADH-dependent aldehyde dehydrogenase (AldH)
CTER_2833	EC:1.2.1.3	13.84	3.52	NADH-dependent aldehyde dehydrogenase
CTER_5570	EC:6.2.1.1	**16.97**	-0.64	acetyl-coenzyme A synthetase/AMP-dependent
CTER_1865	EC:6.2.1.1	13.37	BD	acetyl-coenzyme A synthetase/AMP-dependent
CTER_5426	EC:1.2.1.10	**21.77**	-1.31	bifunctional acetaldehyde/alcohol dehydrogenase (AdhE)
CTER_3280	EC:1.1.1.1	**20.93**	0.97	iron containing alcohol dehydrogenase (Fe-ADH)
CTER_2586	EC:1.1.1.1	**18.41**	0.18	iron containing alcohol dehydrogenase (Fe-ADH)
CTER_1650	EC:1.1.1.1	ND	ND	iron containing alcohol dehydrogenase (Fe-ADH)

Stationary phase

CTER_2504	EC:1.1.1.27	**16.37**	-1.17	lactate dehydrogenase
CTER_4374	EC:1.2.4.1	ND	ND	pyruvate dehydrogenase, E1 component, alpha subunit
CTER_4373	EC:1.2.4.1	ND	ND	pyruvate dehydrogenase, E1 component, beta subunit
CTER_4054	EC:1.8.1.4	14.7	1.03	dihydrolipoamide dehydrogenase, E3 component
CTER_0038	EC:2.3.1.54	**19.23**	-0.85	formate acetyl transferase/pyruvate formate lyase
CTER_1187	EC:2.3.1.54	ND	ND	pyruvate formate lyase
CTER_0232	EC:2.3.1.54	12.91	BD	pyruvate formate lyase
CTER_3262	EC:2.3.1.54	ND	ND	pyruvate formate lyase
CTER_4126	EC:2.3.1.54	ND	ND	pyruvate formate lyase
CTER_4127	EC:2.3.1.54	12.95	BD	pyruvate formate lyase
CTER_0037	EC:1.97.1.4	15.7	-0.18	pyruvate formate lyase-1-activating enzyme
CTER_2583	EC:1.97.1.4	ND	ND	pyruvate formate lyase-1-activating enzyme
CTER_1023	EC:1.2.7.1	**20.1**	-0.48	pyruvate:ferredoxin oxidoreductase, alpha subunit
CTER_1022	EC:1.2.7.1	**19.9**	-1	pyruvate:ferredoxin oxidoreductase, beta subunit
CTER_1024	EC:1.2.7.1	**18.9**	-0.8	pyruvate:ferredoxin oxidoreductase,delta subunit
CTER_1025	EC:1.2.7.1	**20.45**	-0.66	pyruvate:ferredoxin oxidoreductase, gamma subunit
CTER_2215	EC:1.2.7.8	**17**	-0.71	indole pyruvate oxidoreductase, alpha subunit
CTER_2214	EC:1.2.7.8	15.81	-0.26	indole pyruvate oxidoreductase, beta subunit
CTER_0199	EC:1.2.7.8	16.2	0.04	indole pyruvate oxidoreductase, alpha subunit
CTER_0198	EC:1.2.7.8	14.64	-0.14	indole pyruvate oxidoreductase, beta subunit
CTER_3763	EC:1.2.7.3	**16.5**	-0.81	2-oxoglutarate:ferredoxin oxidoreductase, alpha subunit
CTER_3762	EC:1.2.7.3	**16.1**	-0.24	2-oxoglutarate:ferredoxin oxidoreductase, beta subunit
CTER_3761	EC:1.2.7.3	15.03	-0.92	2-oxoglutarate:ferredoxin oxidoreductase, gamma subunit

CTER_3589	EC:1.2.7.-	**18.4**	-0.83	putative pyruvate:flavodoxin oxidoreductase
CTER_3764	NA	ND	ND	4Fe-4S ferredoxin (dicluster domain)
CTER_4519	EC:2.3.1.8	**17.45**	-0.53	phosphate acetyltransferase (PTA)
CTER_4518	EC:2.7.2.1	**18.75**	0	acetate kinase (ACK)
CTER_0993	EC:1.2.1.3	14.35	BD	NADH-dependent aldehyde dehydrogenase (Aldh)
CTER_2833	EC:1.2.1.3	**16.25**	2.43	NADH-dependent aldehyde dehydrogenase (Aldh)
CTER_5570	EC:6.2.1.1	**16.6**	0.13	acetyl-coenzyme A synthetase/AMP-dependent
CTER_1865	EC:6.2.1.1	15.14	-0.02	aceyl-coenzyme A synthetase/AMP-dependent
CTER_5426	EC:1.2.1.10	**21.53**	-1.66	bifunctional acetaldehyde/alcohol dehydrogenase (AdhE)
CTER_3280	EC:1.1.1.1	**19.96**	1.04	iron containing alcohol dehydrogenase (Fe-ADH)
CTER_2586	EC:1.1.1.1	**18.08**	-0.06	iron containing alcohol dehydrogenase (Fe-ADH)
CTER_1650	EC:1.1.1.1	11.83	BD	iron containing alcohol dehydrogenase (Fe-ADH)

BD: Below iTRAQ detectable range as only 1 peptide was detected for the protein, the minimum cutoff is atleast 2 peptides.
ND: Not detected in the proteome, but observed in the genome.
NA: Not available.

4.4.3 Pyruvate catabolism, H_2 and ethanol synthesis pathways

Batch fermentation of *C. termitidis* on 2 g L^{-1} α-celluose and cellobiose have shown H_2, CO_2, ethanol, acetate, formate, and lactate as the major end-products from pyruvate catabolism (Ramachandran et al. 2008). Similar to *C. thermocellum* and *C. cellulolyticum*, the carbon flux in *C. termitidis* is regulated through pyruvate:ferredoxin oxidoreductase (PFOR) (see chapter 1, Figure 1.2). In contrast to *C. thermocellum*, one 4-subunit PFOR (EC:1.2.7.1) complex consisting of β, α, δ, and γ encoded by the gene cluster CTER_1022-CTER_1025, was detected at higher abundance across both the growth phases (see log_2TIC values, Table 4.5). Also, two putative 2-subunit PFOR-like oxidoreductases, indole pyruvate oxidoreductase (EC:1.2.7.8) that acts on aldehyde or oxo group of donors with an iron sulfur protein acceptor, was detected with a overall log_2TIC range spanning between 15.2-17.5 (Table 4.5) across both growth conditions. The β and α subunits detected were encoded by the gene clusters CTER_2214-2215 and CTER_0198 and 0199. This enzyme catalyzes the conversion of 3-(indol-3-yl) pyruvate (in the presence of CoA and oxidized ferredoxin) to S-2-(indol-3-yl)acetyl-CoA, CO_2, 2 reduced ferredoxin and H^+.

One putative 3-subunit PFOR-like oxidoreductase complex, 2-oxoglutarate:ferredoxin oxidoreductase (EC:1.2.7.3) consisting of γ, β, and α subunits encoded by gene cluster CTER_3761-3763, was detected at similar levels as that of a putative indole pyruvate oxidoreductase (EC:1.2.7.8). But, when cultured on α-celluose, CTER_3761-3763 was significantly down-regulated during mid-exponential phase. A putative pyruvate:flavodoxin oxidoreductase (CTER_3589) showed higher abundance in the hexose proteome across both growth phases. BLAST analysis of these putative

PFOR-like proteins CTER_3589, CTER_2214-2215, CTER_0198 and 0199, showed sequence homology to pyruvate-dependent PFOR capable of pyruvate conversion to acetyl-CoA in *C. cellulolyticum* (Desvaux 2005, 2006), *C. papyrosolvens* and *C. acetobutylicum* (Meinecke et al. 1989). In contrast, *C. thermocellum* encoded two 4-subunit PFOR complexes in the genome, out of which Cthe_2390-2393 were highly expressed during exponential phase in the hexose proteome. Unlike *C. termitidis*, the hexose proteome of *C. thermocellum* showed three putative single subunit PFOR-like oxidoreductases (EC:1.2.7.3; EC:1.2.7.8) that were detected at higher levels during exponential phase (Rydzak et al. 2012).

In *C. termitidis*, formate is produced via pyruvate formate lyase (PFL) (chapter 1, Figure 1.2) and the genome showed six genes (CTER_0038, CTER_1187, CTER_0232, CTER_3262, CTER_4126, CTER_4127) that encode enzymes classified as pyruvate formate lyase (EC:2.3.1.54). Only, CTER_0038 was observed in high abundance in the hexose proteome across both growth phases. CTER_1187 was below iTRAQ detectable limit in the hexose proteome during mid-exponential phase and remained undetected when the cells reached staionary. During cell growth on α-cellulose, CTER_0038 was significantly down-regulated during mid-exponential phase similar to *C. thermocellum* (Rydzak et al. 2012) and as the cells entered stationary, the levels relatively improved (Table 4.5). This is consistent with the formate synthesis patterns observed during batch fermentation on cellobiose and α-cellulose in *C. termitidis* as increased formate production was obtained after late exponential phase (see chapter 2). Studies have shown that pyruvate formate lyase-1-activating enzyme is necessary for the formation of glycyl radical residue on the C-terminal region on PFL (Vey et al. 2008; Sawers and Bock

1998). In *C. termitidis* genome, two genes (CTER_0037, CTER_2583) encoded PFL-1-activating enzyme (EC:1.97.1.4), but only CTER_0037 was detected in the hexose proteome during both growth phases. Similar to PFL (CTER_0038), CTER_0037 was significantly down-regulated during mid-exponential phase on α-cellulose. Where as, in *C. thermocellum*, four genes were detected in the genome, and only one was detected in the proteome (Rydzal et al. 2012).

In *C. termitidis*, lower levels of lacate dehydrogenase (EC:1.1.1.27; CTER_2504) were detected in the hexose proteome with a overall $\log_2$TIC value of 16.21 during mid-exponential phase and 16.37 (relatively higher) during stationary phase. Based on the Znet scores (Table 4.5), CTER_2504 was significantly down-regulated during mid-exponential phase and stationary phase cultures grown on α-cellulose. This was consistent with the earlier batch experiments in *C. termitidis*, as lactate production was observed only after late exponential-stationary phase on both substrates corresponding to pH drop, and especially on α-cellulose, the total volumetric production was lower than cellobiose (see chapter 2). Studies in *C. thermocellum* (Yang et al. 2012) and *C. saccharolyticus* (Wilquist and van Neil 2010) have shown that lactate dehydrogenase (LDH) is allosterically regulated by fructose-1-6-bisphosphate (in *C. thermocellum*) and ATP, and inhibited by NAD^+ and PP_i (in *C. saccharolyticus*). In *C. termitidis*, this type of allosteric regulation of LDH (CTER_2504) is possible as lower levels of fructose-1-6-bisphosphate aldolase (CTER_4718) was detected during mid-exponential phase on α-cellulose grown cultures. Hence, on cellobiose (high carbon flux), due to increased FBP or ATP concentrations along with the differences in NAD^+ and PP_i ratios, increased

lactate production was observed between late-exponential to stationary phase (see chapter 2).

Acetyl-CoA branch-point is very critical for NADH reoxidation and energy conservaion mechanisms. In *C. termitidis*, conversion of acetyl-CoA to ethanol can occur either via a bifunctional acetaldehyde/alcohol dehydrogenase (EC:1.2.1.10; CTER_5426), or using a NADH-dependent aldehyde dehydrogenase (EC:1.2.1.3; CTER_0993, CTER_2833) first, and then, iron containing alcohol dehydrogenases (EC:1.1.1.1; CTER_3280, CTER_2586, CTER_1650) (see chapter 1, Figure 1.2). CTER_5426 (AdhE), CTER_3280 (Fe-ADH), and CTER_2586 (Fe-ADH) were observed in high abundance in the hexose proteome compared to CTER_0993 and CTER_2833 (AldH) across both growth phases (see log_2TIC values, Table 4.5) and these results were similar to *C. thermocellum* (Rydzak et al. 2012). Where as, CTER_1650 (Fe-ADH) was undetected in the proteome (both cellulose and cellobiose substrates) during mid-exponential phase, but, was observed in very low amounts in stationary phase. When the cells were cultured on α-cellulose, CTER_5426 (AdhE) was observed at highr abundance with not much significant change compared to CTER_3280 (Fe-ADH) across both conditions during mid-exponential phase. This suggests that ethanol production is preferred via AdhE in *C. termitidis* during cellobiose and cellulose fermentation. These findings are consistent with the end-product synthesis patterns as increased concentrations of H_2/acetate and lower amounts of ethanol was observed during cellulose fermentation (chapter 2).

In *C. termitidis*, acetate production occurs in two steps; 1) conversion of acetyl-CoA to acetyl phosphate via phosphotransacetylase (PTA) or also called as phosphate

acetyltransferase (EC:2.3.1.8; CTER_4519; and 2) conversion of acetyl phosphate to acetate via acetate kinase (EC:2.7.2.1; CTER_4518) (see chapter 1, Figure 1.2). Direct conversion of acetyl-CoA to acetate is not possible in *C. termitidis* due to the absence of acetate thiokinase (ATK), where as *C. thermocellum* encodes all the three enzymes involved during acetate formation in the genome (Lamed and Zeikus 1980; Lin et al. 1998) and proteome (Rydzak et al. 2012). In *C. termitidis*, although, CTER_4519 (PTA) and CTER_4518 (ACK) were detected at higher levels during both mid-exponential and stationary phases (Table 4.5), there was no significant differences in their relative expression between α-cellulose and cellobiose grown cultures. This correlated with end-product analysis as consistent H_2 production was observed during fermentation on both the susbtrates (see chapter 2).

In *C. termtidis*, four putative multisubunit hydrogenases, including three iron only (Fe-Fe) ferredoxin-dependent hydrogenases: i) CTER_4847-4850; ii) CTER_4761-62; iii) CTER_2461-2462, and 1 multisubunit energy conserving Ech-like nickel iron (Ni-Fe) hydrogenase, were identified in the genome and proteome. Exceptions include catalytic subunits CTER_4765 and CTER_2463 that were not detected in the hexose proteome. The multisubunit Fe-Fe hydrogenase (CTER_4847-4850) was detected in higher amounts compared to the other types in the hexose (cellobiose and cellulose) proteome during both mid-exponential and stationary phase cultures and is most likely the major hydrogenase (Table 4.6). There were no significant expressional differences between the Fe-Fe only and Ech hydrogenases, when cultured on both α-cellulose and cellobiose. CTER_2461-63 and CTER_4761-62 were not detected during stationary phase on both the substrates. Among the different catalytic subunits in the Ni-Fe hydrogenase,

CTER_3894 was undetected during stationary phase on α-cellulose and cellobiose (Table 4.6). In contrast, only three catalytic subunits of Fe-Fe only hydrogenase and one multisubunit Ech-like ferredoxin dependent hydrogenases were observed in *C. thermocellum*, and only the Fe-Fe only hydrogenase catalytic subunits were detected at higher levels in the proteome (Rydzak et al. 2012). In order to clearly elucidate the cofactor specificity and regulation of these hydrogenases, enzyme assays and biochemical characterization of these enzymes have to perfomed with *C. termtidis* in the future.

Table 4.6 An overview of hydrogenases in the Genome and Proteome in *C. termitidis*. This table shows log_2TIC and Znet scores of hydrogenases involved in involved in hydrogen sysnthesis in both mid-exponential and stationary phases of α-cellulose versus cellobiose grown cultures of *C. termitidis*. The log_2TIC values in bold correspond to highly abundant proteins across both growth conditions.

Locus Tag	EC No.	log_2TIC	Znet	Name of the protein
			Mid-exponential phase	
CTER_4848	NA	**20.44**	-0.55	iron only hydrogenase (Fe-Fe), ferredoxin-dependent
CTER_4847	NA	**15.42**	-0.65	(Fe-Fe) hydrogenase, ferredoxin-dependent, 24 KD subunit
CTER_4849	NA	**20.95**	-0.65	(Fe-Fe) hydrogenase, ferredoxin-dependent, 51 KD subunit
CTER_4850	NA	**18.28**	-1.29	(Fe-Fe) hydrogenase, ferredoxin-dependent, 24 KD subunit
CTER_4761	NA	14.16	-0.05	iron only hydrogenase, iron-sulfur binding domain (2Fe-2S), 30 KD
CTER_4762	NA	13.85	0.87	iron only hydrogenase, iron-sulfur binding domain (2Fe-2S), 51 KD
CTER_4765	NA	ND	ND	iron only hydrogenase, iron-sulfur binding domain (2Fe-2S), 24 KD
CTER_2461	NA	14.85	-1.31	iron only hydrogenase, iron-sulfur binding domain (2Fe-2S), 30 KD
CTER_2462	NA	13	BD	iron only hydrogenase, iron-sulfur binding domain (2Fe-2S), 51 KD
CTER_2463	NA	ND	ND	iron only hydrogenase, iron-sulfur binding domain (2Fe-2S), 24 KD
CTER_2553	NA	15.2	1.42	iron only hydrogenase, iron-sulfur binding domain (2Fe-2S), 51 KD
CTER_3893	NA	15.17	-0.35	nickel-iron hydrogenase (Ni-Fe), 49 KD subunit
CTER_3894	NA	13	BD	nickel-iron hydrogenase (Ni-Fe), 30 KD subunit
CTER_3895	NA	14.15	0.25	nickel-iron hydrogenase (Ni-Fe), 20 KD subunit
CTER_0657	NA	13.7	0.22	nickel-iron hydrogenase (Ni-Fe), 49 KD subunit

Stationary phase

CTER_4848	NA	**20.46**	-0.82	iron only hydrogenase (Fe-Fe), ferredoxin-dependent
CTER_4847	NA	15.3	-0.29	(Fe-Fe) hydrogenase, ferredoxin-dependent, 24 KD subunit
CTER_4849	NA	**20.6**	-0.86	(Fe-Fe) hydrogenase, ferredoxin-dependent, 51 KD subunit
CTER_4850	NA	**18.06**	-0.99	(Fe-Fe) hydrogenase, ferredoxin-dependent, 24 KD subunit
CTER_4761	NA	ND	ND	iron only hydrogenase, iron-sulfur binding domain (2Fe-2S), 30 KD
CTER_4762	NA	ND	ND	iron only hydrogenase, iron-sulfur binding domain (2Fe-2S), 51 KD
CTER_4765	NA	ND	ND	iron only hydrogenase, iron-sulfur binding domain (2Fe-2S), 24 KD
CTER_2461	NA	ND	ND	iron only hydrogenase, iron-sulfur binding domain (2Fe-2S), 30 KD
CTER_2462	NA	ND	ND	iron only hydrogenase, iron-sulfur binding domain (2Fe-2S), 51 KD
CTER_2463	NA	ND	ND	iron only hydrogenase, iron-sulfur binding domain (2Fe-2S), 24 KD
CTER_2553	NA	15.29	0.19	iron only hydrogenase, iron-sulfur binding domain (2Fe-2S), 51 KD
CTER_3893	NA	15.46	-0.31	nickel-iron hydrogenase (Ni-Fe), 49 KD subunit
CTER_3894	NA	ND	ND	nickel-iron hydrogenase (Ni-Fe), 30 KD subunit
CTER_3895	NA	14.1	BD	nickel-iron hydrogenase (Ni-Fe), 20 KD subunit
CTER_0657	NA	15.76	-0.21	nickel-iron hydrogenase (Ni-Fe), 49 KD subunit

BD: Below iTRAQ detectable range as only 1 peptide was detected for the protein, the minimum cutoff is atleast 2 peptides.
ND: Not detected in the proteome, but observed in the genome.
NA: Not available.

4.5 Conclusions

In this chapter, an in-depth quantitative proteomic analysis was performed on the mesophilic, cellulolytic bacterium *C. termitidis* for the first time to understand the differential expression of gene and gene products involved in core metabolic pathways, and its relation to thermodynamics of end-product formation. Two dimensional RP-HPLC/MS/MS after iTRAQ labeling was performed on mid-exponential and stationary phase samples cultured on 2 g L^{-1} cellobiose and α-cellulose. The log_2TIC values obtained for all the identified proteins determine the relative abundance across both conditions, where as Znet scores determine the relative expression on α-cellulose with respect to cellobiose.

Most of the proteins involved in glycolysis, pyruvate catabolism, malate transhydrogenase pathway, H_2 and ethanol synthesis pathways did not change across both growth conditions, but there were a few exceptions. The regulation of carbon flux through PFOR seemed to be very crucial as higher levels of PFOR was detected across both conditions. Ethanol synthesis occurred via AdhE during cellobiose and cellulose fermentation. Although both AdhE and Fe-ADH were detected at higher abundance on cellulose grown cultures, AdhE acitivity was lower when compared to cellobiose during both growth phases. Acetate was produced via PTA/AK and their levels were higher in both growth condtions. This was consistent with the metabolic profiling, as increased amounts of acetate and lower ethanol concentrations corresponded to increased H_2 production on α-cellulose. H_2 synthesis occurs via ferredoxin-dependent hydrogenase, but further experimental analysis is required to clearly define its regulatory functions with respect to cofactor specificity. These findings correlate well with the end-product

synthesis patterns exhibited by *C. termtidis* on the two susbtrates. Hence, knowledge of the proteome along with further biochemical characterization of enzymes, transcriptome or metabolome analysis could be a very powerful strategy to manage and regulate carbon and electron flux for the optimized synthesis of biofuels and other desired end-products.

Chapter 5: Proteomic analyses of *Clostridium termitidis* strain CT1112 cells cultured on hexose sugars reveal sequential pentose and hexose fermentation

This Chapter is based, in-part, on the following publication: "Ramachandran, U., Blunt, W., Shamshurin, D., Spicer, V., Ezzati, P., Krokhin, O.V., Wilkins, J.A., Cicek, N., Sparling, R., and Levin, D.B. 2013. Proteomic analyses of *Clostridium termitidis* strain CT1112 cells cultured on hexose sugars reveal sequential pentose and hexose fermentation. BMC Microbiology (submitted)."

5.1 Abstract

Initial characterization of *Clostridium termitidis*, a mesophilic, anaerobic, and cellulolytic bacterium, has demonstrated its ability to produce hydrogen, ethanol, and various other soluble end-products on substrates containing hexose sugars like cellobiose and α-cellulose. In this chapter, we present proteomic evidence that putative proteins consistent with xylose fermentation were found at high levels when cells were grown on hexoses (cellobiose and α-cellulose) in the absence of added xylose. This led to the hypothesis that simultaneous fermentation of pentoses and hexoses should be possible in this organism, which we confirmed using experiments using growth, end-product synthesis and substrate depletion. We also demonstrate the organism's capability to ferment xylan. Quantitative proteomic analysis, using 4-plex 2D-HPLC-MS/MS, of *C. termitidis* cultures containing 2 g L^{-1} α-cellulose or 2 g L^{-1} cellobiose showed significant expression of enzymes regulating xylose metabolism via the pentose/glucoronate interconversion and pentose phosphate pathways. An in-house GPU-based peptide/protein identification engine and analysis workflow elucidated differential expression levels (Z-scores) for enzymes related to xylose uptake, transport, and

metabolism. The *C. termitidis* genome revealed the presence of xylose uptake transporters that belonged to the ABC (ATP-binding cassette) superfamily whose presence was confirmed in the proteome leading to the possibility of simultaneous utilization of xylose and cellobiose. As confirmation, growth characteristics and end-product (H_2, CO_2, acetate, formate, and ethanol) synthesis patterns of *C. termitidis* grown in batch cultures with 1 g L^{-1} xylose, cellobiose, xylose + cellobiose (mixed substrate), or xylan were determined. The growth on mixed substrate showed simultaneous utilization of hexose and pentose sugars for the first time. The maximum concentrations of H_2, CO_2, and ethanol on 1 g L^{-1} xylose were 8.78 ± 0.45, 5.35 ± 0.99, and 3.07 ± 0.36 mmol L^{-1} culture, respectively, where as on 1 g L^{-1} xylan, concentrations were 5.37 ± 0.20, 3.49 ± 0.18, and 1.57 ± 0.11 mmol L^{-1} culture, respectively. Although the maximum concentrations of H_2, CO_2, and ethanol were similar in cultures with xylose compared to cellobiose, the volumetric production rates were higher (0.43 ± 0.08, 0.33 ± 0.05, and 0.27 ± 0.04 mmol product L^{-1} culture h^{-1}, respectively).

5.2 Introduction

Plant cell walls consist of cellulose (cellobiose), hemicellulose (xyloglucan, arabinoxylan, and glucomannan), pectin (homogalacturonan, rhamnogalacturonan, and xylogalacturonan), lignin, and proteoglycan. The crystallinity of cellulose and its structural organization with hemicellulose make it more challenging for cellulolytic bacteria to breakdown these complex polymers to release hexose and pentose sugars used for fermentation (Houghton et al. 2006). Recent advances in "Omic" technologies (bioinformatics, genomics, proteomics, transcriptomics, and metabolomics) have facilitated a deeper understanding of central carbon metabolism in bacteria, leading to rational strategies for engineering biosynthetic pathways to generate desired end-products like hydrogen, ethanol, and other value-added co-products (Yan and Liao 2009; Lee et al. 2008).

We have used proteomic and genomic approaches to elucidate simultaneous hexose and pentose fermentation abilities in a mesophilic, anaerobic, cellulolytic bacterium, *Clostridium termitidis* initially characterized by Hethener et al. (1992). Further characterization by Ramachandran et al. (2008) indicated that it can synthesize hydrogen (H_2) and ethanol. Whole genome sequence analysis and shotgun proteomic analyses led us to investigate the ability of *C. termitidis* to utilize xylose and xylan as substrates. Use of xylan by *C. termitidis* had not previously been reported.

Cultures grown on 2 g L^{-1} α-cellulose and cellobiose, respectively, were subjected to differential protein expression analysis using 2D-HPLC-MS/MS with 4-plex iTRAQ. Protein identification and quantification using an in-house GPU-based peptide identification engine (McQueen et al. 2012) revealed significant differential expression of

proteins involved in xylose metabolism via pentose phosphate and pentose/glucoronate interconversion pathways in *C. termitidis*, even in the absence of pentose in the medium. An overview of the draft annotation revealed a large population of genes encoding the ABC superfamily, among which, xylose transporter proteins necessary for xylose uptake and transport across the cytoplasmic membrane were identified. To further validate simultaneous hexose and pentose metabolism, batch fermentation and end-product analysis were performed with *C. termitidis* cultures grown on xylose, cellobiose, xylan, or xylose + cellobiose.

5.3 Materials and Methods

5.3.1 Microbial source, media, and growth

The type strain of *Clostridium termitidis* CT1112 was obtained from American Type Culture Collection (ATCC 51846). Most of the reagents and chemicals for media and substrates for hexose proteomic experiments were used as described earlier in chapter 4 (section 4.3.1). Culture stocks, handling, passaging, sampling time, sample preparation for protein, HPLC, and GC analyses were exactly similar to the methods described earlier in chapter 4 (section 4.3.1).

Batch experiments to investigate the ability of *C. termitidis* to utilize xylose were conducted in Balch tubes (Bellco Glass Co.) with a total working volume of 27 mL. Sterile, anaerobic cellobiose and xylose were added to the tubes containing 9 mL 1191 medium as previously described (chapter 2) to a final concentration of 1 g L^{-1} and were incubated at 37 °C for 32-36 h. Where as, for the mixed substrate cellobiose plus xylose (at 1:1 ratio), 1 g L^{-1} anaerobic cellobiose (2.9 mM; 5.8 mM hexose equivalents) and 1 g L^{-1} anaerobic xylose (6.7 mM; 5.6 mM hexose equivalents) were added so that the final

concentration was 2 g L^{-1} (11.4 mM hexose equivalents). These were incubated under same conditions. Beechwood Xylan (Sigma Aldrich) was added as a powder to a final concentration of 1 g L^{-1} before autoclaving. During the experiment, three independent biological replicate samples were taken every 4 h until the stationary phase was reached.

5.3.2 Cell growth and pH measurements

Optical density, Bradford and pH measurements were determined as described in chapter 4 (section 4.3.2). The instruements used are also described in the same section as above.

5.3.3 Soluble and gaseous end-products analysis

The supernatants obtained for the batch experiments used to detect pentose utilization were analyzed for detecting soluble end-products based on the protocols described previously (chapter 2). HPLC and GC analysis were performed as per the instruements and methods described in chapter 4 (section 4.3.3).

5.3.4 Protein isolation, purification, and quantitation

The methods, materials, equipments, reagents, assay kits for protein isolation, purification, quantitation, and iTRAQ labeling were exactly similar to that described in chapter 4 (section 4.3.4).

5.3.5 2-D Liquid chromatography-mass spectrometry analysis

After labeling, the peptides were desalted and separated in two dimensions according to the protocols described in chapter 4 (section 4.3.5). The concentrations of all the buffers and the methods used for peptide fractionation were similar to the procedures as described in the same section mentioned above.

5.3.6 Protein identification and statistical analysis

After performing deep 2-D LC/MS/MS, step-by-step analysis of the raw data using statistical methods and softwares was done as per procedures described in chapter 4 (section 4.3.6). Following required criteria and search parameters, the peptideswere identified using specific search engines against the *C. termitidis* genome (AORV00000000) (Lal et al. 2013). Also, log_2TIC and Z-scores for identified proteins were further calculated. All the methods for protein identification and statistical analysis are similar to chapter 4 (section 4.3.6).

5.4 Results and Discussion

5.4.1 Proteomic analyses of *C. termitidis* reveal sequential xylose and hexose utilization

The initial characterization of *C. termitidis* showed growth with xylose as a carbon source (Hethener et al. 1992). Nevertheless, the current whole genome analysis of *C. termitidis* revealed all the genes necessary for xylose utilization except for a transaldolase encoding gene. Likewise, two-dimensional iTRAQ analysis displayed a high abundance of most of the proteins associated with pentose interconversion and subsequent metabolism in the pentose phosphate pathway except for transaldolase (EC 2.2.1.2) in both mid-exponential and stationary phases (Figure 5.1, Table 5.1), and across both growth conditions tested (α-cellulose and cellobiose grown cultures). In the mid-exponential experiment, xylose isomerase (EC 5.3.1.5) was in the top 75 (of ~ 2000) proteins of both the *C. termitidis* α-cellulose and cellobiose samples based on the integration of their iTRAQ reporter intensities alone. An overall log_2 TIC value of 19.6 (over a range spanning from 11.6-23.7) indicated the relatively high representation of

xylose isomerase under both conditions, while the Znet score (Table 5.1) indicates there was a significant up-regulation of protein expression when the cells grow on α-cellulose. The log_2TIC values correlate well across the proteins involved in pentose metabolism and transport between the growth phases (Tables 5.1 and 5.2).

Due to the absence of transaldolase (EC 2.2.1.2), *C. termitidis* utilizes a possible alternative pathway for sedoheptulose-7-phosphate breakdown (Figure 5.1). Recent studies in *E. coli* have shown that a bifunctional ATP-dependent 6-phoshofructokinase (EC 2.7.1.11) can phosphorylate sedoheptulose-7-phosphate into sedoheptulose-1,7-bisphosphate in transaldolase-deficient mutants (Nakahigashi et al. 2009). Further, sedoheptulose-1,7-bisphosphate is converted to erythrose-4-phosphate and dihydroxyacetone phosphate in the presence of bifunctional fructose-1,6-bisphosphate aldolase (EC 4.1.2.13). Subsequently, transketolase (EC 2.2.1.1) catalyzes the conversion of erythrose-4-phosphate into glyceraldehyde-3-phosphate and fructose-6-phosphate, which enters glycolysis (Figure 5.1). This type of alternate pathway was also observed in a lower algal species, *Cyanophora paradoxa*, in which transaldolase was replaced by bifunctional fructose-1,6-bisphosphate class II aldolases for sedoheptulose-1,7-bisphosphate breakdown (Fletchner et al. 1999).

In *C. termitidis*, the two glycolytic proteins, 6-phoshofructokinase (EC 2.7.1.11) and fructose-1,6-bisphosphate aldolase (EC 4.1.2.13), were observed in high abundance in the hexose proteome (Table 5.1). Three genes (CTER_0067, CTER_4719, CTER_5379) in the *C. termitidis* genome encode enzymes classified as 6-phoshofructokinases (EC 2.7.1.11) and two genes (CTER_4718, CTER_1264) encode fructose-1,6-bisphosphate aldolases (EC 4.1.2.13). All of the genes belonging to enzyme

classes EC 2.7.1.11 and EC 4.1.2.13 were also detected in the proteome, except for CTER_5379. Ribulose-5-phosphate 3-epimerase (EC 5.1.3.1) was below detectable limits in the hexose proteome until stationary phase was reached.

Both *C. termitidis* and *C. thermocellum* lack an overt transaldolase in their respective genomes. However, in contrast to *C. thermocellum*, the non-oxidative branch of the pentose phosphate pathway in *C. termitidis* is expected to generate essential intermediates such as ribose-5-phosphate and erythrose-4-phosphate, since it expresses all the genes needed for pentose interconversion (Rydzak et al. 2012; Carere et al. 2012). In *C. termitidis*, there were multiple genes detected in the genome for the different subunits of transketolase (2.2.1.1) in both mid-exponential and stationary phases. All other subunits, except for CTER_5397 in the mid-exponential phase and CTER_5396 (CTER_5396-5397), CTER_1675 (CTER_1675-1676), and CTER_4233 (CTER_4233-4234) in the stationary phase, were not detected in the proteome. In contrast, two-dimensional iTRAQ analyses of *C. thermocellum* cellobiose grown cultures sampled during exponential phase revealed higher expression levels of one of the two transketolases (Cthe_2704-2705), while the other transketolase (Cthe_2444) was detected in lower amounts. Also, ribose 5-phosphate isomerase was detected in the proteome, whereas ribose 5-phosphate epimerase was present in the genome, but undetected in the proteome (Rydzak et al. 2012).

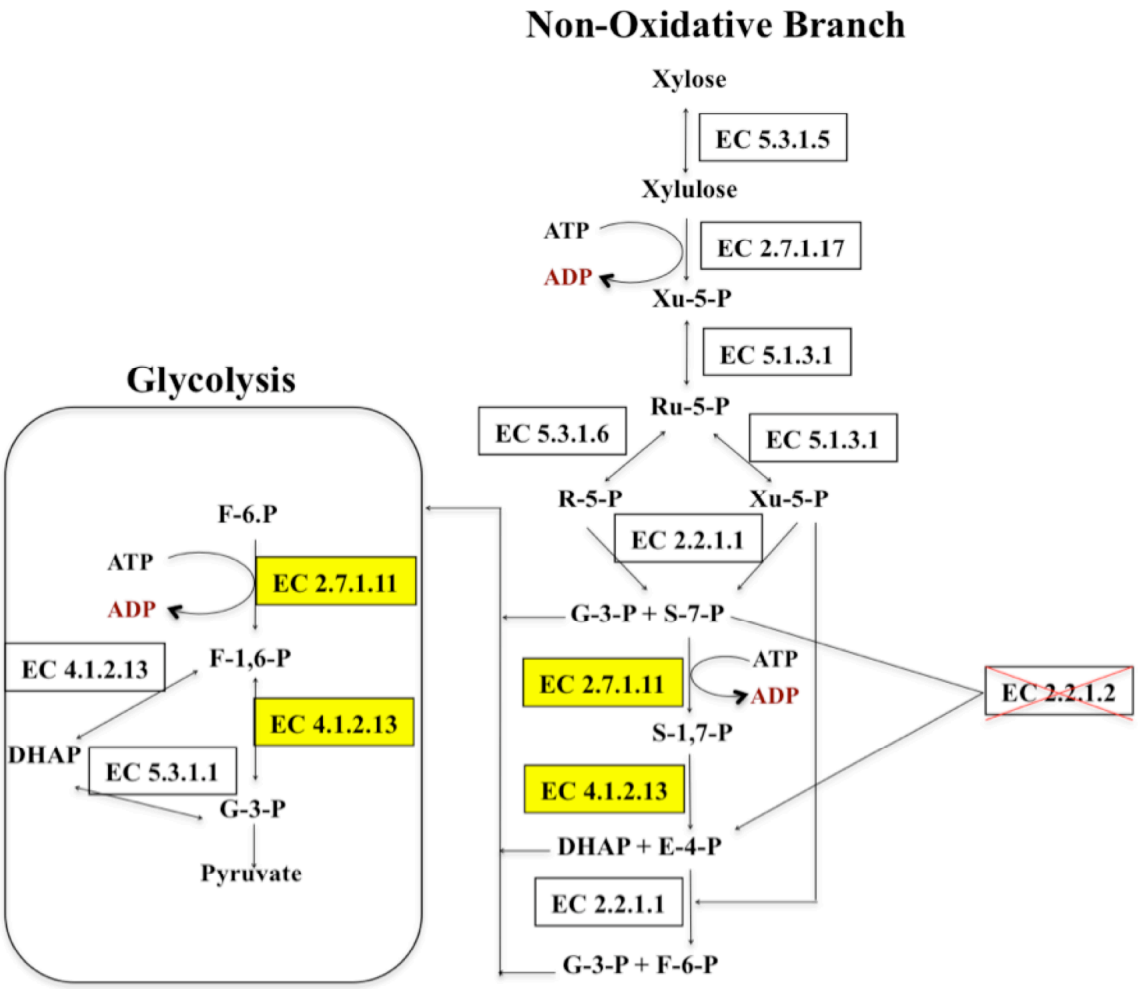

Figure 5.1 Pentose interconversion and Pentose phosphate pathway in *C. termitidis*. This figure indicates all possible proteins associated with xylose metabolism. In this putative model, transaldolase (EC 2.2.1.2) is absent and replaced by ATP-dependent 6-phosphofructokinase (EC 2.7.1.11) and fructose-1,6-bisphosphate aldolase (2.7.1.11) that catalyzes the conversion of sedoheptulose-7-phosphate (S-7-P) to erythrose-4-phosphate (E-4-P) and dihydroxyacetone phosphate (DHAP). E-4-P is further converted to glyceraldehyde-3-P (G-3-P) and fructose-6-phosphate (F-6-P) in the presence of transketolase (2.2.1.1), which further enters glycolysis.

Table 5.1 Proteins involved in Xylose metabolism in the Genome and Proteome in *C. termitidis*. This table shows log2TIC and Znet scores of proteins involved in pentose interconversion and subsequent metabolism using pentose phosphate pathway in both mid-exponential and stationary phases of α-cellulose versus cellobiose grown cultures of *C. termitidis*. The log_2TIC values in bold correspond to highly abundant proteins across both growth conditions.

Locus Tag	EC No.	log2TIC	Znet	Name of the protein
		Mid-exponential phase		
CTER_2434	EC:3.2.1.8	**18.3**	2.02	beta-1,4-xylanase
CTER_2436	EC:3.2.1.8	12.46	0.05	beta-1,4-xylanase
CTER_1803	EC:3.2.1.8	12.56	0.93	beta-1,4-xylanase
CTER_1086	NA	14.96	0.02	putative xylanase/chitin deacetylase
CTER_5018	NA	12.89	BD	putative xylanase/chitin deacetylase
CTER_4329	EC:5.3.1.5	**19.69**	2	xylose isomerase
CTER_4331	EC:2.7.1.17	**18.3**	1.86	D-xylulose kinase
CTER_4934	EC:5.1.3.1	14	BD	ribulose-phosphate 3-epimerase
CTER_2022	EC:5.3.1.6	14.06	-0.7	ribose 5-phosphate isomerase B
CTER_4017	EC:2.7.6.1	**16.59**	-0.59	ribose-phosphate pyrophosphokinase
CTER_2745	EC:2.2.1.1	**19.29**	0.62	transketolase
CTER_4974	EC:2.2.1.1	12.91	BD	transketolase N-terminal subunit

CTER_4973	EC:2.2.1.1	12.8	BD	transketolase C-terminal subunit
CTER_3783	EC:2.2.1.1	13.29	BD	transketolase N-terminal subunit
CTER_5397	EC:2.2.1.1	ND	ND	transketolase N-terminal subunit
CTER_5396	EC:2.2.1.1	12.8	BD	transketolase C-terminal subunit
CTER_4718	EC:4.1.2.13	**21.06**	-0.08	fructose-1,6-bisphosphate aldolase, class II
CTER_1264	EC:4.1.2.13	**18.09**	0.81	fructose-1,6-bisphosphate aldolase
CTER_0067	EC:4.1.2.4	**18.44**	-0.41	6-phosphofructokinase
CTER_4719	EC:4.1.2.4	**20.39**	-0.41	6-phosphofructokinase
CTER_5379	EC:4.1.2.4	ND	ND	6-phosphofructokinase
		Stationary phase		
CTER_2434	EC:3.2.1.8	**17.74**	1.97	beta-1,4-xylanase
CTER_1803	EC:3.2.1.8	13.12	4.56	beta-1,4-xylanase
CTER_1086	NA	15.81	-0.18	putative xylanase/chitin deacetylase
CTER_5018	NA	15.82	2.1	putative xylanase/chitin deacetylase
CTER_4776	NA	13.2	BD	putative xylanase/chitin deacetylase
CTER_4329	EC:5.3.1.5	**19.02**	2.27	xylose isomerase
CTER_4331	EC:2.7.1.17	**17.36**	1.86	D-xylulose kinase
CTER_4934	EC:5.1.3.1	14.92	0.22	ribulose-phosphate 3-epimerase
CTER_2022	EC:5.3.1.6	14.91	-0.84	ribose 5-phosphate isomerase B
CTER_4017	EC:2.7.6.1	**17.36**	-0.02	ribose-phosphate pyrophosphokinase
CTER_2745	EC:2.2.1.1	**18.54**	0.33	transketolase
CTER_4974	EC:2.2.1.1	15.3	1.37	transketolase N-terminal subunit
CTER_4973	EC:2.2.1.1	15.93	1.96	transketolase C-terminal subunit

CTER_4234	EC:2.2.1.1	13.02	BD	transketolase N-terminal subunit
CTER_4233	EC:2.2.1.1	ND	ND	transketolase C-terminal subunit
CTER_5397	EC:2.2.1.1	12.84	BD	transketolase N-terminal subunit
CTER_5396	EC:2.2.1.1	ND	ND	transketolase C-terminal subunit
CTER_1676	EC:2.2.1.1	12.74	BD	transketolase N-terminal subunit
CTER_1675	EC:2.2.1.1	ND	ND	transketolase C-terminal subunit
CTER_4718	EC:4.1.2.13	**19.88**	-0.01	fructose-1,6-bisphosphate aldolase, class II
CTER_1264	EC:4.1.2.13	**17.82**	0.12	fructose-1,6-bisphosphate aldolase
CTER_0067	EC:4.1.2.4	**18.09**	-0.77	6-phosphofructokinase
CTER_4719	EC:4.1.2.4	**19.42**	0.17	6-phosphofructokinase
CTER_5379	EC:4.1.2.4	ND		6-phosphofructokinase

BD: Below iTRAQ detectable range as only 1 peptide was detected for the protein, the minimum cutoff is atleast 2 peptides.
ND: Not detected in the proteome, but observed in the genome.
NA: Not available.

Table 5.2 Proteomic analysis of xylose transporters in *C. termitidis*. The major components of ABC-type transporters are observed in the *C. termitidis* proteome specific for xylose uptake during mid-exponential and stationary phases of α-cellulose versus cellobiose grown cultures of *C. termitidis*. The log_2TIC values in bold correspond to highly abundant proteins across both growth conditions.

Locus Tag	log2TIC	Znet	Name of the protein
			Mid-exponential phase
CTER_0912	**15.83**	1.07	ABC-type xylose transport system, periplasmic component
CTER_0914	**18.37**	2.31	ABC-type xylose transport system, periplasmic component
CTER_0915	**15.64**	0.68	ABC-type xylose transport system, ATPase component
CTER_0916	14.59	0.85	ABC-type xylose transport system, permease component
CTER_5427	14.77	-1.49	ABC-type xylose transport system, permease component
CTER_5428	**18.68**	-1.47	ABC-type xylose transport system, ATPase component
CTER_5429	**19.29**	-1.41	ABC-type xylose transport system, periplasmic component
			Stationary phase
CTER_0912	**15.34**	1.44	ABC-type xylose transport system, periplasmic component
CTER_0914	**18.11**	2.36	ABC-type xylose transport system, periplasmic component
CTER_5427	14.45	-0.9	ABC-type xylose transport system, permease component
CTER_5428	**18.68**	-1.9	ABC-type xylose transport system, ATPase component
CTER_5429	**19.89**	-1.88	ABC-type xylose transport system, periplasmic component

Among the 712 putative ABC-type transporters (see appendix, supplementary Table 1), two putative operons including a periplasmic component, ATP-binding domain, and the permease component, were detected in the genome. Based on the log_2TIC, which is the sum of all the peptides detected across both α-cellulose and cellobiose growth conditions, the gene products of operon 1 (CTER_0912-0916) and operon 2 (CTER_5427-5429) were detected in high abundance in mid-exponential phase (Table 5.2). In stationary phase, the gene products of operon 2 remained in high abundance, however the gene products of CTER_0915 and CTER_0916 from operon 1 were undetectable. Based on the Znet scores, operon 1 was up-regulated in the α-cellulose grown cultures compared with cellobiose grown cells (Table 5.2).

In *C. termitidis*, mid-exponential and stationary phase cultures, β-1,4-xylanase (EC 3.2.1.8) was observed in abundance in both genome and proteome (Table 5.1). Multiple genes (CTER_2434, CTER_2436, CTER_1803) encode EC 3.2.1.8 family enzymes in the *C. termitidis* genome and of these, CTER_2434 was up-regulated in α-cellulose compared with cellobiose grown cultures in mid-exponetial phase, whereas the gene product of CTER_1803 was up-regulated in stationary phase cultures of α-cellulose only.

In this study, *C. termitidis* was grown on α-cellulose and cellobiose (hexose sugar carbon sources). Despite the absence of added xylose in the medium, up-regulation of xylanases and other key enzymes associated with xylose metabolism was observed on α-cellulose grown cells. A possible explanation for these observations could be that *C. termitidis* encounters both cellulose and hemicellulose components in naturally occurring lignocellulosic substrates. This suggests that the presence of cellulose triggers expression

of enzymes associated with xylan hydrolysis. Hence, bioinformatic and proteomic analyses have provided new insights into the central carbon metabolism of *C. termitidis*, especially with respect to the xylose utilization pathway, as described in Figure 5.1. The presence of a putative functional pathway for xylose fermentation, including the uptake system, would indicate the possibility for co-utilization of xylose and cellobiose, a useful feature for consolidated bioprocessing of raw lignocellulolytic substrates.

5.4.2 Growth characteristics

Cell growth was quantified for each substrate by measuring optical densities (OD_{600}) and protein concentration, as quantified using the Modified Bradford Method (Bradford 1976) (Figures 5.2 A-D). Cultures containing xylose and xylan showed no lag phase and reached stationary phase by 20 h, with a maximum OD_{600} of 0.47 ± 0.05 and 0.40 ± 0.01, respectively, and a maximum protein concentration of 46.04 ± 5.90 μg/mL and 38.67 ± 4.14 μg mL^{-1}, respectively. The cellobiose grown cultures also displayed no lag phase and reached stationary phase at 28 h, with a maximum OD_{600} of 0.49 ± 0.15 and a protein concentration of 32.95 ± 2.70 μg mL^{-1} (Table 5.3).

The protein content for all substrates was found to be significantly less than the values for *C. termitidis* growth on cellobiose reported by Ramachandran et al. (2008). This may be attributed to the fact that this work was done with 1 g L^{-1} of cellobiose, whereas the previous work was done with 2 g L^{-1} cellobiose. This explanation does not account for why only slightly higher protein contents were found in 1 g L^{-1} xylose + 1 g L^{-1} cellobiose, unless preferential uptake of a single substrate limited growth. The maximum OD_{600} values, however, obtained by *C. termitidis* cultures grown on the mixed substrate were identical.

Generation times for *C. termitidis* cultures grown with cellobiose, xylose and xylose + cellobiose, were found to be 7.0 ± 0.5, 6.3 ± 0.2, and 7.2 ± 0.7 h g^{-1}, respectively. These values closely correspond with the 6.9 h generation time reported by Ramachandran et al. (2008) for *C. termitidis* cultured on 2 g L^{-1} cellobiose. Interestingly, the generation time for *C. termitidis* cultures grown with the insoluble substrate xylan (polymer) was found to be 7.1 ± 0.3 h g^{-1}, a value that is more comparable to those reported for soluble substrates than insoluble substrates, such as the doubling-time of 18.9 h reported by Ramachandran et al. (2008) for growth of *C. termitidis* on α-cellulose. Lin et al. (2011) studied *Thermoanaerobacter* sp. X514 for its capability to simultaneously utilize pentose and hexose sugars. Growth was quantified on glucose, xylose, fructose, cellobiose, and several combinations of glucose + xylose together. When cultured on 50 mM (17.1 g L^{-1}) cellobiose, the maximum OD reached was 0.25 and the cells entered stationary phase by 38-40 h of growth. Monosaccharide sugars including 50 mM (7.5 g L^{-1}) xylose reached a maximum OD of 0.3, with the stationary phase reaching around 25-30 h of growth. The cultures on 50 mM glucose (9 g L^{-1}) + 50 mM xylose exhibited co-utilization of both the substrates and reached a maximum OD of 0.35 and stationary phase was reached between 28-30 h of growth. Batch experiments of *C. termitidis* showed a similar phenomenon of co-utilization of hexoses and pentoses when cultured on mixed substrate containing xylose and cellobiose.

A)

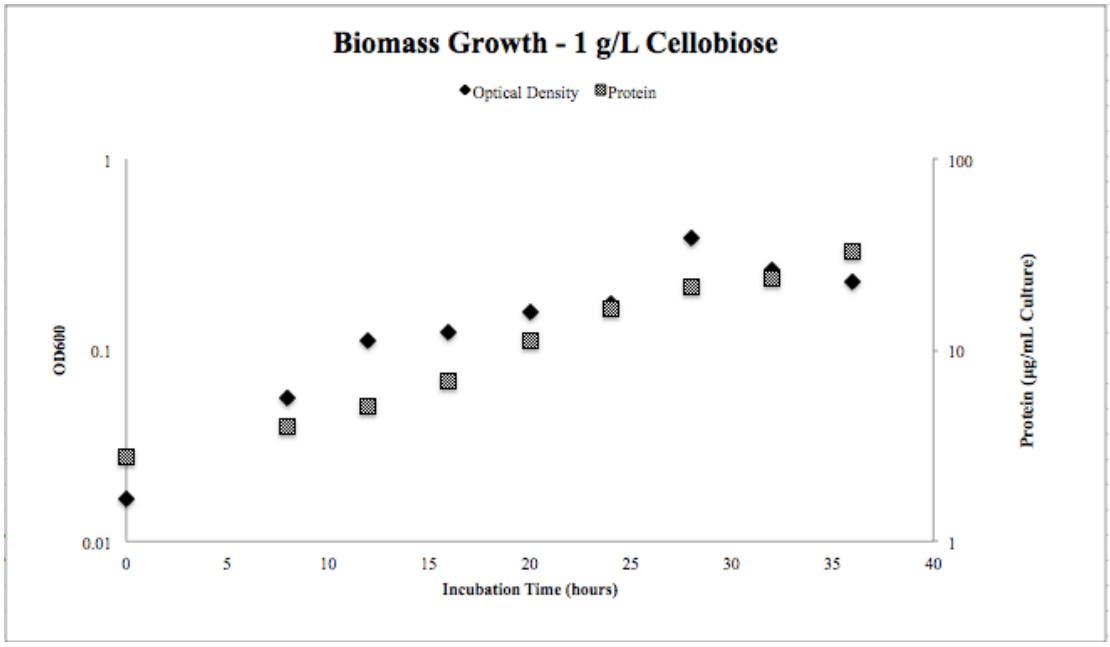
Biomass Growth - 1 g/L Cellobiose
Optical Density
Protein
OD600
Protein (µg/mL Culture)
Incubation Time (hours)
1
0.1
0.01
100
10
1
0
5
10
15
20
25
30
35
40

B)

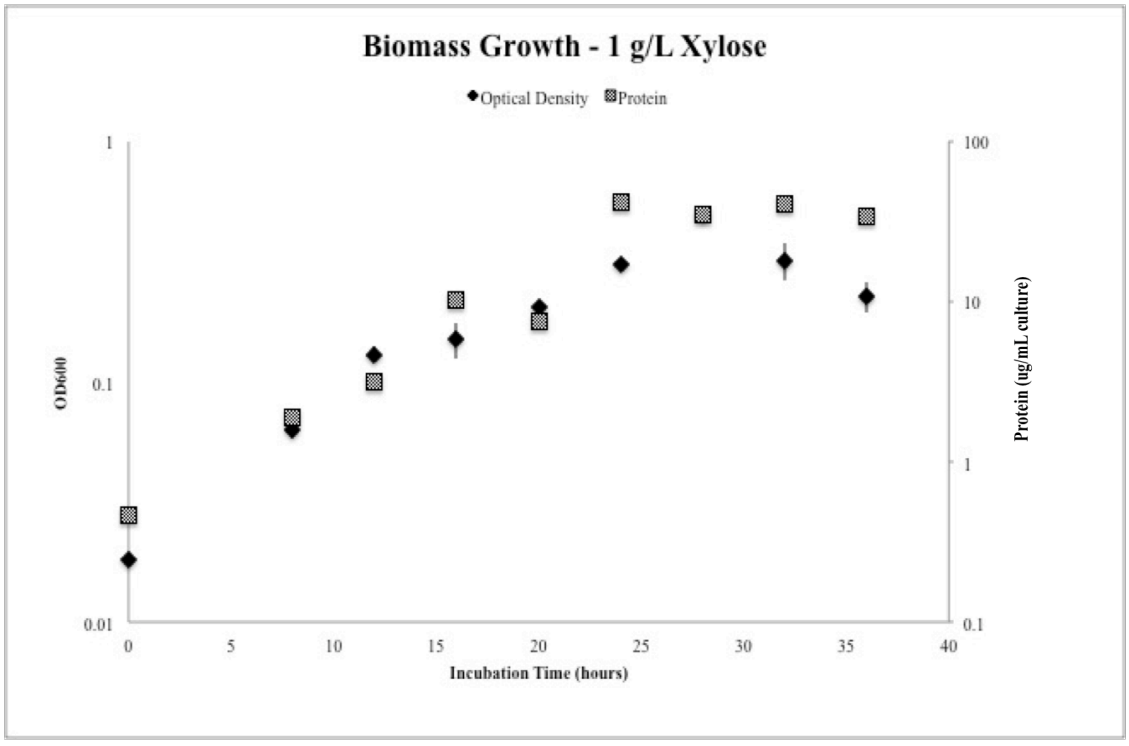
Biomass Growth - 1 g/L Xylose
Optical Density
Protein
OD600
Protein (ug/mL culture)
Incubation Time (hours)
1
0.1
0.01
100
10
1
0.1
0
5
10
15
20
25
30
35
40

C)

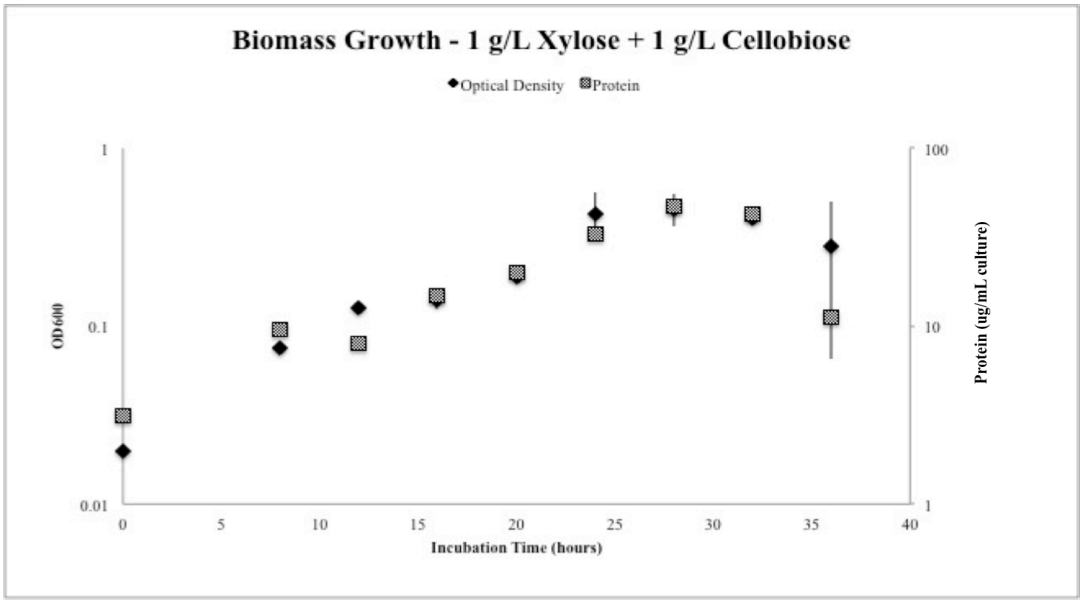
Biomass Growth - 1 g/L Xylose + 1 g/L Cellobiose
Optical Density
Protein
OD600
Protein (ug/mL culture)
Incubation Time (hours)
1
0.1
0.01
100
10
1
0
5
10
15
20
25
30
35
40

D)

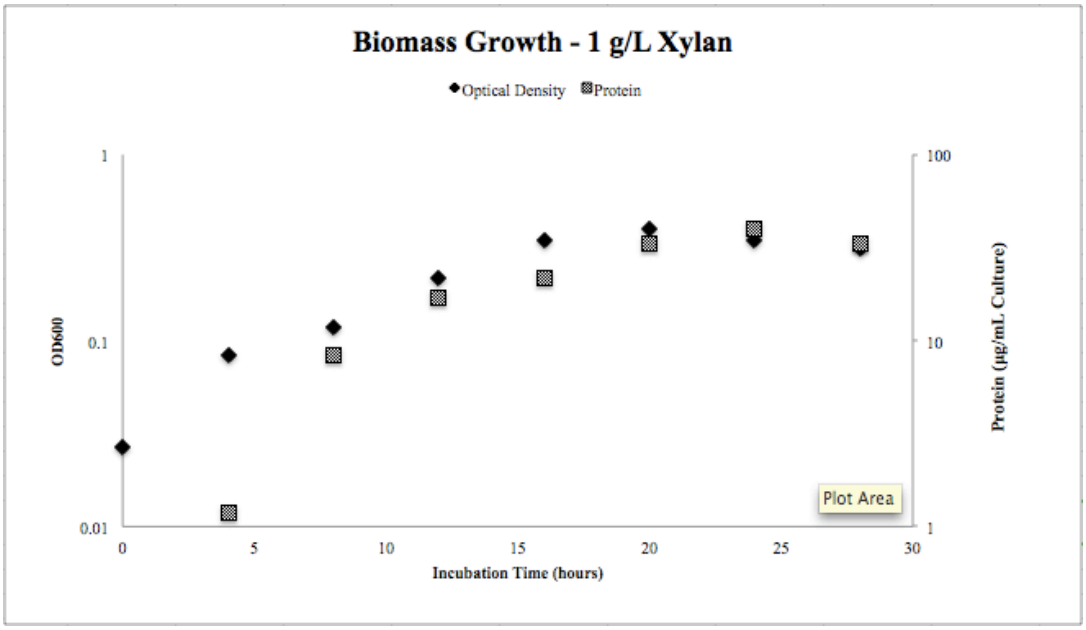
Biomass Growth - 1 g/L Xylan
Optical Density
Protein
OD600
Protein (µg/mL Culture)
Incubation Time (hours)
Plot Area
1
0.1
0.01
100
10
1
0
5
10
15
20
25
30

Figure 5.2 Biomass growth measured by optical density at 600 nm and protein content for *C. termitidis* cultured on **A)** 1 g L^{-1} cellobiose; **B)** 1 g L^{-1} Xylose; **C)** 1 g L^{-1} xylose + 1 g L^{-1} cellobiose; and **D)** 1 g L^{-1} xylan. Data points represent the means of 3 independent replicates. Bars above and below the means represent the standard deviation (SD).

Table 5.3 Volumetric production of end-products and other growth characteristics for *C. termitidis* cultured on the tested substrates at a concentration of 1 g L^{-1} at the end of growth (between 32-36 h).

	Maximum Concentration									
Substrate	**Substrate Consumption mM hex. Eq.**	**Lactate**	**Formate**	**Acetate**	**Ethanol**	**H_2**	**CO_2**	**Protein**	**OD**	**Final pH**
				mmol L^{-1} culture				**µg mL^{-1}**		
Cellobiose	5.42 ± 0.28	2.16 ± 0.28	1.98 ± 1.51	7.78 ± 1.30	2.77 ± 0.45	8.76 ± 0.39	5.58 ± 0.50	32.95 ± 2.70	0.49 ± 0.15	6.78 ± 0.14
Xylose	5.49 ± 0.05	1.37 ± 0.39	3.37 ± 1.38	8.76 ± 1.39	3.07 ± 0.36	8.78 ± 0.45	5.35 ± 0.99	41.87 ± 5.18	0.47 ± 0.05	6.67 ± 0.06
Xylose + cellobiose	7.59 ± 0.2	3.13 ± 0.03	3.45 ± 1.55	9.08 ± 2.36	3.18 ± 0.43	10.86 ± 0.26	6.18 ± 0.26	50.13 ± 2.89	0.43 ± 0.03	6.46 ± 0.00
Xylan	-	0.06 ± 0.02	1.14 ± 0.24	7.33 ± 0.50	1.57 ± 0.11	5.37 ± 0.20	3.49 ± 0.18	38.67 ± 4.14	0.40 ± 0.01	6.84 ± 0.03

5.4.3 Gas production

Gas production (H_2 and CO_2) by *C. termitidis* grown on various substrates is shown in Figures 5.3 A-D. The gas production profiles coincided with the growth pattern with all three substrate conditions. H_2 production was greatest for the mixed substrate (xylose + cellobiose), followed by cellobiose, xylose, and xylan, despite the fact that the cell biomass (as determined by total protein concentration) of *C. termitidis* grown on the mixed substrate was not significantly different from the cell mass produced from the other substrates. This result is in good agreement with the maximum pH drop being greatest in this treatment. At stationary phase, the H_2:CO_2 ratios produced by *C. termitidis* grown on the mixed substrate were slightly higher (1.8) than those produced by *C. termitidis* grown cellobiose, xylose, or xylan alone (1.6, 1.6, and 1.5, respectively).

Maximum volumetric production rates for all the major end-products are presented in Table 5.4. The rates were determined by plotting concentration against time on a semi-log scale, and the rates were calculated as the arithmetic mean ± standard deviations for the individual rates between 16-28 h time points. Maximum production rates of H_2 were considerably higher than those previously reported in literature. The maximum volumetric production rates for CO_2 were found to be similar for all the substrates tested (refer to Table 5.4) and compares very well with the value of 0.33 reported by Ramachandran et al. (2008). Again, volumetric production of CO_2 for xylan cultures more closely matched the rates associated with soluble sugars than insoluble substrates, such as α-cellulose.

Taguchi et al. (1994) isolated *Clostridium sp.* No. 2. from the termite *Cototoermes formosanus* for its ability to ferment glucose, arabinose, and xylose to produce hydrogen.

In preliminary batch studies with this organism, growth was tested on 3 g L^{-1} of each substrate in 1 L PY media at three different temperatures: 31, 36, and 41°C. End-product analysis showed that *Clostridium sp.* No. 2. completely utilized 3 g L^{-1} xylose, glucose and arabinose. The total volumetric H_2 production for xylose fermentation under these conditions ranged from 39.5 to 48 mmol and the H_2 evolution rate ranged from 9.6 mmol h^{-1} at 31°C to 13.8 mmol h^{-1} at 36 and 41°C. The specific yield for H_2 was reported to be 2 mol H_2 mol substrate $^{-1}$ at 31°C up to 2.3 and 2.4 mol H_2 mol substrate^{-1} for growth at 36°C and 41°C, respectively. In comparison with *C. termitidis* growth on 1 g L^{-1} xylose, the maximum total H_2 production was obtained as 8.78 ± 0.45 mmol L^{-1} culture. The volumetric production rate was only 0.43 ± 0.08 mmol L^{-1} h^{-1}. The yield of H_2 for *C. termitidis* growth on 1 g L^{-1} xylose was 8.78 ± 0.45 mmol product g substrate^{-1} (1.52 ± 0.08 mol product per mol hexose equivalent added) and this value is greater than the H_2 yield for *Clostridium sp.* No. 2. on 3 g L^{-1} xylose.

Caldicellulosiruptor lactoaceticus sp. nov., a cellulolytic, extreme thermophile phylogenetically related to *C. saccharolyticus* with very desirable H_2-synthesis capabilities, also exhibits the ability to ferment xylose, xylan, pectin apart from α-cellulose and cellobiose (Mladenovska et al. 1995). The gaseous end-products produced on pentoses by *C. saccharolyticus* were similar to that of *C. termitidis* except for the H_2 production, which ranged from 50-94% of the theoretical maximum, depending on substrate tested and the amount of lactate produced (Kadar et al. 2004).

A)

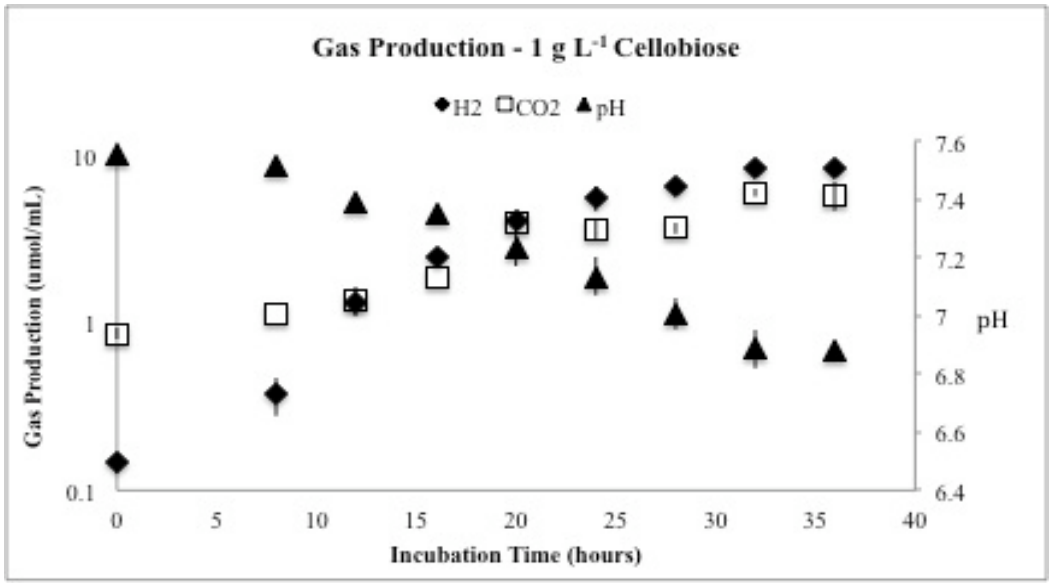
Gas Production - 1 g L-1 Cellobiose
H2
CO2
pH
Gas Production (umol/mL)
10
1
0.1
7.6
7.4
7.2
7
6.8
6.6
6.4
pH
0
5
10
15
20
25
30
35
40
Incubation Time (hours)

B)

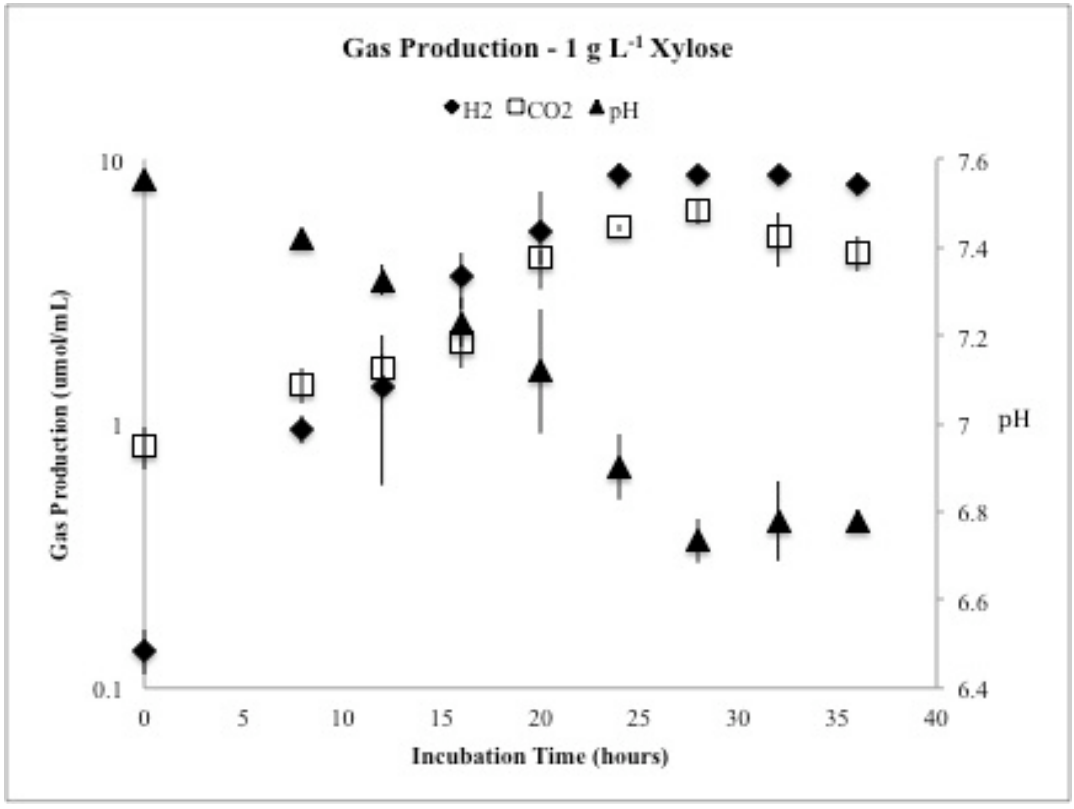
Gas Production - 1 g L-1 Xylose
H2
CO2
pH
Gas Production (umol/mL)
10
1
0.1
7.6
7.4
7.2
7
6.8
6.6
6.4
pH
0
5
10
15
20
25
30
35
40
Incubation Time (hours)

C)

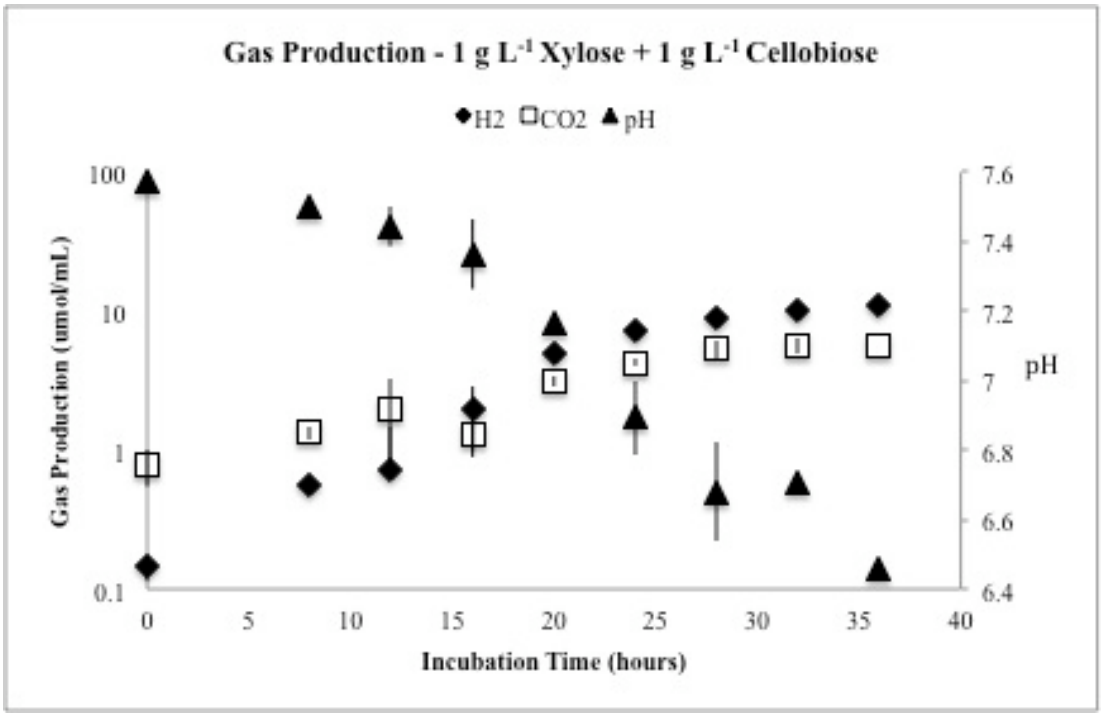
Gas Production - 1 g L-1 Xylose + 1 g L-1 Cellobiose
H2
CO2
pH
Gas Production (umol/mL)
100
10
1
0.1
7.6
7.4
7.2
7
6.8
6.6
6.4
pH
0
5
10
15
20
25
30
35
40
Incubation Time (hours)

D)

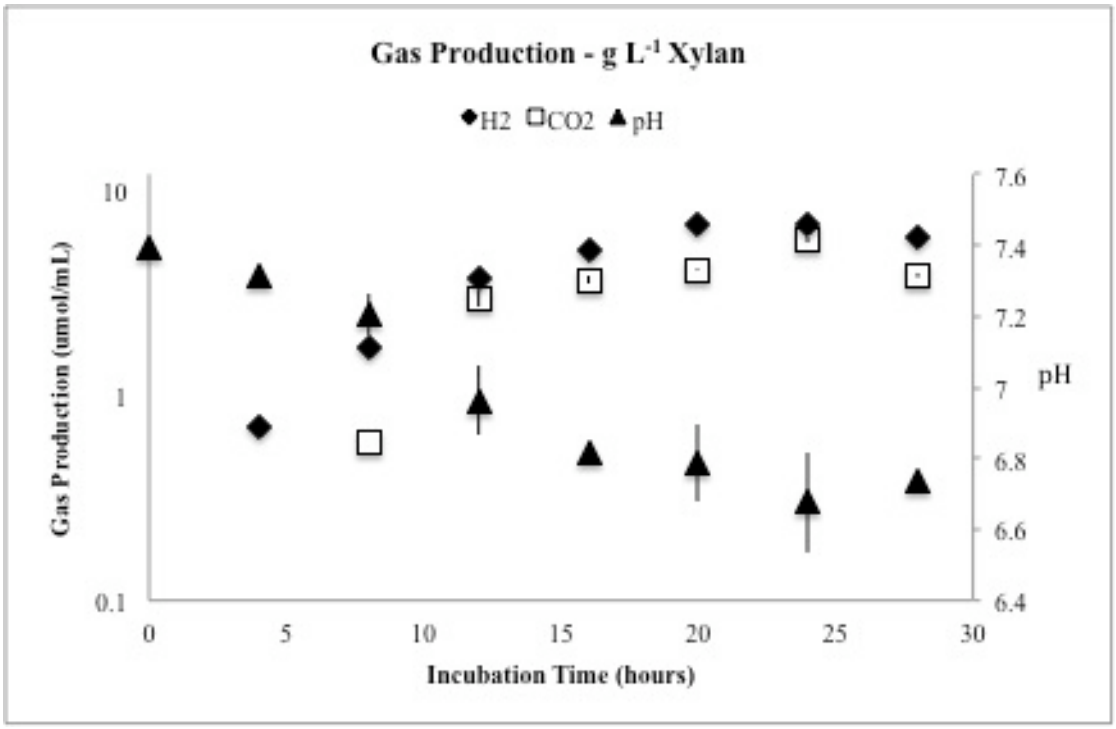
Gas Production - g L-1 Xylan
H2
CO2
pH
Gas Production (umol/mL)
10
1
0.1
7.6
7.4
7.2
7
6.8
6.6
6.4
pH
0
5
10
15
20
25
30
Incubation Time (hours)

Figure 5.3 Gas production for *C. termitidis* cultured on A) 1 g L^{-1} cellobiose; B) 1 g L^{-1} Xylose; C) 1 g L^{-1} xylose + 1 g L^{-1}cellobiose; and D) 1 g L^{-1}xylan. Data points represent the means of 3 independent replicates. Bars above and below the means represent the standard deviation (SD).

Table 5.4 Maximum volumetric production rates for soluble and gaseous end-products synthesized by *C. termitidis* using different carbon sources (between 16-28 h).

Volumetric Production Rates					
Substrate	**Formate**	**Acetate**	**Ethanol**	**H_2**	**CO_2**
	mmol product L^{-1} culture h^{-1}				
Cellobiose	0.04 ± 0.02	0.28 ± 0.19	0.13 ± 0.04	0.45 ± 0.23	0.41 ± 0.27
Xylose	0.26 ± 0.12	0.65 ± 0.04	0.27 ± 0.04	0.43 ± 0.08	0.33 ± 0.05
Xylose + cellobiose	0.19 ± 0.19	0.72 ± 0.07	0.17 ± 0.14	0.53 ± 0.16	0.33 ± 0.11
Xylan	0.05 ± 0.02	0.26 ± 0.13	0.11 ± 0.05	0.26 ± 0.07	0.27 ± 0.05

Table 5.5 Substrate specific yields of major end-products synthesized by *C. termitidis* using different carbon sources (between 32-36 h).

Yield						
Substrate	**Lactate**	**Formate**	**Acetate**	**Ethanol**	**H_2**	**CO_2**
	mol product per mol hexose equivalent added					
Cellobiose	0.39 ± 0.06	0.18 ± 0.02	1.18 ± 0.08	0.43 ± 0.03	1.43 ± 0.04	1.10 ± 0.05
Xylose	0.23 ± 0.07	0.70 ± 0.28	1.47 ± 0.23	0.44 ± 0.05	1.52 ± 0.08	1.07 ± 0.11
Xylose + cellobiose	0.26 ± 0.03	0.27 ± 0.11	0.80 ± 0.21	0.28 ± 0.04	1.95 ± 0.02	0.54 ± 0.03
Xylan[a]	0.25 ± 0.07	1.05 ± 0.20	8.58 ± 1.68	3.18 ± 0.43	5.52 ± 0.32	3.63 ± 0.13

[a]yield for xylan reported in mmol product per gram substrate added

5.4.4 Production of soluble end-products

The major soluble end-products synthesized by *C. termitidis* were acetate, formate, ethanol, and lactate (Figures 5.4 A-D). Acetate was the dominant soluble end-product, being present in higher concentration under all substrate conditions. Its synthesis corresponded to the growth curve, beginning from the start of exponential phase, and being produced at an increasing rate until stationary phase was reached between 24 h and 28 h. Soluble xylose displayed the greatest substrate specific yield of acetate (Table 5.5) when normalized per mole of hexose equivalent added, followed by cellobiose, and lastly, xylose + cellobiose. Xylan is normalized to the mass of substrate added, owing to the unkown composition.

Lactate production was found to be negligible in cultures with xylan. In cultures where cellobiose or xylose were present, lactate production remained minimal during most of the growth phase, and then exhibited a sudded rise as the cells neared stationary phase (Figure 5.4 A-D). In 1 g L^{-1} cellobiose, final concentrations of lactate were 2.16 ± 0.28 mM, but were 3.13 ± 0.03 mM in 1 g L^{-1} xylose + 1 g L^{-1} cellobiose, while xylose grown cells generated 1.37 ± 0.39 mM lactate (Table 5.3). According to Table 5.3, most of the pH drop is caused by the production of acetate. Lactate production was observed after 28 h on 1 g L^{-1} cellobiose, which coincided with a pH drop below 6.9 during stationary phase, where as on 1 g L^{-1} xylose + 1 g L^{-1} cellobiose, lactate production was observed after 24 h when the pH dropped below 6.9. Lower amounts of lactate was observed on 1 g L^{-1} xylose, with negligible concentrations observed on 1 g L^{-1} xylan (Figure 5.4 A-D).

Formate production was most notable in cultures containing soluble xylose, and its prodution corresponded to the growth curve, beginning at 8 h and increasing in rate until stationary phase was reached at 20 h, and the final formate concentration in xylose cultres was 3.37 ± 1.38 mM, and 3.45 ± 1.55 mM in xylose + cellobiose. Formate production was much lower in 1 g L^{-1} xylan and 1 g L^{-1} cellobiose, and generally did not exceed concentrations of 2 mM at any point during growth in either case. The specific production rates with respect to dry cell weight for all the end-products are presented in Table 5.6.

Ethanol production began with the onset of exponential-phase and plateaued before the cells were in stationary phase at 16 h for both xylose and xylan. The maximum substrate specific yield of ethanol was 4.33 ± 0.40 mmol product g substrate^{-1} (0.44 ± 0.05 mol product per mol hexose equivalent added) for xylose and 3.18 ± 0.43 mmol product g substrate^{-1} for xylan, respectively (Table 5.5). Cellobiose cultures produced a maximum ethanol yield of 0.43 ± 0.03 mol product per mol hexose equivalent added (2.61 ± 0.31 mmol product g substrate^{-1} added), but ethanol production continued throughout the growth phase. The same phenomenon was observed for cultures grown on the mixed substrate (xylose + cellobiose). The major soluble end-products of carbohydrate fermentation by *Thermoanaerobacter* sp. X514 were acetate, lactate, and ethanol (Lin et al. 2011). For 50 mM xylose grown cultures of *Thermoanaerobacter* sp. X514, an ethanol yield of 9.6 mM was obtained. In comaprison, *C. termitidis* on 1 g L^{-1} (6.7 mM) xylose exhibited an ethanol yield of 0.44 ± 0.05 mol product per mol hexose equivalent added (4.33 ± 0.40 mmol product g substrate^{-1} added).

Clostridium phytofermentans is an anaerobic, cellulolytic mesophile that has been shown to grow on both xylose and xylan, amongst many other substrates characteristically found in biomass. The major end products were ethanol, acetate, H_2, and CO_2, and the minor end products included formate and lactate (Warnick et al. 2002). Jin et al. (2011) reported that for growth on AFEX-pretreated corn stover, *C. phytofermentans* was able to hydrolyze nearly 89% of the xylan after a 10-day incubation, in addition to 76% glucan utilization. This collectively resulted in an ethanol yield of 2.8 g L^{-1} for glucan loading of 0.5% (vol/vol) of AFEX-pretreated corn stover. These studies were carried out in 125 mL serum bottles with an N_2-containing headspace. In comparison with this work, the maximum ethanol yield for *C. termitidis* obtained was 0.17 g L^{-1} and 0.07 g L^{-1} for 1 g L^{-1} xylose and 1 g L^{-1} xylan, respectively. The maximum concentration of H_2 produced from *C. termitidis* growth on 1 g L^{-1} substrate is higher for all the substrate combinations tested, and this corresponds to higher acetate production (Table 5.3). The ethanol, yield, however, is much higher for *C. phytofermentans* cultured on 1 g L^{-1} switchgrass at 37 °C for 14 days. Despite the comparison between soluble and insoluble substrates and different carbon loading conditions, *C. phytofermentans* exhibits more rapid growth and higher ethanol production, but *C. termitidis* is a more robust producer of hydrogen.

Owing to the fact that xylose is a 5-C monosaccharide and cellobiose is a 12-C disaccharide, expressing them in terms of their respective molarity resulting from addition of 1 g L^{-1} of each does not make for an appropriate comparative basis, as the molecular weight of cellobiose is much higher. To circumvent this, all sugar concentrations in Figure 5.5 A and Figure 5.5 B are expressed by converting the

concentration of each sugar to number of glucose equivalents that it would take to get the equivalent amount of carbon. *C. termitidis* completely utilized 6.7 mM xylose (1 g L^{-1}), where as *Thermoanaerobacter* sp. X514 did not completely deplete the substrates when grown on 50 mM (9 g L^{-1}) glucose + 50 mM (7.5 g L^{-1}) xylose together (Lin et al. 2011).

When used as single substrates, *C. termitidis* consumed both xylose and cellobiose (pure substrates) to below 0.1 mM. However, the rates of consumption of these substrates were different. Xylose was no longer detectable in the cultures after 24 h, where as cellobiose was not depleted until 36 h. Significant utilization of both carbon sources began with the onset of exponential phase between 0-8 h. From Figure 5.5 A, it can be seen that the rate of xylose consumption during the late-exponential phase is higher than the rate of cellobiose utilization. The cells consumed 50% of the pure substrates between 24-28 h for cellobiose grown cultures and 20-24 h for xylose grown cultures. In cultures with xylose + cellobiose, the patterns of substrate consumption are more complex (Figure 5.5 B). The substrates were not completely depleted at the end point at 36 h. Based on the end-product synthesis pattern, it was observed that the cells did not utilize any more substrates after 32 h, which coincided with a pH drop below 6.48. This pH drop was associated with increased acetate and lactate synthesis in the *C. termitidis* cultures grown on the mixed substrates when compared with pure substrates after 32 h. Based on the characteristic depletion of xylose and cellobiose in the cultures grown on mixed substrates, the total substrate utilized in hexose equivalents were obtained as 7.59 ± 0.2 mM (Table 5.3) after 32 h until the end-point.

A)

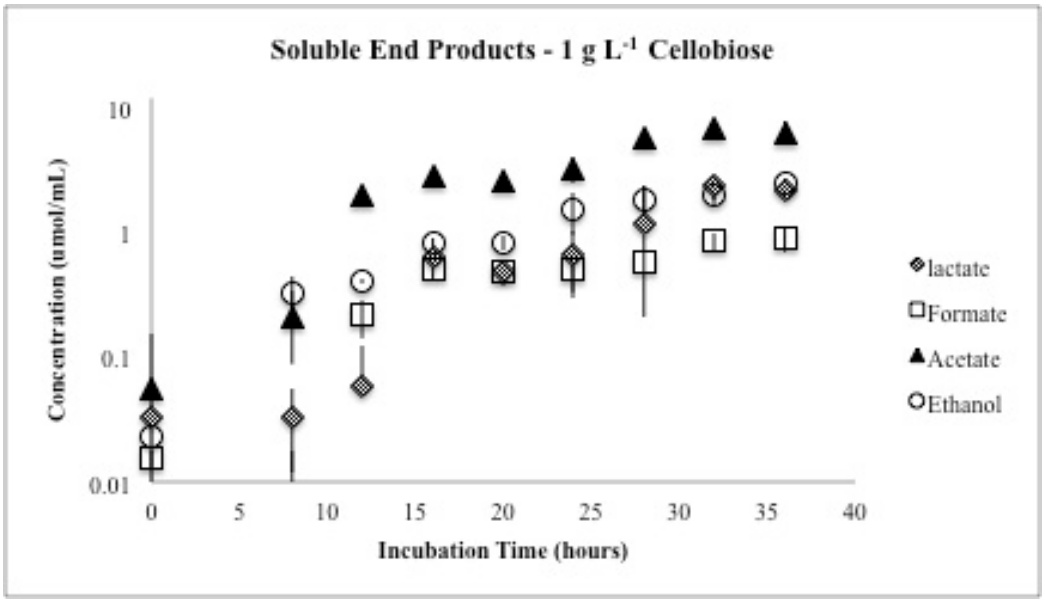
Soluble End Products - 1 g L-1 Cellobiose
Concentration (umol/mL)
10
1
0.1
0.01
0
5
10
15
20
25
30
35
40
Incubation Time (hours)
lactate
Formate
Acetate
Ethanol

B)

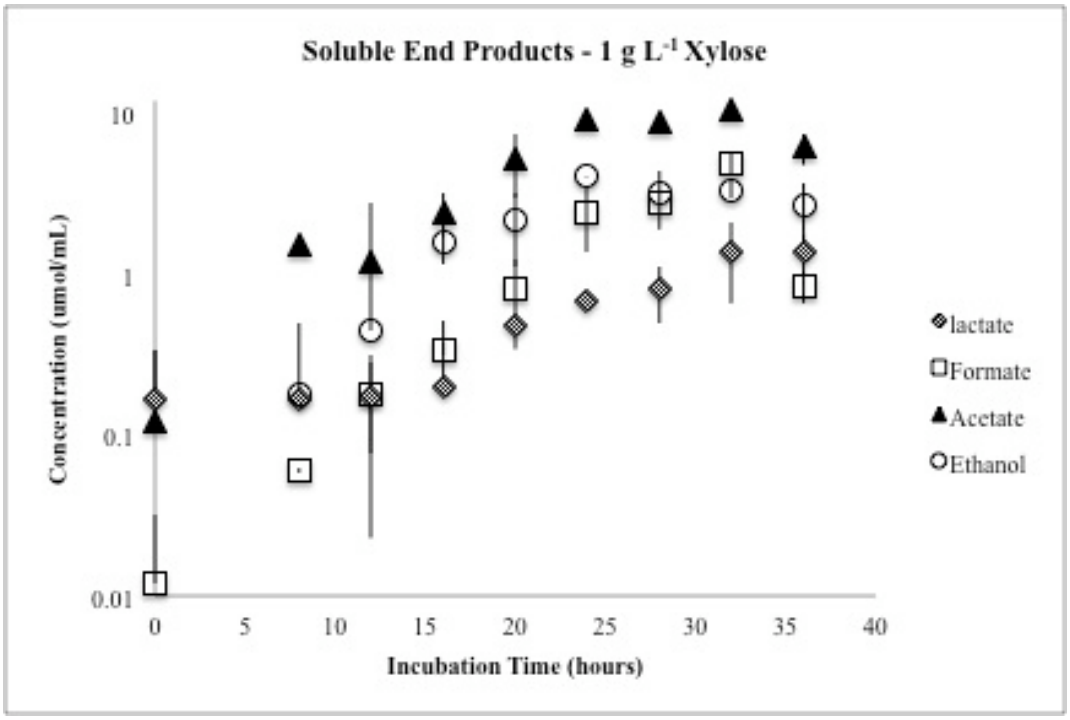
Soluble End Products - 1 g L-1 Xylose
Concentration (umol/mL)
10
1
0.1
0.01
0
5
10
15
20
25
30
35
40
Incubation Time (hours)
lactate
Formate
Acetate
Ethanol

C)

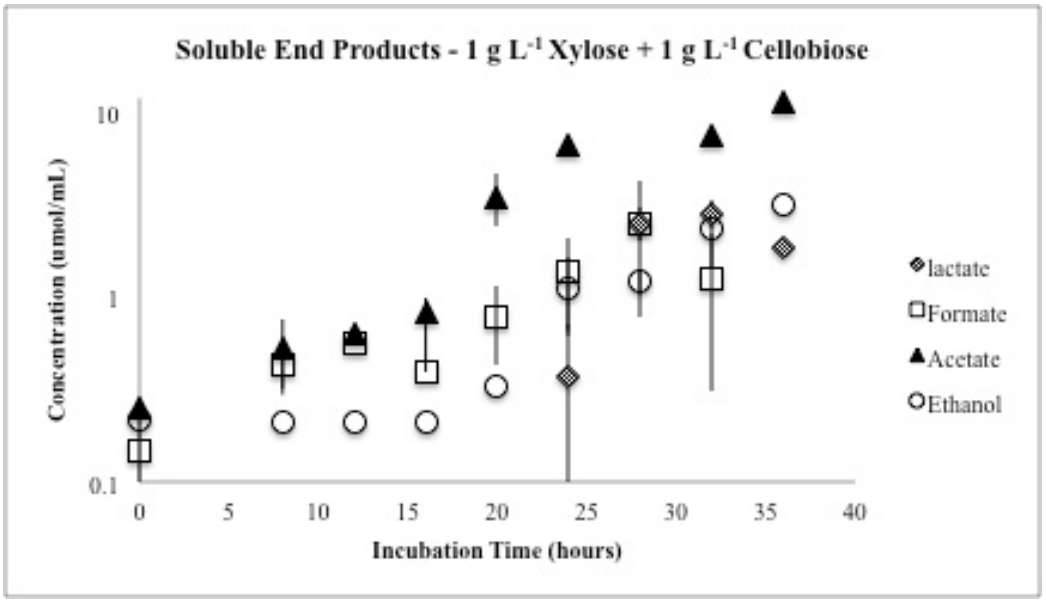
Soluble End Products - 1 g L-1 Xylose + 1 g L-1 Cellobiose
Concentration (umol/mL)
10
1
0.1
0
5
10
15
20
25
30
35
40
Incubation Time (hours)
lactate
Formate
Acetate
Ethanol

D)

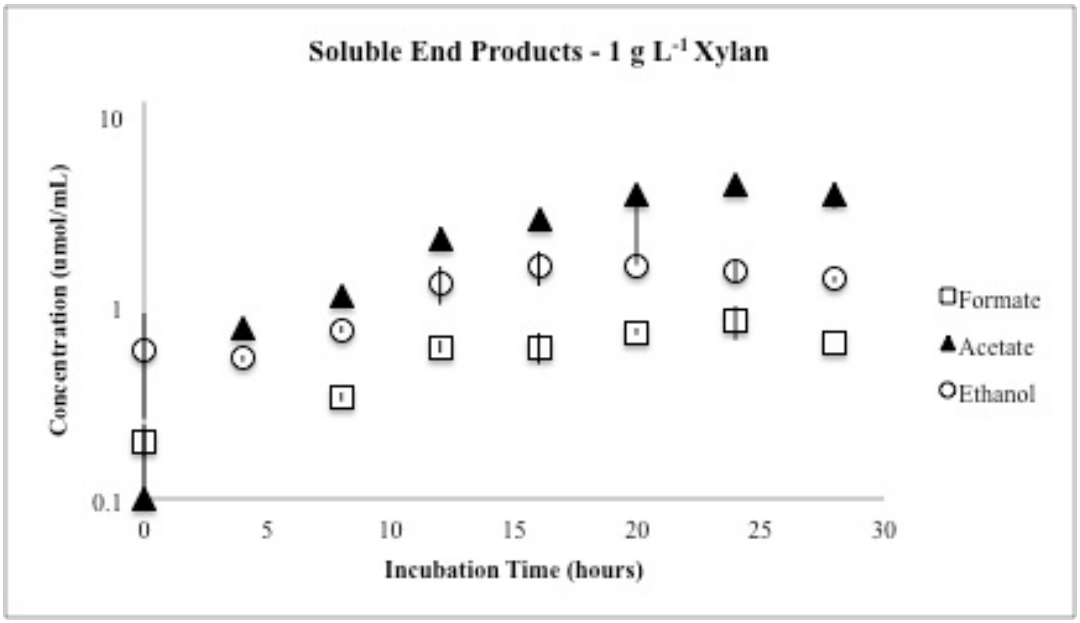
Soluble End Products - 1 g L-1 Xylan
Concentration (umol/mL)
10
1
0.1
0
5
10
15
20
25
30
Incubation Time (hours)
Formate
Acetate
Ethanol

Figure 5.4 Soluble end products for *C. termitidis* cultured on A) 1 g L^{-1} cellobiose; B) 1 g L^{-1} xylose; C) 1 g L^{-1} xylose + 1 g L^{-1} cellobiose; and D) 1 g L^{-1} xylan. Data points represent the means of 3 independent replicates. Bars above and below the means represent the standard deviation (SD).

Table 5.6 Specific production rates of major end-products synthesized by *C. termitidis* cultured on different substrates (between 16-28 h).

Specific Production Rates					
Substrate	**Formate**	**Acetate**	**Ethanol**	**H_2**	**CO_2**
	mmol product g^{-1} DCW h^{-1}				
Cellobiose	2.14 ± 0.33	5.43 ± 1.78	3.13 ± 1.02	6.09 ± 3.89	2.74 ± 0.60
Xylose	5.01 ± 0.33	7.66 ± 0.76	4.32 ± 0.45	5.12 ± 0.30	4.70 ± 0.30
Xylose + cellobiose	1.47 ± 0.42	10.17 ± 4.72	3.97 ± 1.05	8.61 ± 2.87	4.87 ± 1.87
Xylan	0.85 ± 0.33	4.49 ± 2.07	2.05 ± 0.81	3.68 ± 0.95	4.29 ± 0.84

A)

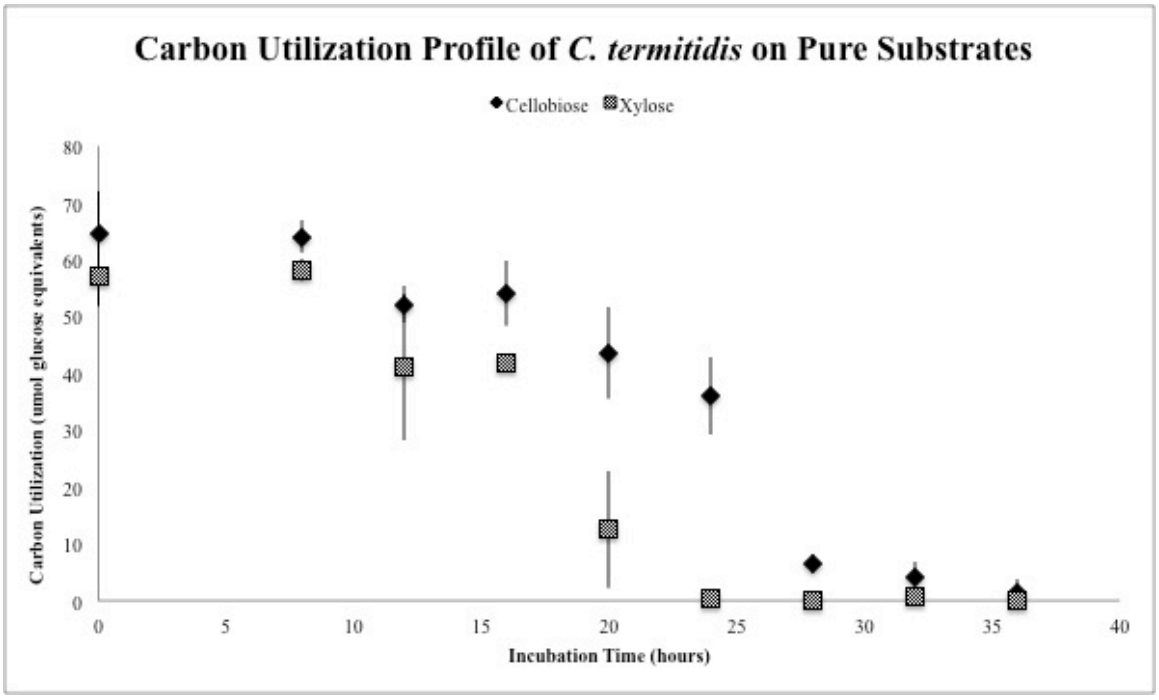
Carbon Utilization Profile of C. termitidis on Pure Substrates
Cellobiose
Xylose
Carbon Utilization (umol glucose equivalents)
Incubation Time (hours)
0
10
20
30
40
50
60
70
80
0
5
10
15
20
25
30
35
40

B)

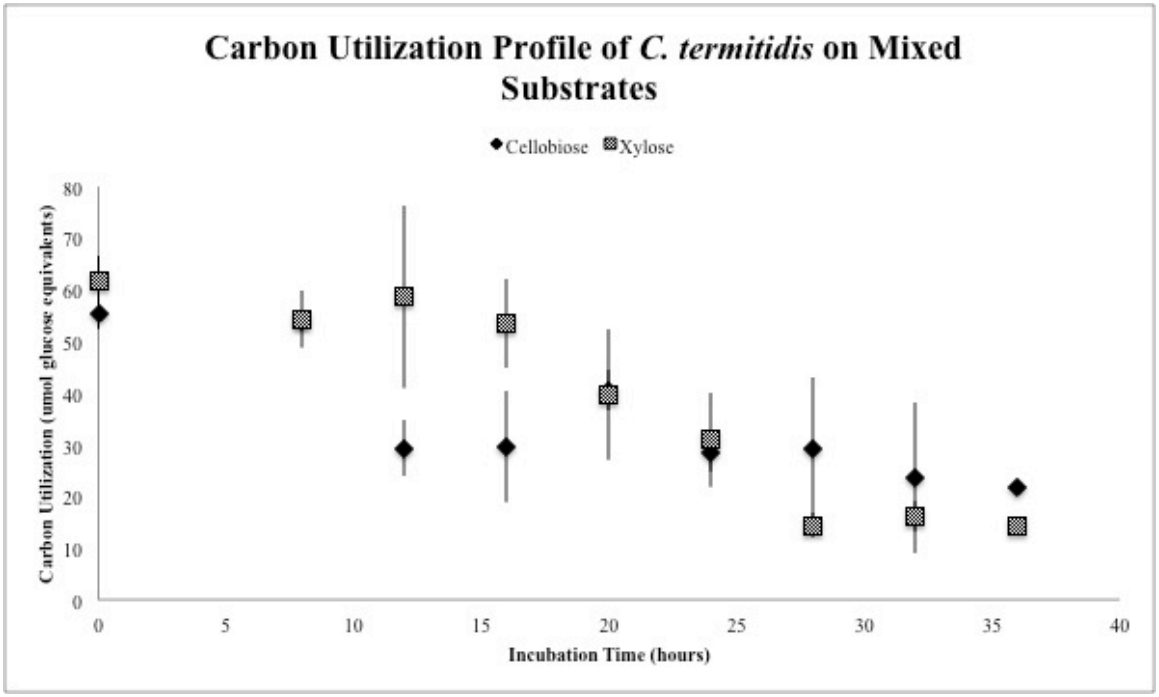
Carbon Utilization Profile of C. termitidis on Mixed Substrates
Cellobiose
Xylose
Carbon Utilization (umol glucose equivalents)
Incubation Time (hours)
0
10
20
30
40
50
60
70
80
0
5
10
15
20
25
30
35
40

Figure 5.5 Sugar profile for *C. termitidis* cultures grown on A) Mono-substrates xylose or cellobiose; B) Mixed substrates containing 1 g L^{-1} xylose and 1 g L^{-1} cellobiose Data points represent the means of 3 independent replicates. Bars above and below the means represent the standard deviation (SD).

Average carbon recovery for cultures of xylose, cellobiose, and xylose + cellobiose were found to be 1.13, 0.97, and 1.04, respectively, and the corresponding OR balances were 0.92, 0.95, and 0.83, respectively. This indicates that all end-products were accounted for. The carbon balance for xylan cultures could not be completed due to lack of adequate quantification methodology, and is left as a future challenge that is not addressed in this work.

5.5 Conclusions

In this chapter, both xylan and concurrent pentose and hexose fermentation were described for the first time for *C. termitidis* and the growth characteristics and end-product synthesis on xylose described. Fundamentally, the proteomic analyses revealed high levels of proteins putatively related to xylose metabolism despite the absence of added xylose to the growth medium. This led to the hypothesis that cells are primed for xylose metabolism even in the absence of xylose, suggesting that sequential fermentation of xylose and cellobiose should be possible in *C. termitidis*. This was demonstrated using the batch experiments and end-product analysis on soluble (xylose, cellobiose, cellobiose + xylose), and insoluble (xylan) substrates.

Chapter 6: Conclusions and Future Studies

6.1 Discussion of major findings

Cellulosic biomass from agriculture, municipal sources, and forestry could be used as impending feedstocks for biofuels and value-added bioproducts production ousting fossil fuels and diminishing green house gas emissions (Levin et al. 2007; Mabee et al. 2006). Cellulolytic Clostridia are gaining importance due to their ability to perform consolidated biprocessing for bioconversion of lignocellulosic biomass to desired end-products. Also, recent advancements in genomic and proteomic technologies have given us an opportunity to clearly understand microbial metabolism for the efficient lignocellulosic biomass conversion to biofuels (hydrogen, ethanol) using specific microorganisms that will maximize substrate (pentoses and hexoses) conversion. In this dissertation, an anerobic, cellulolytic, mesophilic bacterium, *C. termitidis* was extensively investigated for its metabolic potential to convert lignocellulosic substrates to H_2/ethanol, which was subsequently verified using functional genomic and proteomic analyses.

Chapter 1 provides literature about the significance, efficient processing and challenges for lignocellulose-based biofuels production, thereby defining the objectives of using a suitable under-characterized candidate, *C. termitidis*, which is anaerobic, cellulolytic, mesophilic bacterium capable of utilizing both the products of cellulose and hemicellulose hydrolysis. In chapter 2, metabolic profiling of *C. termitidis* was performed to characterize end-product synthesis pathways on the two susbtrates, cellobiose and α-cellulose at a concentration of 2 g L^{-1}. Irrespective of longer doubling time on α-

cellulose, compared with cellobiose, *C. termitidis* preferred sythesizing H_2 with the carbon flow directed towards acetate production and this coincided with decreased CO_2 and ethanol production. As the pH dropped below 6.2, H_2 and ethanol synthesis were significantly reduced. This pattern was different from *C. cellulolyticum*, which showed higher generation times on both the substrates with decreased H_2 and increased ethanol synthesis on cellulose. These results prove that hypothesis 1 was successful as the rates of growth and synthesis patterns of H_2 and ethanol were different between *C. termitidis* cellobiose and α-cellulose grown cultures. The batch experiments on these two substrates also showed no pyruvate overflow at concentrations of 2 g L^{-1} and the growth arrest was due to pH drop below 6.2. This pH drop also coincided with lactate production. This pattern was different from that observed in *C. cellulolyticum* as pyruvate overflow was also coupled with growth arrest (Guedon et al. 1999). Higher concentrations of H_2 and lower ethanol concentrations were observed on α-cellulose, when compared with cellobiose cultures. Hence, hypothesis 2 was refuted as the metabolic bottlenecks with respect to carbon flux were different between *C. termitidis* and *C. cellulolyticum*.

It is essential to consider carefully the complex metabolism of these anaerobic Clostridia used as an ideal candidate biofuel producer for developing hypotheses for maximal production yields. In chapter 3, hypothesis 3 stated pH-control, continuous gas sparging with N_2 in an open system with constant agitation, would significantly affect the end-product yields, especially H_2/ethanol, was confirmed using controlled batch experiments on 2 g L^{-1} cellobiose and α-cellulose in a bioreactor. These findings showed that gas sparging/pH-control significantly increased the specific and volumetric yields of

H_2 during fermentation with cellobiose and α-cellulose, where as ethanol synthesis was not preferred by *C. termitidis*, as compared to the earlier batch tube experiments.

Based on the metabolic characterization of the end-product synthesis pathways, further investigation on the functional proteomic for the first time was performed on the newly sequenced *C. termitidis*. In Chapter 4, compositional and quantitative proteomic studies of *C. termitidis* grown on cellulose vs cellobiose under two growth states (mid-exponential and stationary phases) were performed using novel multidimensional HPLC peptide fractionation protocols (Dwivedi et al. 2008) combined with state-of-the-art mass spectrometry analysis using industry-leading TOF QSTAR® Elite Hybrid mass spectrometer (AB SCIEX). Major findings included ethanol synthesis pathway regulation being regulated via bifucntional AdhE on cellobiose and cellulose. Cellulose cultures showed relatively lower AdhE regulation during mid-exponential and stationary phases when compared with cellobiose cultures. Also, higher levels of phosphotransacetylase (PTA) and acetate kinase (ACK) were detected in the proteome across both growth conditions (when cultured on cellulose or cellobiose). Increased volumetric production of acetate and H_2 corresponded to lower amounts of ethanol and lactate on cellulose cultures (chapter 1) and these findings correlated well with the protein expresson profiles of PFOR, ferredoxin-dependent hydrogenases, PFL, LDH, AdhE, AldH, Fe-ADH, PTA, and ACK.

In the current chapter, the effect of physiological changes on carbon and electron flux during hexose and pentose fermentation was studied in *C. termitidis*. Initial biochemical characterization of *C. termitidis* by Hethener et al. (1992) showed a positive reaction for xylose (pentose) sugar fermentation test. Also, the hexose proteomic studies

and whole genome analysis revealed higher levels of putative proeins associated with xylose catabolism, when the cells were grown on hexoses with the absence of added xylose in the medium. Hence, hypothesis 4 that is verified in chapter 5 was succesful as sequential fermentation of hexose and pentose sugars was proved and confirmed by growth, end-product analysis and substrate depletion experiments. Despite the absence of a transaldolase encoding gene, an alternative model of the pentose phosphate pathway was proposed in *C. termitidis* along with its ability to ferment xylan for the first time in this chapter. In addition to the xylose metabolism specific proteins, *C. termitidis* encodes a ABC-type transport system for pentoses and hexoses uptake. Two putative functional operons (operon 1: CTER_0912-0916 and operon 2: CTER_5427-5429) were detected in high levels on both the substrates during mid-exponential phase.

6.2 Conclusions and Future Studies

For efficient and optimized synthesis of biofuels by CBP, a clear elucidation of genomics (gene identification, functions), metabolism, effect of growth conditions and end-product concentrations on carbon flow and metabolic fluxes, and proteomics (identification and expression analysis of key enzymes, both spatial and temporal) is necessary for the selected naturally occurring cellulolytic bacteria and its future application for improved production of desired end-products. This thesis reports on a mesophilic *Clostridium* that has the ability to utilize both pentose and hexose sugars for efficient lignocellulosic conversion into biofuels (H_2/ethanol). Proteomic analyses of *C. termitidis* cultured on cellobiose and cellulose have provided a snapshot of differences in the protein expression levels across the conditions tested (chapter 4). These results shed light on the differences in pathway flux and metabolic shifts, but it do not show a

complete picture on the regulatory components of the biochemical reactions. Hence, future studies involving transcriptomics, metabolomics, and biochemical characterization would aid in the complete understanding of regulation of metabolic shifts for the production of desired end-products in *C. termitidis*.

A putative functional pentose phosphate pathway was proposed for xylose metabolism in *C. termitidis,* based on the proteomic analyses of *C. termitidis* cells cultured on cellulose and cellobiose (chapter 5). Key proteins involved in xylose metabolism were observed at higher abundance, suggesting that the cells were primed for xylose metabolism even in the absence of the pentose sugar in the medium. It would be of great interest to perform complete compositional and quantitative proteomic analyses on xylose grown cultures versus cellulose or cellobiose cultures. In this case, the differences in the relative expression levels of proteins involved in pentose phosphate pathway could be observed specifically with xylose grown cultures. Also, xylan metabolism was shown for the first time in *C. termitidis* (chapter 5). Proteomic analyses of cultures grown on a complex polymer like xylan, would be interesting to compare with the proteome observed in cellulose grown cells. Further, sequential fermentation of hexose and pentose sugars were shown for the first time in this study (chapter 5). Future experiments could be designed to verify the possibility of simultaneous hexose and pentose fermentation in *C. termitidis*. Batch experiments on mixed substrates such as xylose+cellobiose, xylose+cellulose, and xylan+cellulose could be done to verify simultaneous hexose and pentose fermentation in *C. termitidis*. This type of simultaneous fermentation will be an essential feature to use *C. termitidis* in industrial application for its capability to utilize hexose and pentose sugars together.

Open bioreactor experiements in *C. termitidis* with pH control and continuous N_2 sparging have demonstrated the possible shift in the metabolism towards H_2 synthesis rather than ethanol synthesis (chapter 3). In the future, it could be verified by conducting proteomic analysis on mid-exponential and stationary phase samples obtained from bioreactor experiments on cellobiose and cellulose under different physiological conditions. Based on the batch experiments conducted on xylose and xylan substrates (chapter 5), open bioreactor experiments with pH control/N_2 sparging could be conducted in the future to observe metabolic shifts between H_2 and ethanol synthesis pathways. The capability of utilizing hexose and pentose sugars sequentially could be further exploited by performing scale-up experiments in open system first on mixed susbtrates and then conducting proteomic analysis on the samples obtained during mid-exponential and stationary phase cultures. All these features could possibly be used to select *C. termitidis* as a potential candidate for large-scale hydrogen and ethanol production from raw lignocellulosics either as mono-cultures or in co-cultures in the future.

In most co-culture systems, individual members of the consortium are not well characterized. End-product synthesis patterns are significantly affected due to different fermentative properties of bacteria present in the consortium. The utilization of renewable biomass resources for the production of different chemicals and energy could eradicate the issues caused by organic waste materials (Lay 2000). Hence, bioenergy obtained by various microbial fermentative processes play a significant role in the regulation of global carbon cycling and further considered as an environment friendly process. An efficient and sustainable co-culture will only exist if appropriate syntrophic interactions are exhibited between the two bacterial strains (Powell 1985). In their natural habitats, many

different microorganisms coexist by interacting with one another, while they are even more effective during their interaction with other groups of organisms, whereas some organisms are effective only when they have a synergistic association with other groups of microorganisms (Chang et al. 2008).

Studies have shown that the syntrophic effect of associated microorganisms during cellulose degradation were not directly dependent on the cellulase system, but instead due to the production of essential nutrients, maintenance of anaerobic environment, or eradication of toxic end-products (Hungate 1944). In water retting ponds (Tamburini et al. 2003) and paddy field soils (Liesack et al. 2000), anaerobic cellulolytic *Clostridia* and aerobic *Bacillus* coexists at various places where cellulose degradation occurs. The syntrophic effect of these two bacteria has been shown to be effective for efficient cellulose hydrolysis (Kato et al. 2004). The other major drawback of using two pure strains in a co-culture is their competition for utilizing the same substrate. In that case, one bacteria out-competes the other resulting in the decline of growth of the other bacteria due to the lack of nutrients, and eventually cell death. One such example is the use of a co-culture containing *C. cellulolyticum* (Desvaux et al. 2000) with a non-cellulolytic *Clostridium* sp. capable of utilizing cellobiose or glucose, for biofuels synthesis. The cellulolytic bacterium *C. cellulolyticum* actively hydrolyzed cellulose to release cellobiose units that were necessary for both the bacteria in the co-culture, thereby outnumbering the co-cultured *Clostridium* sp.

Anaerobic thermophilic bacteria such as *Thermoanaerobium brockii* (Lamed and Zeikus 1980), *Thermoanerobacter ethanolicus* (Maki et al. 2009), and *Thermoanaerobacterium saccharolyticum* (Venkateswaran and Demain 1986) share a

syntrophic relationship with *C. thermocellum,* which hydrolyzes cellulose to cellobiose, and cellodextrans, and hemicellulose to xylobiose, arabinoxylans, and xylooligosaccharides by expressing cellulases and hemicellulases. Ethanol is produced from the cellulose hydrolytic products by *C. thermocellum*, where as the former species convert the hemicellulose hydrolytic products to ethanol, further avoiding competition for substrates between strains, and maximizing product formation (Maki et al. 2009).

Bacterial co-cultures are a means to enhance efficient substrate utilization and increase the production of desirable fermentable products (Maki et al. 2009). In order to establish a stable co-culture, growth and media requirements along with other physiological properties such as pH, temperature, carbon source, and atmosphere are necessary for providing optimum conditions for equal growth for both the strains. The other key factors that affect the sustenance of the co-culture include the inoculation ratio, growth rates, yeast extract concentration, and alkalinity of the co-culture system (Geng et al. 2010). Apart from the dependence on growth and media requirements of each strain, stable co-cultures are also affected by metabolic interactions such as competition for substrates, and other criteria like production of growth stimulating or growth inhibiting compounds. Hence, keeping these factors in mind in the future, the co-culture of the desired strains with *C. termitidis* may improve yields along with efficient substrate conversion.

References

Adams, J. 2008. Transcriptome: connecting the genome to gene function. Nature Education 1: 1.

Agbor, V.B., Cicek, N., Sparling, R., Berlin, A., and Levin, D.B. 2011. Biomass pretreatment: Fundamentals toward application. Biotechnology Advances 29(6): 675-685.

Aggarwal, K., Choe, L.H., Lee, K.H. 2006. Shotgun proteomics using the iTRAQ isobaric tags. Briefings in Functional Genomics and Proteomics 5(2): 112-120.

Arita, M. 2009. What can metabolomics learn from genomics and proteomics. Current opinion in Biotechnology 20(6): 610-615.

Biebl, H. 2001. Fermentation of glycerol by *Clostridium pasteurianum* - batch and continuous culture studies. Journal of Industrial Microbiology and Biotechnology 27(1): 18-26.

Bielen, A.A.M., Willquist, K., Engman, J., van der Oost, J., van Niel, E.W.J., and Kengen, S.W.M. 2010. Pyrophosphate as a central energy carrier in the hydrogen-

producing extremely thermophilic *Caldicellulosiruptor saccharolyticus*. Fems Microbiology Letters 307(1): 48-54.

Boisset, C., Chanzy, H., Henrissat, B., Lamed, R., Shoham, Y., and Bayer, E.A. 1999. Digestion of crystalline cellulose substrates by the *Clostridium thermocellum* cellulosome: Structural and morphological aspects. Biochemical Journal 340: 829-835.

Bradford, M.M. 1976. A rapid and sensitive for the quantitation of microgram quantitites of protein utilizing the principle of protein-dye binding. Analytical Biochemistry 72: 248-254.

Brener, D., and Johnson, B.F. 1984. Relationship between Substrate Concentration and Fermentation Product Ratios in *Clostridium thermocellum* Cultures. Applied and Environmental Microbiology 47(5): 1126-1129.

Britt, P.F., Buchanan, A.C., Cooney, M.J., and Martineau, D.R. 2000. Flash vacuum pyrolysis of methoxy-substituted lignin model compounds. Journal of Organic Chemistry 65(5): 1376-1389.

Brown, L.R. 2006. Exploding U.S. grain demand for automotive fuel threatens world food security and political stability. Earth Policy Institute.

Brown M.A., Levine, M.D., Romm, J.P.R.A.H., and Koomey, J.H. 1998. Engineering-economic studies of energy technologies to reduce greenhouse gas emissions: opportunites and challenges. Annual review of energy environment 23:31-39.

Carere, C.R., Rydzak, T., Verbeke, T.J., Cicek, N., Levin, D.B., Sparling, R. 2012. Linking genome content to biofuel production yields: a meta-analysis of major catabolic pathways among select H_2 and ethanol producing bacteria. BMC Microbiology 12(1):295.

Carere, C.R., Sparling, R., Cicek, N., and Levin, D.B. 2008. Third generation biofuels via direct cellulose fermentation. International Journal of Molecular Science 9(7): 1342-1360.

Chang, J.J., Chou, C.H., Ho, C.Y., Chen, W.E., Lay, J.J., and Huang, C.C. 2008. Syntrophic co-culture of aerobic *Bacillus* and anaerobic *Clostridium* for biofuels and biohydrogen production. International Journal of Hydrogen Energy 33(19): 5137-5146.

Chen, J.S. 1995. Alcohol dehydrogenase- multiplicity and relatedness in the solvent-producing Clostridia. Fems Microbiology Reviews 17(3): 263-273.

Chen, W.M., Tseng, Z.J., Lee, K.S., and Chang, J.S. 2005. Fermentative hydrogen production with *Clostridium butyricum* CGS5 isolated from anaerobic sewage sludge. International Journal of Hydrogen Energy 30(10): 1063-1070.

Conway, T., Sewell, G.W., Osman, Y.A., and Ingram, L.O. 1987. Cloning and sequencing of the alcohol dehydrogenase-Iike gene from *Zymomonas mobilis*. Journal of Bacteriology 169(6): 2591-2597.

Craig, R., Cortens, J.P., Beavis, R.C. 2004. Open source system for analyzing, validating, and storing protein identification data. Journal of Proteome Research 3(6):1234-1242.

Daniels, L., Rajagopal, B.S., Belay, N. 1986. Assimilatory reduction of sulfate and sulfite by methanogenic bacteria. Applied and Environmental Microbiology 51: 703-709.

Darrett, R., and Grisham, C.M. 1995. Biochemistry. Saunders College Publishing, New York, NY.

Demain, A.L., Newcomb, M., and Wu, J.H.D. 2005. Cellulase, clostridia, and ethanol. Microbiology and Molecular Biology Reviews 69(1): 124-+.

Desvaux, M., Guedon, E., and Petitdemange, H. 2000. Cellulose catabolism by *Clostridium cellulolyticum* growing in batch culture on defined medium. Applied and Environmental Microbiology 66(6): 2461-2470.

Desvaux, M. 2005. *Clostridium cellulolyticum*: model organism of mesophilic cellulolytic clostridia. Fems Microbiology Reviews 29(4): 741-764.

Desvaux, M. 2006. Unravelling carbon metabolism in anaerobic cellulolytic bacteria. Biotechnology Progress 22(5): 1229-1238.

Desvaux, M., Guedon, E., and Petitdemange, H. 2000. Cellulose catabolism by *Clostridium cellulolyticum* growing in batch culture on defined medium. Applied and Environmental Microbiology 66(6): 2461-2470.

Desvaux, M., Guedon, E., and Petitdemange, H. 2001a. Kinetics and metabolism of cellulose degradation at high substrate concentrations in steady-state continuous cultures of *Clostridium cellulolyticum* on a chemically defined medium. Applied and Environmental Microbiology 67(9): 3837-3845.

Desvaux, M., Guedon, E., and Petitdemange, H. 2001b. Metabolic flux in cellulose batch and cellulose-fed continuous cultures of *Clostridium cellulolyticum* in response to acidic environment. Microbiology-Sgm 147: 1461-1471.

Devries, W., and Stoutham, A. H. 1967. Pathway of Glucose Fermentation in Relation to Taxonomy of Bifidobacteria. Journal of Bacteriology 93(2): 574-576.

Dwivedi, R.C., Spicer, V., Harder, M., Antonovici, M., Ens, W., Standing, K.G., Wilkins, J.A., and Krokhin, O.V. 2008. Practical implementation of 2D HPLC scheme with

accurate peptide retention prediction in both dimensions for high-throughput bottom-up proteomics. Analytical Chemistry 80(18): 7036-7042.

EIA: Annual energy outlook 1999, with projections to 2020. In: DOE/EIA-0383. vol. 99. Washington, DC: Energy Information Administration, USA Department of Energy.; 1998.

Ethanol clean air facts, American coalition for ethanol– ACE- http://www.ethanol.org/ (Consulted 10/11/2004).

Farrell, A. E. 2006. Ethanol can contribute to energy and environmental goals. Science 312(5781):1748.

Feng, X., Mouttaki, H., Lin, L., Huang, R., Wu, B., Hemme, C.L., He, Z., Zhang, B., Hicks, L.M., Xu, J., Zhou, J., and Tang, Y.J. 2009. Characterization of the central metabolic pathways in *Thermoanaerobacter sp.* strain X514 via isotopomer-assisted metabolite analysis. Applied and Environmental Microbiology 75(15): 5001-5008.

Fernandes, A.N., Thomas, L.H., Altaner, C.M., Callow, P., Forsyth, V.T., Apperley, D.C., Kennedy, C.J., and Jarvis, M.C. 2011. Nanostructure of cellulose microfibrils in spruce wood. Proceedings of the National Academy of Sciences USA 108(47): 1195-203.

Flechner, A., Gross, W., Martin, W.F., Schnarrenberger, C. 1999. Chloroplast class I and class II aldolases are bifunctional for fructose-1,6-biphosphate and sedoheptulose-1,7-biphosphate cleavage in the Calvin cycle. FEBS Letters 447(2-3): 200-202.

Fry, S. 2001. Plant cell walls Encyclopedia of life sciences. Chichester: Nature Publishing Group.

Geng, A., He, Y.L., Qian, C.L., Yan, X., and Zhou, Z.H. 2010. Effect of key factors on hydrogen production from cellulose in a co-culture of *Clostridium thermocellum* and *Clostridium thermopalmarium*. Bioresource Technology 101(11): 4029-4033.

Giallo, J., Gaudin, C., Belaich, J.P. 1985. Metabolism and solubilization of cellulose by *Clostridium cellulolyticum* H10. Applied and Environmental Microbiology 49: 1216-1221.

Giallo, J., Gaudin, C., Belaich, J.P., Petitdemange, E., Caillet-Mangin, F. 1983. Metabolism of glucose and cellobiose by a cellulolytic mesophilic *Clostridiuim sp.* strain H1O. Applied Environmental and Microbiology 45: 843-849.

Gilar, M., Olivova, P., Daly, A.E., Gebler, J.C. 2005. Two-dimensional separation of peptides using RP-RP-HPLC system with different pH in first and second separation dimensions. Journal of Separation Science 28(14): 1694-1703.

Gottschalk, G. 1986. Bacterial Metabolism. second ed: Springer-Verlag publishers 1-359.

Groom, M.J., Gray, E.M., and Townsend, P.A. 2008. Biofuels and biodiversity: Principles for creating better policies for biofuel production. Conservation Biology 22(3): 602-609.

Guedon, E., Desvaux, M., and Petitdemange, H. 2000. Kinetic analysis of *Clostridium cellulolyticum* carbohydrate metabolism: Importance of glucose 1-phosphate and glucose 6-phosphate branch points for distribution of carbon fluxes inside and outside cells as revealed by steady-state continuous culture. Journal of Bacteriology 182(7): 2010-2017.

Guedon, E., Desvaux, M., and Petitdemange, H. 2002. Improvement of cellulolytic properties of *Clostridium cellulolyticum* by metabolic engineering. Applied and Environmental Microbiology 68(1): 53-58.

Guedon, E., Payot, S., Desvaux, M., and Petitdemange, H. 1999. Carbon and electron flow in *Clostridium cellulolyticum* grown in chemostat culture on synthetic medium. Journal of Bacteriology 181(10): 3262-3269.

Hemme, C.L., Fields, M.W., He, Q., Deng, Y., Lin, L., Tu, Q., Mouttaki, H., Zhou, A., Feng, X., Zuo, Z., Ramsay, B.D., He, Z., Wu, L., Van Nostrand, J., Xu, J., Tang, Y.J., Wiegel, J., Phelps, T.J., and Zhou, J. 2011. Correlation of genomic and physiological traits of *Thermoanaerobacter* species with biofuel yields. Applied and Environmental

Microbiology 77(22): 7998-8008.

Hethener, P., Brauman, A., and Garcia, J.L. 1992. *Clostridium termitidis sp*-Nov, a cellulolytic bacterium from the gut of the wood-feeding termite, *Nasutitermes lujae*. Systematic and Applied Microbiology 15(1): 52-58.

Heyndrickx, M., Devos, P., and Deley, J. 1991. Fermentation Characteristics of *Clostridium pasteurianum* Lmg-3285 Grown on Glucose and Mannitol. Journal of Applied Bacteriology 70(1): 52-58.

Houghton, J., Weatherwax, S., and Ferrell, J. 2006. Lignocellulosic Biomass Characteristics. In: Biofuels Joint Road Map. Edited by U.S. Department of Energy: 39-56.

Hungate, R.E. 1944. Studies on Cellulose Fermentation: The Culture and Physiology of an Anaerobic Cellulose-digesting Bacterium. Journal of Bacteriology 48(5): 499-513.

Islam, R., Cicek, N., Sparling, R., and Levin, D. 2006. Effect of substrate loading on hydrogen production during anaerobic fermentation by *Clostridium thermocellum* 27405. Applied Microbiology and Biotechnology 72(3): 576-583.

Islam, R., Cicek, N., Sparling, R., Levin, D.B. 2009. Influence of initial cellulose concentration on the carbon flow distribution during batch fermentation by *Clostridium thermocellum* ATCC 27405. Applied Microbiology and Biotechnology 82(1): 141-148.

Jin, M., Balan, V., Gunawan, C., Dale, B.E. 2011. Consolidated bioprocessing (CBP) performance of *Clostridium phytofermentans* on AFEX-treated corn stover for ethanol production. Biotechnology and Bioengineering 2011, 108(6): 1290-1297.

Johnson, J.L., and Chen, J.S. 1995. Taxonomic Relationships among Strains of *Clostridium acetobutylicum* and Other Phenotypically Similar Organisms. FEMS Microbiology Reviews 17(3): 233-240.

Kadam, K.L., Chin, C.Y., and Brown, L.W. 2008. Flexible biorefinery for producing fermentation sugars, lignin and pulp from corn stover. Journal of Industrial Microbiology and Biotechnology 35(5): 331-341.

Kanehisa, M., and Goto, S. 2000. KEGG: kyoto encyclopedia of genes and genomes. Nucleic Acids Research 28(1): 27-30.

Kadar Z, de Vrije T, van Noorden GE, Budde MA, Szengyel Z, Reczey K, Claassen PA. 2004. Yields from glucose, xylose, and paper sludge hydrolysate during hydrogen production by the extreme thermophile *Caldicellulosiruptor saccharolyticus*. Applied Biochemistry and Biotechnology 113-116: 497-508.

Kato, S., Haruta, S., Cui, Z.J., Ishii, M., and Igarashi, Y. 2004. Effective cellulose degradation by a mixed-culture system composed of a cellulolytic *Clostridium* and aerobic non-cellulolytic bacteria. FEMS Microbiology Ecology 51(1): 133-142.

Kessler, D., Leibrecht, I., and Knappe, J. 1991. Pyruvate-Formate-Lyase-Deactivase and Acetyl-CoA reductase activities of *Escherichia coli* reside on a polymeric protein particle encoded by AdhE. FEMS Letters 281(1-2): 59-63.

Lal, S., Ramachandran, U., Zhang, X.L., Munir, R., Sparling, R., Levin, D.B. 2013. Draft genome sequence of the cellulolytic mesophilic anaerobic bacterium *Clostridium termitidis* strain CT1112 (DSM 5398). Genome Announcements 1(3): e00281-13.

Lamed, R., and Zeikus, J.G. 1980. Ethanol-Production by Thermophilic Bacteria - Relationship between Fermentation Product Yields of and Catabolic Enzyme-Activities in *Clostridium thermocellum* and *Thermoanaerobium brockii.* Journal of Bacteriology 144(2): 569-578.

Lamed, R., and Zeikus, J. G. 1981. Thermostable, ammonium-activated malic enzyme of *Clostridium thermocellum*. Biochimica et Biophysica Acta 660(2): 251–255.

Lay, J.J. 2000. Modeling and optimization of anaerobic digested sludge converting starch to hydrogen. Biotechnology and Bioengineering 68(3): 269-278.

Lee, S.K., Chou, H., Ham, T.S., Lee, T.S., Keasling, J.D. 2008. Metabolic engineering of microorganisms for biofuels production: from bugs to synthetic biology to fuels. Current Opinions in Biotechnology 19(6): 556-563.

Lengler, W.J., Drews, J., and Schlegel, G.H. 1999. Biology of prokaryotes. Library of Congress: 1-921.

Levin, D.B., Carere, C., Ramachandran, U., Rydzak, T., Saunders, J. 2011. Fermentative Biofuels: Prospects of Practical Application (Book Chapter), 69 pages, Chapter 12, pp. 601-634. Carbon Neutral Fuels and Energy Carriers, TE Veziroglu & N. Muradov (Eds.). Taylor & Francis Group, Publishers, Boca Raton, Florida, USA.

Levin, D.B., Islam, R., Cicek, N., and Sparling, R. 2006. Hydrogen production by *Clostridium thermocellum* 27405 from cellulosic biomass substrates. International Journal of Hydrogen Energy 31(11): 1496-1503.

Levin, D.B., Pitt, L., and Love, M. 2004. Biohydrogen production: prospects and limitations to practical application. International Journal of Hydrogen Energy 29(2): 173-185.

Levin, D.B., Zhu, H., Beland, M., Cicek, N., and Holbein, B.E. 2007. Potential for renewable microbial hydrogen and methane biogas energy production from residual biomass in Canada. Bioresource Technology 98: 654-660.

Liesack, W., Schnell, S., and Revsbech, N.P. 2000. Microbiology of flooded rice paddies. FEMS Microbiology Reviews 24(5): 625-645.

Lim, D. 2003. Microbiology. Kendall/Hunt publishers: 1-781.

Lin, L., Song, H., Tu, Q., Qin, Y., Zhou, A., Liu, W., He, Z., Zhou, J., Xu, J. 2011. The *Thermoanaerobacter glycobiome* reveals mechanisms of pentose and hexose co-utilization in bacteria. PLoS Genetics 7(10):e1002318.

Lin, W. R., Lee, C. C., Hsu, J. J., Hamel, J. F., Demain, A. L. 1998. Properties of acetate kinase activity in *Clostridium thermocellum* cell extracts. Applied Biochemistry and Biotechnology 69(2): 137–145.

Lochner, A., Giannone, R. J., Keller, M., Antranikian, G., Graham, D. E., Hettich, R. L. 2011. Label-free Quantitative Proteomics for the Extremely Thermophilic Bacterium *Caldicellulosiruptor obsidiansis* Reveal Distinct Abundance Patterns upon Growth on Cellobiose, Crystalline Cellulose, and Switchgrass. Journal of Proteome Research 10(12): 5302-5314.

Lovins, A.B., and Aranow, B. T., Ed. 2004. In winning the oil endgame: Innovation for profits, jobs and security. Rocky Mountain Institute, Snowmass, CO: 1-122.

Lynd, L.R. 1996. Overview and evaluation of fuel ethanol from cellulosic biomass: Technology, economics, the environment, and policy. Annual Review of Energy and the Environment 21: 403-465.

Lynd, L.R., Weimer, P.J., van Zyl, W.H., and Pretorius, I.S. 2002. Microbial cellulose utilization: Fundamentals and biotechnology. Microbiology and Molecular Biology Reviews 66(4): 739-739.

Lynd, L.R., van Zyl, W.H., McBride, J.E., and Laser, M. 2005. Consolidated bioprocessing of cellulosic biomass: an update. Current Opinion in Biotechnology 16(5): 577-583.

Ma, H.W., and Zeng, A.P. 2003. Reconstruction of metabolic networks from genome data and analysis of their global structure for various organisms. Bioinformatics 19(2): 270-277.

Mabee, W.E., Fraser, E.D.G., McFarlane, P.N., and Saddler, J.N. 2006. Canadian biomass reserves for biorefining. Applied Biochemistry and Biotechnology 129(1-3): 22-40.

Mabee, W.E., Gregg, D.J., and Saddler, J.N. 2005. Assessing the emerging biorefinery sector in Canada. Applied Biochemistry and Biotechnology 121: 765-778.

Maicas, S., Ferrer, S., and Pardo, I. 2002. NAD(P)H regeneration is the key for heterolactic fermentation of hexoses in *Oenococcus oeni*. Microbiology-Sgm 148: 325-332.

Maki, M., Leung, K.T., and Qin, W.S. 2009. The prospects of cellulase-producing bacteria for the bioconversion of lignocellulosic biomass. International Journal of Biological Sciences 5(5): 500-516.

Market Research Analyst. 2008. World Ethanol Production 2008-2012. http://www.marketresearchanalyst.com/2008/01/26/world-ethanol-production-forecast 2008-2012.

McMurry, J., and T. P. Begley (ed). 2005. The organic chemistry of biological pathways. Roberts and Co. Publishers.

McQueen, P., Spicer, V., Rydzak, T., Sparling, R., Levin, D., Wilkins, J.A., Krokhin, O. 2012. Information-dependent LC-MS/MS acquisition with exclusion lists potentially generated on-the-fly: Case study using a whole cell digest of *Clostridium thermocellum*. Proteomics 12(8): 1160-1169.

Meinecke, B., Bertram, J., and Gottschalk, G. 1989. Purification and characterization of the pyruvate-ferredoxin oxidoreductase from *Clostridium acetobutylicum*. Archives of Microbiology 152(3): 244–250.

Mladenovska Z, Mathrani IM, Ahring BK. 1995. Isolation and characterization of *Caldicellulosiruptor lactoaceticus sp.* nov., an extremely thermophilic, cellulolytic, anaerobic bacterium. Archives of Microbiology 163: 223-230.

Nair, R.V., Bennett, G.N., and Papoutsakis, E.T. 1994. Molecular characterization of an aldehyde/alcohol dehydrogenase gene from *Clostridium acetobutylicum* ATCC-824. Journal of Bacteriology 176(3): 871-885.

Nakahigashi, K., Toya, Y., Ishii, N., Soga, T., Hasegawa, M., Watanabe, H., Takai, Y., Honma, M., Mori, H., Tomita, M. 2009. Systematic phenome analysis of *Escherichia coli* multiple-knockout mutants reveals hidden reactions in central carbon metabolism. Molecular Systems Biology 5: 306.

Neveling, U., Klasen, R., Bringer-Meyer, S., and Sahm, H. 1998. Purification of the pyruvate dehydrogenase multienzyme complex of *Zymomonas mobilis* and identification and sequence analysis of the corresponding genes. Journal of Bacteriology 180(6): 1540-1548.

Nielsen, J., Villadsen, J., and Lidén, G. (eds). 2003. Bioreaction Engineering Principles. second ed. New York: Kluwer Academic/Plenum Publishers.

NRCan, N.R.C. 2004. Canadian Hydrogen: Current status and Future Prospects. Dalcor Consultants Ltd. and Intuit Strategy Inc.

Ogata, H., Goto, S., Sato, K., Fujibuchi, W., Bono, H., Kanehisa, M. 1999. KEGG: Kyoto Encyclopedia of Genes and Genomes. Nucleic Acids Research 27(1): 29-34.

Ozkan, M., Yılmaz, E.I., Lynd, L.R., Özcengiz, G. 2004. Cloning and expression of the *Clostridium thermocellum* L-lactate dehydrogenase gene in *Escherichia coli* and enzyme characterization. Canadian Journal of Microbiology 50: 845-851.

Pan, X.J., Arato, C., Gilkes, N., Gregg, D., Mabee, W., Pye, K., Xiao, Z.Z., Zhang, X., and Saddler, J. 2005. Biorefining of softwoods using ethanol organosolv pulping: Preliminary evaluation of process streams for manufacture of fuel-grade ethanol and co-products. Biotechnology and Bioengineering 90(4): 473-481.

Parikka, M. 2004. Global biomass fuel resources. Biomass and Bioenergy 27(6): 613-620.

Pauly M., and Keegstra, K. 2008. Cell-wall carbohydrates and their modification as a resource for biofuels. The Plant Journal 54(4): 559-68.

Petitdemange, E., Caillet, F., Giallo, J., and Gaudin, C. 1984. *Clostridium cellulolyticum* Sp-Nov, a Cellulolytic, Mesophilic Species from Decayed Grass. International Journal of Systematic Bacteriology 34(2): 155-159.

Peralta-Yahya, P.P., and Keasling, J.D. 2010. Advanced biofuel production in microbes. Biotechnology Journal 5(2): 147-162.

Perkins, D.N., Pappin DJC, Creasy DM, Cottrell JS. 1999. Probability-based protein identification by searching sequence databases using mass spectrometry data. Electrophoresis 20(18): 3551-3567.

Powell, G.E. 1985. Stable Coexistence of Syntrophic Associations in Continuous Culture. Journal of Chemical Technology and Biotechnology 35(1): 46-50.

Ragauskas, A.J., Williams, C.K., Davison, B.H., Britovsek, G., Cairney, J., Eckert, C.A., Frederick, W.J., Hallett, J.P., Leak, D.J., Liotta, C.L., Mielenz, J.R., Murphy, R., Templer, R., and Tschaplinski, T. 2006. The path forward for biofuels and biomaterials. Science 311(5760): 484-489.

Ramachandran, U., Wrana, N., Cicek, N., Sparling, R., and Levin, D.B. 2008. Hydrogen production and end-product synthesis patterns by *Clostridium termitidis* strain CT1112 in

batch fermentation cultures with cellobiose or alpha-cellulose. International Journal of Hydrogen Energy 33(23): 7.

Ramachandran, U., Wrana, N., Cicek, N., Sparling, R., and Levin, D.B. 2011. Isolation and characterization of a hydrogen- and ethanol-producing *Clostridium sp* strain URNW. Canadian Journal of Microbiology 57(3): 236-243.

Raman, B., McKeown, C.K., Rodriguez, M. Jr., Brown, S. D., Mielenz, J. R. 2011. Transcriptomic analysis of *Clostridium thermocellum* ATCC 27405 cellulose fermentation. BMC Microbiology 11: 134.

Reid, M.F., and Fewson, C.A. 1994. Molecular Characterization of Microbial Alcohol Dehydrogenases. Critical Reviews in Microbiology 20(1): 13-56.

Rydzak, T., Levin, D.B., Cicek, N., Sparling, R. 2009. Growth phase-dependant enzyme profile of pyruvate catabolism and end-product formation in *Clostridium thermocellum* ATCC 27405. Journal of Biotechnology 140(3-4): 169-75.

Rydzak, T., Levin, D. B., Cicek, N., Sparling, R. 2011. End-product induced metabolic shifts in *Clostridium thermocellum* ATCC 27405. Applied Microbiology and Biotechnology 92(1): 199–209.

Rydzak, T., McQueen, P.D., Krokhin, O.V., Spicer, V., Ezzati, P., Dwivedi, R.C., Shamshurin, D., Levin, D.B., Wilkins, J.A., Sparling, R. 2012. Proteomic analysis of *Clostridium thermocellum* core metabolism: relative protein expression profiles and growth phase-dependent changes in protein expression. BMC Microbiology 12: 214.

Sander R. Compilation of Henry's law constants for inorganic and organic species of potential importance in environmental chemistry. Air Chemistry Department, Max-Planck Institute of Chemistry, Mainz, Germany, 1999.

Sauer, U. 2004. High-throughput phenomics: experimental methods for mapping fluxomes. Current Opinion in Biotechnology 15(1): 58-63.

Sawers, G. and Bock, A. 1988. Anaerobic regulation of pyruvate formate-lyase from *Escherichia coli* K-12. Journal of Bacteriology 170(11): 5330–5336.

Searchinger, T., Heimlich, R., Houghton, R.A., Dong, F.X., Elobeid, A., Fabiosa, J., Tokgoz, S., Hayes, D., and Yu, T.H. 2008. Use of US croplands for biofuels increases greenhouse gases through emissions from land-use change. Science 319(5867): 1238-1240.

Simpson, T.W., Sharpley, A.N., Howarth, R.W., Paerl, H.W., and Mankin, K.R. 2008. The new gold rush: Fueling ethanol production while protecting water quality. Journal of Environmental Quality 37(2): 318-324.

Sparling, R., Islam, R., Cicek, N., Carere, C., Chow, H., Levin, D.B. 2006. Formate synthesis by *Clostridium thermocellum* during anaerobic fermentation. Canadian Journal of Microbiology 52: 681-688.

Sparling, R., Carere, C., Rydzak, T., Schellenberg, J., Levin, D. B. 2012. Comparative Genomics and Bioenergetics of Dark Fermentation (Chapter 10). In State of the Art and Progress in Production of Biohydrogen. Edited by Azbar N, Levin DB. Sharjah, UAE: Bentham eBooks 160-188.

Stephanopoulos, G. 1998. Metabolic engineering. Biotechnology and Bioengineering 58(2-3): 119-120.

Stevenson, D.M., and Weimer, P.J. 2005. Expression of 17 genes in *Clostridium thermocellum* ATCC 27405 during fermentation of cellulose or cellobiose in continuous culture. Applied and Environmental Microbiology 71(8): 4672–4678.

Stoops, J.K., Cheng, R.H., Yazdi, M.A., Maeng, C.Y., Schroeter, J.P., Klueppelberg, U., Kolodziej, S.J., Baker, T.S., and Reed, L.J. 1997. On the unique structural organization of the *Saccharomyces cerevisiae* pyruvate dehydrogenase complex. Journal of Biological Chemistry 272(9): 5757-5764.

Stryer, L. (ed). 1995. Biochemistry. Fourth ed. W.H. Freeman and Company.

Taguchi, F., Mizukami, N., Hasegawa, K., Saito-Taki, T. 1994. Microbial conversion of arabinose and xylose to hydrogen by a newly isolated *Clostridium sp.* No. 2. Canadian Journal of Microbiology 40(3): 228-233.

Tamburini, E., Leon, A.G., Perito, B., and Mastromei, G. 2003. Characterization of bacterial pectinolytic strains involved in the water retting process. Environmental Microbiology 5(9): 730-736.

Thauer, R.K., Jungermann, K., and Decker, K. 1977. Energy conservation in chemotrophic anaerobic bacteria. Bacteriology Reviews 41(1): 100-180.

Tolonen, A.C., Haas, W., Chilaka, A.C., Aach, J., Gygi, S.P., Church, G.M. 2011. Proteome-wide systems analysis of a cellulosic biofuel-producing microbe. Molecular and systems Biology 7: 461.

Tzortzis, G., Goulas, A.K., Gee, J.M., and Gibson, G.R. 2005. A novel galactooligosaccharide mixture increases the bifidobacterial population numbers in a continuous in vitro fermentation system and in the proximal colonic contents of pigs in vivo. Journal of Nutrition 135(7): 1726-1731.

Van de Werken, H.J., Verhaart, M.R., VanFossen, A.L., Willquist, K., Lewis, D.L., Nichols, J.D., Goorissen, H.P., Mongodin, E.F., Nelson, K.E., van Niel, E.W., Stams,

A.J., Ward, D.E., de Vos, W.M., van der Oost, J., Kelly, R.M., and Kengen, S.W. 2008. Hydrogenomics of the extremely thermophilic bacterium *Caldicellulosiruptor saccharolyticus.* Applied and Environmental Microbiology 74(21): 6720-6729.

Van Maris, A., Abbott, D.A., Bellissimi, E., van den Brink, J., Kuyper, M., Luttik, M.A., Wisselink, H.W., Scheffers, W.A., van Dijken, J.P., and Pronk, J.T. 2006. Alcoholic fermentation of carbon sources in biomass hydrolysates by *Saccharomyces cerevisiae*: current status. Antonie Van Leeuwenhoek International Journal of General and Molecular Microbiology 90(4): 391-418.

Van Wyk, J.P.H. 2001. Biotechnology and the utilization of biowaste as a resource for bioproduct development. Trends in Biotechnology 19(5): 172-177.

Venkateswaran, S., and Demain, A.L. 1986. The *Clostridium thermocellum*- *Clostridium thermosaccharolyticum* Ethanol Production Process- Nutritional Studies and Scale-Down. Chemical Engineering Communications 45(1-6): 53-60.

Vey, J. L., Yang, J., Li, M., Broderick, W. E., Broderick, J. B., Drennan, C. L. 2008. Structural basis for glycyl radical formation by pyruvate formate-lyase activating enzyme. Proceedings of the National Academy of Sciences U S A 105(42): 16137–16141.

Walker, G.M. 2011. 125th Anniversary review: fuel alcohol: current production and future challenges. Journal of Institute of Brewing 117(1): 3–22

Warnick, T.A., Methe, B.A., Leschine, S.B. 2002. *Clostridium phytofermentans sp.* nov., a cellulolytic mesophile from forest soil. International Journal of Systematic and Evolutionary Microbiology 52(Pt 4): 1155-1160.

Wiegel, J. 1980. Formation of ethanol by bacteria- A pledge for the use of extreme thermophilic anaerobic bacteria in industrial ethanol fermentation processes. Experientia 36(12): 1434-1446.

Willquist, K., and van Niel, E.W.J. 2010. Lactate formation in *Caldicellulosiruptor saccharolyticus* is regulated by the energy carriers pyrophosphate and ATP. Metabolic Engineering 12(3): 282-290.

Wisniewski, J.R., Zougman, A., Nagaraj, N., Mann, M. 2009. Universal sample preparation method for proteome analysis. Nature Methods 6(5): 359-362.

Xue, Y.F., Xu, Y., Liu, Y., Ma, Y.H., and Zhou, P.J. 2001. *Thermoanaerobacter tengcongensis* sp nov., a novel anaerobic, saccharolytic, thermophilic bacterium isolated from a hot spring in Tengcong, China. International Journal of Systematic and Evolutionary Microbiology 51: 1335-1341.

Yang, S., Giannone, R. J., Dice, L., Yang, Z. K., Engle, N. L., Tschaplinski, J. T., Hettich R. L., Brown, S. D. 2012. *Clostridium thermocellum* ATCC 27405 transcriptonomic, metabolomic, and proteomic profiles after ethanol stress. BMC Genomics 13: 336.

Yan, R.T., and Chen, J.S. 1990. Coenzyme a-Acylating Aldehyde Dehydrogenase from *Clostridium beijerinckii* Nrrl-B592. Applied and Environmental Microbiology 56(9): 2591-2599.

Yan, Y., and Liao, J. 2009. Engineering metabolic systems for production of advanced fuels. Journal of Indian Microbiology and Biotechnology 36(4): 471-479.

Zhang, Y.H., and Lynd, L.R. 2005. Cellulose utilization by *Clostridium thermocellum*: bioenergetics and hydrolysis product assimilation. Proceedings of the National Academy of Sciences U S A 102(20): 7321-7325.

Zieske, L.R. 2006. A perspective on the use of iTRAQ (TM) reagent technology for protein complex and profiling studies. Journal of Experimental Botany 57(7): 1501-1508.

Appendix

Supplementary Table 1. Bioinformatic analysis of different families of transporters in *C. termitidis* genome. The highlighted families of transporters are specific to carbohydrates uptake.

Transporter Classification Family No.	Transporter Classification Family Name	Gene Count
TC:1.A.62	The Homotrimeric Cation Channel (TRIC) Family	1
TC:1.B.17	The Outer Membrane Factor (OMF) Family	1
TC:1.E.14	The LrgA Holin (LrgA Holin) Family	1
TC:2.A.1	The Major Facilitator Superfamily (MFS)	30
TC:2.A.14	The Lactate Permease (LctP) Family	2
TC:2.A.15	The Betaine/Carnitine/Choline Transporter (BCCT) Family	1
TC:2.A.36	The Monovalent Cation:Proton Antiporter-1 (CPA1) Family	1
TC:2.A.44	The Formate-Nitrite Transporter (FNT) Family	1
TC:2.A.50	The Glycerol Uptake (GUP) Family	1
TC:2.A.66	The Multidrug/Oligosaccharidyl-lipid/Polysaccharide (MOP) Flippase Superfamily	16
TC:2.A.67	The Oligopeptide Transporter (OPT) Family	2
TC:2.A.79	The Threonine/Serine Exporter (ThrE) Family	2
TC:2.A.86	The Autoinducer-2 Exporter (AI-2E) Family (Formerly the PerM Family, TC #9.B.22)	4
TC:2.A.98	The 10 TMS Putative Sulfate Exporter (PSE) Family	1
TC:3.A.1	The ATP-binding Cassette (ABC) Superfamily	712
TC:3.A.10	The H⁺-translocating Pyrophosphatase (H⁺-PPase) Family	2
TC:3.A.11	The Bacterial Competence-related DNA Transformation Transporter (DNA-T) Family	2
TC:3.A.12	The Septal DNA Translocator (S-DNA-T) Family	1
TC:3.A.15	The Outer Membrane Protein Secreting Main Terminal Branch (MTB) Family	3
TC:3.A.4	The Arsenite-Antimonite (ArsAB) Efflux Family	2
TC:3.A.5	The General Secretory Pathway (Sec) Family	8
TC:3.A.6	The Type III (Virulence-related) Secretory Pathway (IIISP) Family	11
TC:3.A.7	The Type IV (Conjugal DNA-Protein Transfer or VirB) Secretory Pathway (IVSP) Family	1
TC:4.B.1	The Nicotinamide Ribonucleoside (NR) Uptake Permease (PnuC) Family	1
TC:4.C.1	The Proposed Fatty Acid Transporter (FAT) Family	8
TC:8.A.1	The Membrane Fusion Protein (MFP) Family	2
TC:8.A.3	ıic Membrane-Periplasmic Auxiliary-1 (MPA1) Protein with Cytoplasmic (C) Domain (MPA1-C or M	3
TC:8.A.7	The Phosphotransferase System Enzyme I (EI) Family	1
TC:9.A.30	The Tellurium Ion Resistance (TerC) Family	2
TC:9.B.20	The Putative Mg²⁺ Transporter-C (MgtC) Family	1
TC:9.B.30	The Hly III (Hly III) Family	1
TC:9.B.33	The Sensor Histidine Kinase (SHK) Family	1
TC:9.B.46	The <I>Staphylococcus aureus</I> Putative Quorum Sensing Peptide Exporter, AgrB (AgrB) Family	4

Supplementary Table 2. 1-D LC/MS/MS analysis of *C. termitidis* mid-exponential phase samples cultured on 1191 medium containing 2g/L α-cellulose (highlighted proteins are involved in central carbon metabolism), using AB SCIEX TripleTOF™ 5600 system.

N	Confidence	%Cov (95)	Accession	Name
4	102.57	76.77	2504593713	Ct_00047420 triosephosphate isomerase
5	95.24	70.13	2504590118	Ct_00011340 Phosphoenolpyruvate carboxykinase (GTP)
6	92.34	70.35	2504594340	Ct_00053720 Alcohol dehydrogenase, class IV
11	72.06	69.22	2504589706	Ct_00007200 Pyruvate/oxaloacetate carboxyltransferase
17	65.69	71.72	2504593736	Ct_00047650 glyceraldehyde-3-phosphate dehydrogenase, type I
20	64.39	49.72	2504589785	Ct_00007990 pyruvate, phosphate dikinase
23	60.58	68.66	2504592229	Ct_00032520 Alcohol dehydrogenase, class IV
25	59.46	61.32	2504593776	Ct_00048050 NADH:ubiquinone oxidoreductase, NADH-binding
28	56.79	49.41	2504589708	Ct_00007220 Acetyl-CoA carboxylase, carboxyltransferase component
31	54.93	73.25	2504593646	Ct_00046750 6-phosphofructokinase
32	53.51	79.73	2504593645	Ct_00046740 fructose-1,6-bisphosphate aldolase, class II
36	51.69	62.69	2504589998	Ct_00010140 Pyruvate:ferredoxin oxidoreductase and related 2-oxoacid:ferredoxin oxidoreductases, alpha subunit
39	47.55	47.94	2504593775	Ct_00048040 hydrogenases, Fe-only
41	45.7	69.08	2504590972	Ct_00019900 ATP synthase, F1 beta subunit
43	43.96	39.57	2504591703	Ct_00027250 transketolase
59	36.04	53.8999 9747	2504593445	Ct_00044740 acetate kinase
60	35.66	65.38	2504589997	Ct_00010130 Pyruvate:ferredoxin oxidoreductase and related 2-oxoacid:ferredoxin oxidoreductases, beta subunit
95	27.66	37.99	2504592804	Ct_00038300 Glucose-6-phosphate isomerase
106	24.79	23.98	2504589026	Ct_00000380 formate acetyltransferase 1
109	24.6	59.65	2504590235	Ct_00012510 Fructose-1,6-bisphosphate aldolase
138	21.82	28.79	2504589626	Ct_00006400 pyruvate kinase
168	19.42	11.23	2504592534	Ct_00035580 pyruvate:ferredoxin (flavodoxin) oxidoreductase
215	16.34	35.8	2504589393	Ct_00004060 L-lactate dehydrogenase

Supplementary Table 3. 1D LC/MS/MS analysis of *C. termitidis* stationary phase samples cultured on 1191 medium containing 2g/L α-cellulose (highlighted proteins are involved in central carbon metabolism), using AB SCIEX TripleTOF^{TM} 5600 system.

N	Confidence	%Cov (95)	Accession	Name
2	147.16	73.75	2504593423	Ct_00044510 ABC-type sugar transport system
6	90.67	65.85	2504594340	Ct_00053720 Alcohol dehydrogenase, class IV
7	88.48	66.25	2504593713	Ct_00047420 triosephosphate isomerase
8	84.59	67.94	2504590118	Ct_00011340 Phosphoenolpyruvate carboxykinase (GTP)
11	69.83	55.94	2504589744	Ct_00007580 ABC-type dipeptide transport system
12	68.04	80.94	2504593736	Ct_00047650 glyceraldehyde-3-phosphate dehydrogenase, type I
13	67.7	60.39	2504592229	Ct_00032520 Alcohol dehydrogenase, class IV
16	63.31	64.12	2504589706	Ct_00007200 Pyruvate/oxaloacetate carboxyltransferase
21	55.29	65.74	2504589998	Ct_00010140 Pyruvate:ferredoxin oxidoreductase and related 2-oxoacid:ferredoxin oxidoreductases, alpha subunit
22	53.14	52.81	2504593776	Ct_00048050 NADH:ubiquinone oxidoreductase, NADH-binding
23	52.85	49.21	2504589708	Ct_00007220 Acetyl-CoA carboxylase, carboxyltransferase component
32	43.93	45.28	2504593775	Ct_00048040 hydrogenases, Fe-only
33	42.14	65.29	2504593646	Ct_00046750 6-phosphofructokinase
38	38.92	62.81	2504589997	Ct_00010130 Pyruvate:ferredoxin oxidoreductase and related 2-oxoacid:ferredoxin oxidoreductases, beta subunit
41	37.88	70.09	2504593645	Ct_00046740 fructose-1,6-bisphosphate aldolase, class II
42	37.43	29.46	2504589785	Ct_00007990 pyruvate, phosphate dikinase
44	37.15	59.58	2504589392	Ct_00004050 Malic enzyme
47	34.69	48.6	2504593445	Ct_00044740 acetate kinase
52	29.58	40.4	2504589009	Ct_00000210 isocitrate dehydrogenase, NADP-dependent
54	28.96	34.43	2504591703	Ct_00027250 transketolase
67	25.77	26.94	2504589026	Ct_00000380 formate acetyltransferase 1
72	24.5	21.81	2504593421	Ct_00044490 Cellobiose phosphorylase
96	21.31	31.49	2504593439	Ct_00044680 stage IV sporulation protein A
149	15.31	44.4	2504590235	Ct_00012510 Fructose-1,6-bisphosphate aldolase
200	12	30.46	2504593899	Ct_00049280 Transketolase, C-terminal subunit

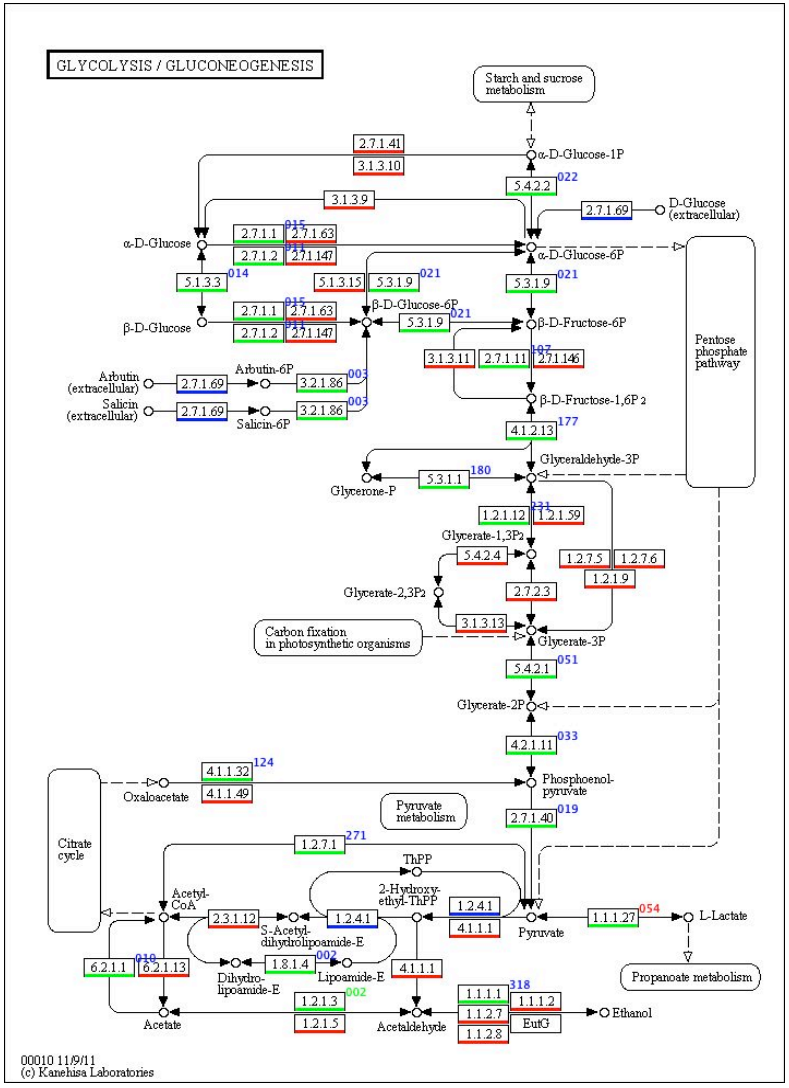
GLYCOLYSIS / GLUCONEOGENESIS
Starch and sucrose metabolism
α-D-Glucose-1P
D-Glucose (extracellular)
α-D-Glucose
α-D-Glucose-6P
β-D-Glucose-6P
β-D-Glucose
β-D-Fructose-6P
Pentose phosphate pathway
Arbutin (extracellular)
Arbutin-6P
Salicin (extracellular)
Salicin-6P
β-D-Fructose-1,6P 2
Glyceraldehyde-3P
Glycerone-P
Glycerate-1,3P2
Glycerate-2,3P2
Carbon fixation in photosynthetic organisms
Glycerate-3P
Glycerate-2P
Phosphoenol-pyruvate
Oxaloacetate
Pyruvate metabolism
Citrate cycle
ThPP
2-Hydroxy-ethyl-ThPP
Acetyl-CoA
S-Acetyl-dihydrolipoamide-E
Pyruvate
L-Lactate
Propanoate metabolism
Dihydro-lipoamide-E
Lipoamide-E
Acetate
Acetaldehyde
Ethanol
EutG
00010 11/9/11
(c) Kanehisa Laboratories

Supplementary Figure 1. Glycolysis pathway analyses during mid-exponential phase in *C. termitidis* grown on α-cellulose versus cellobiose using an in-house software package "Kegg colorbook". Protein level Z-scores and their supporting peptide data are also mapped onto KEGG pathways (adapted from Ogata et al. 1999; Kanehisa et al. 2000). The gene overview file generated in an IMG-JGI workflow relates genes (and thus their corresponding proteins) to a wide range of classification models, including enzyme class (EC) numbers and COG categories. In the map overlay, reaction-boxes with green color-code indicates their presence both in the genome as well as the proteome, blue color-code indicates that they are encoded in the genome and not identified in the proteome, and red color-code signifies their absence in both the genome and proteome.

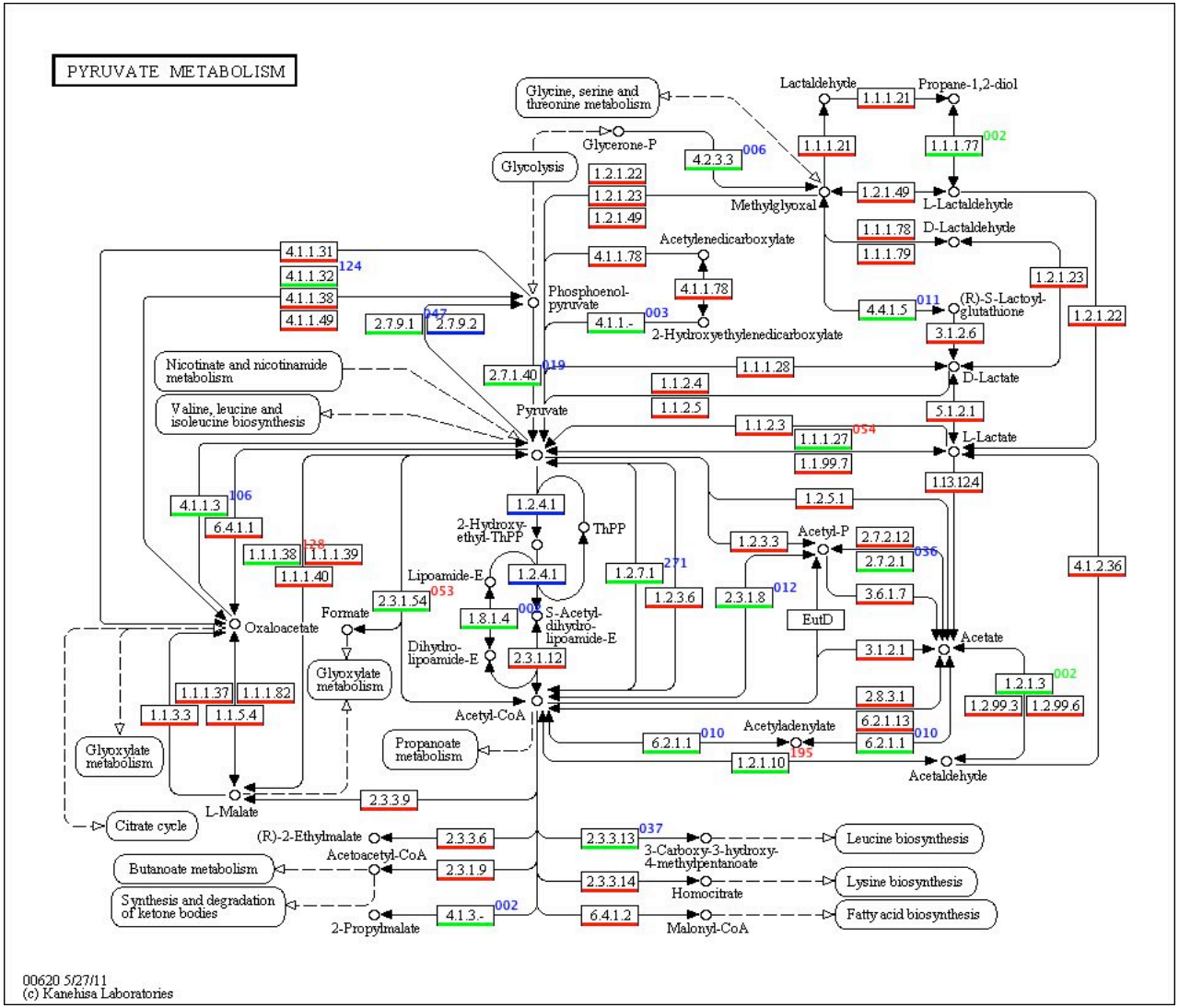
PYRUVATE METABOLISM
Glycine, serine and threonine metabolism
Glycerone-P
Glycolysis
Lactaldehyde
Propane-1,2-diol
1.1.1.21
1.1.1.77
002
4.2.3.3
006
1.2.1.22
1.2.1.23
1.2.1.49
Methylglyoxal
L-Lactaldehyde
1.1.1.78
D-Lactaldehyde
1.1.1.79
Acetylenedicarboxylate
4.1.1.78
4.1.1.31
4.1.1.32
124
4.1.1.38
4.1.1.49
Phosphoenol-pyruvate
4.1.1.78
4.1.1.-
003
2-Hydroxyethylenedicarboxylate
2.7.9.1
047
2.7.9.2
4.4.1.5
011
(R)-S-Lactoyl-glutathione
3.1.2.6
1.2.1.22
Nicotinate and nicotinamide metabolism
Valine, leucine and isoleucine biosynthesis
2.7.1.40
019
Pyruvate
1.1.1.28
D-Lactate
1.1.2.4
1.1.2.5
5.1.2.1
1.1.2.3
1.1.1.27
054
L-Lactate
1.1.99.7
1.13.12.4
4.1.1.3
106
6.4.1.1
1.2.4.1
2-Hydroxy-ethyl-ThPP
ThPP
1.2.5.1
1.2.3.3
Acetyl-P
2.7.2.12
2.7.2.1
036
1.1.1.38
138
1.1.1.39
1.1.1.40
Lipoamide-E
1.2.4.1
1.2.7.1
271
1.2.3.6
2.3.1.8
012
3.6.1.7
4.1.2.36
2.3.1.54
053
Formate
1.8.1.4
004
S-Acetyl-dihydro-lipoamide-E
EutD
Oxaloacetate
Dihydro-lipoamide-E
2.3.1.12
3.1.2.1
Acetate
Glyoxylate metabolism
1.2.1.3
002
1.1.1.37
1.1.1.82
1.2.99.3
1.2.99.6
1.1.3.3
1.1.5.4
Acetyl-CoA
2.8.3.1
6.2.1.13
Acetyladenylate
6.2.1.1
010
6.2.1.1
010
Glyoxylate metabolism
Propanoate metabolism
1.2.1.10
195
Acetaldehyde
2.3.3.9
L-Malate
Citrate cycle
(R)-2-Ethylmalate
2.3.3.6
2.3.3.13
037
3-Carboxy-3-hydroxy-4-methylpentanoate
Leucine biosynthesis
Acetoacetyl-CoA
Butanoate metabolism
2.3.1.9
2.3.3.14
Homocitrate
Lysine biosynthesis
Synthesis and degradation of ketone bodies
2-Propylmalate
4.1.3.-
002
6.4.1.2
Malonyl-CoA
Fatty acid biosynthesis
00620 5/27/11
(c) Kanehisa Laboratories

Supplementary Figure 2. Pyruvate catabolic pathway analyses during mid-exponential phase in *C. termitidis* grown on α-cellulose versus cellobiose using an in-house software package "Kegg colorbook". Protein level Z-scores and their supporting peptide data are also mapped onto KEGG pathways (adapted from Ogata et al. 1999; Kanehisa et al. 2000). The gene overview file generated in an IMG-JGI workflow relates genes (and thus their corresponding proteins) to a wide range of classification models, including enzyme class (EC) numbers and COG categories. In the map overlay, reaction-boxes with green color-code indicates their presence both in the genome as well as the proteome, blue color-code indicates that they are encoded in the genome and not identified in the proteome, and red color-code signifies their absence in both the genome and proteome. Kegg color book, was used for visualizing all the possible metabolic pathways with respect to *C. termitidis* proteome and genome with specific color-coding for clear elucidation.

```
00.07 00.81 01377
1.00 SD (-0.74 00.88): 00309 (00157 00152) 22.44
1.64 SD (-1.26 01.39): 00142 (00096 00046) 10.31
1.96 SD (-1.52 01.65): 00103 (00076 00027) 07.48


-3.20 0001
-2.80 0001
-2.40 0004
-2.20 0001
-2.00 0003
-1.80 0007 *
-1.60 0011 *
-1.40 0011 *
-1.20 0027 ****
-1.00 0039 *****
-0.80 0058 ********
-0.60 0073 **********
-0.40 0115 ******************
-0.20 0198 ******************************
00.00 0270 ****************************************
00.20 0205 ******************************
00.40 0105 ***************
00.60 0051 *******
00.80 0042 ******
01.00 0028 ****
01.20 0018 **
01.40 0018 **
01.60 0021 ***
01.80 0010 *
02.00 0013 *
02.20 0014 **
02.40 0009 *
02.60 0013 *
02.80 0003
03.00 0004
03.20 0003
04.40 0001
peak-based centroid: 00.08
```

Supplemenatary Figure 3. Z-limits of stationary phase iTRAQ experiment- cellulose vs cellobiose.

```
00.10 00.79 01370
1.00 SD (-0.68 00.89): 00345 (00190 00155) 25.18
1.64 SD (-1.19 01.39): 00139 (00098 00041) 10.15
1.96 SD (-1.44 01.65): 00088 (00064 00024) 06.42


-3.00 0001
-2.40 0001
-2.20 0002
-2.00 0002
-1.80 0007 *
-1.60 0006 *
-1.40 0012 **
-1.20 0031 *****
-1.00 0033 ******
-0.80 0054 **********
-0.60 0096 ******************
-0.40 0109 ********************
-0.20 0194 ************************************
00.00 0216 ****************************************
00.20 0193 ************************************
00.40 0116 *********************
00.60 0072 *************
00.80 0035 ******
01.00 0051 *********
01.20 0028 *****
01.40 0027 *****
01.60 0021 ***
01.80 0015 **
02.00 0016 **
02.20 0014 **
02.40 0005
02.60 0003
02.80 0002
03.00 0005
03.20 0001
03.80 0001
04.00 0001
peak-based centroid: 00.11
```

Supplemenatary Figure 4. Z-limits of mid-exponential phase iTRAQ experiment-cellulose vs cellobiose.